Microfluidic Assays for Perfusion Culture and Chemical Monitoring of Living Cells

by

Shusheng Lu

A dissertation submitted in partial fulfillment
of the requirements for the degree of
Doctor of Philosophy
(Chemistry)
in the University of Michigan
2017

Doctoral Committee:

Professor Robert T. Kennedy, Chair
Professor Mark E. Meyerhoff
Professor Michael D. Morris
Professor Leslie S. Satin

DEDICATION

To my family and friends.

ACKNOWLEDGEMENTS

I would like to thank, first and foremost, my advisor Dr. Robert Kennedy, for his contribution to this research and all his guidance and support throughout my time at University of Michigan. I also would like to thank the remaining members of my committee, Dr. Mark Meyerhoff, Dr. Michael Morris, and Dr. Leslie Satin, for their feedback and suggestions for my projects and for taking the time to serve on my committee.

I am grateful for all former and present members in the Kennedy lab for their guidance and suggestions, especially Dr. Ting Zhang for training me the foundation of skills necessary for my thesis work, Dr. Colleen Dugan for the help with adipocytes culture and for valuable discussions about the cell co-culture project, and Dr. Cynthia Cipolla for helpful discussions about islets. I also would like to thank my collaborators, Dr. Leslie Satin and Dr. Eric Glynn for their work on the glucose sensitivity project, Dr. Rohit Kulkarni, Dr. Masaru Akiyama and Dr. Tomozumi Takatani for their work on the Ca^{2+} measurement project, and Dr. Arvan Peter and Dr. Shuaishuai Zhu for their work on the C-peptide project.

Finally, I would like to thank my family, especially my parents, with their unconditional love, and my fiancée Qian Lu, for her love, support and constant encouragement throughout my graduate school years.

TABLE OF CONTENTS

DEDICATION ii
ACKNOWLEDGEMENTS iii
LIST OF FIGURES vi
LIST OF ABBREVIATIONS ix
ABSTRACT xi
CHAPTER 1 Introduction 1
Microfluidics and Micro Total Analysis System 1
Microfluidics for Cell Studies 3
Microfluidic Capillary Electrophoresis Immunoassay 5
Diabetes Background 7
Obesity and Adipocytes Background 20
Dissertation Overview 25
References 27
CHAPTER 2 Microchip Electrophoresis Devices for Chemical Gradient Generation and 24 h Operation and Application to Perfusion and Chemical Monitoring of Living Cells 33
Introduction 33
Experimental Section 36
Results and Discussion 43
Conclusion 51
References 53
CHAPTER 3 A Microfluidic System to Study Cell-cell Interaction 55
Introduction 55
Experimental Section 58
Results and Discussion 68
Conclusion 80

References 81
CHAPTER 4 Microchip for Monitoring C-Peptide-Bearing Superfolder Green Fluorescent Protein (CpepSfGFP) Secretion from Living Islets 84
Introduction 84
Experimental Section 85
Results and discussion 85
Conclusion 90
References 91
CHAPTER 5 Investigation of the Role of X-Box Binding Protein 1 in Insulin Regulated Pancreatic α-Cell Function 92
Introduction 92
Experimental Section 95
Results and discussion 100
Conclusion 105
References 106
CHAPTER 6 Summary and Future Directions 108
Summary 108
Future Directions 111
Conclusion 122
References 123

LIST OF FIGURES

Figure 1.1. Microchip electrophoresis developed for insulin monitoring. 7

Figure 1.2. Images of islets of Langerhans. 9

Figure 1.3. Simplified schematic of the triggering and amplifying pathways of GSIS. ...10

Figure 1.4. Biphasic and pulsatile insulin secretion. 11

Figure 1.5. Plasma glucose and serum insulin level in normal and diabetic subjects when infused with 6 mg kg^{-1} glucose for 1 min every 10 min. 12

Figure 1.6. Insulin secretion rate (ISR) profiles from a control and a type 2 diabetic patient during continuous enteral nutrition. 12

Figure 1.7. Blood glucose profile of human and mouse. 13

Figure 1.8. Using glucose ramp to measure glucose sensitivity. 14

Figure 1.9. Insulin release from a perfused pancreas and a perfused single islet. 16

Figure 1.10. Preproinsulin Process. 18

Figure 2.1. Overview of the microfluidic platform for monitoring insulin secretion from single islets. 38

Figure 2.2. Sample electropherograms and a sample calibration curve. 44

Figure 2.3. Islet morphology comparison. 45

Figure 2.4. Average long-term insulin secretion. 46

Figure 2.5. 25 h islet insulin secretion. 48

Figure 2.6. COMSOL models simulating on-chip mixing. 49
Figure 2.7. Programmed on-chip glucose changes with pumps mimicked by fluorescein. 50
Figure 2.8. Insulin secretory dynamics in the 3 treatment groups. 51
Figure 3.1. Microfluidic chip layout. 62
Figure 3.2. Side view of adipocytes and islet perfusion culture. 63
Figure 3.3. Workflow of Experiments. 64
Figure 3.4. The assembled chip in compression frame with only the cell culture portion. 65
Figure 3.5. Sample electropherograms and a sample calibration curve. 70
Figure 3.6. COMSOL Model of Adipocyte chamber, islet chamber and cellular release. 72
Figure 3.7. FFA concentration measured with off-line NEFA enzyme assay. 74
Figure 3.8. Summary of insulin secretion stimulated with 3h palmitate (PA) pretreatment and adipocytes co-culture. 75
Figure 3.9. Statistical analysis of 1st phase insulin secretion peak value and average secretion rate. 76
Figure 3.10. Statistical analysis of 2nd phase average insulin secretion rates and oscillation frequency. ** $p < 0.01$; * $p < 0.05$. 77
Figure 3.11. Representative insulin secretion from individual islets stimulated with 3h palmitate (PA) pretreatment and adipocytes co-culture. 77
Figure 3.12. Intracellular Ca^{2+} concentration of control islets and islets pretreated with 100 μM palmitic acid for 3 h. 79

Figure 4.1. Microfluidic chip for monitoring C-peptide secretion from single islet modified from the previous design. 86
Figure 4.2. Electropherograms of CpepSfGFP before modifying the microchip (left) and after (right). 87
Figure 4.3. Kinetics of transgenic CpepSfGFP and mouse insulin from isolated CpepSfGFP islets. 88
Figure 4.4. Comparison of CpepSfGFP secretion stimulated by 60 mM K^+ and 25 mM glucose. 89
Figure 5.1. Designs of microfluidic devices for Ca^{2+} imaging studies. 94
Figure 5.2. Open-top PDMS/glass microfluidic chip for Ca^{2+} imaging. 97
Figure 5.3. Screenshot of Ca^{2+} imaging in Metamorph software. 100
Figure 5.4. The cell chamber model built with COMSOL software and the mean concentration of different areas labeled near the bottom of the cell chamber. 102
Figure 5.5. Effects of altered XBP1 expression on [Ca^{2+}] in aTC6 cells. 104
Figure 6.1. Diagram of the microchip electrophoresis. 114
Figure 6.2. GSIS from islets chronically exposed to fatty acids. 117
Figure 6.3. On-line elution profile from 3T3-L1 adipocytes. 119
Figure 6.4. The expression of adipocyte-secreted factors in 3T3-L1 cells. 120
Figure 6.5. A microchip design culturing 2 islets. 121

LIST OF ABBREVIATIONS

Ab	Antibody
ANOVA	Analysis of variance
B/F	Bound-to-free ratio
BSA	Bovine serum albumin
BSS	Balanced salt solution
CE	Capillary electrophoresis
CpepSfGFP	C-peptide-bearing Superfolder Green Fluorescent Protein
DMEM	Dulbecco's Modified Eagle Medium
EDTA	Ethylenediaminetetraacetic acid
ELISA	Enzyme-linked immunosorbent assay
EOF	Electroosmotic flow
ER	Endoplasmic reticulum
FFA	Free fatty acid
FITC	Fluorescein isothiocyanate
G	Glucose
GLUT2	Glucose transporter-type 2
GSIS	Glucose stimulated insulin secretion
HBSS	Hank’s buffered salt solution
HEPES	4-(2-hydroxyethyl)-1-piperazineethanesulfonic acid
HV	High voltage
Hz	Hertz
K_{ATP}	ATP-sensitive potassium channels
K_d	Dissociation constant
KRB	Krebs ringer buffer
LIF	Laser-induced fluorescence
LOD	Limit of detection
MCE	Microchip electrophoresis
mM	Milimolar
MS	Mass spectrometry
NEFA	Non-esterified fatty acid
µg	Microgram
µL	Microliter
µTAS	micro total analysis systems
nM	Nanamolar
PDMS	Polydimethyl siloxane
PK/PD	Pharmacokinetics and pharmacodynamics

pL	Picoliter
pM	Picomolar
R^2	Coefficient of determination of a linear regression
RIA	Radioimmunoassay
RPMI	Roswell Memorial Park Institute
RSD	Relative standard deviation
SD	Standard deviation
SEM	Standard error of mean
UPR	Unfolded protein response
UV	Ultraviolet
kV	Kilovolts
W	Watts
XBP-1	X-Box Binding Protein 1

ABSTRACT

Insulin is secreted from islets of Langerhans to control glucose homeostasis. Deficient insulin secretion is a hallmark of type 2 diabetes. New tools for studying insulin secretion are of interest to better understand this process. An advanced method for measuring insulin secretion is based on using electrophoresis. In the method, a single islet is incubated on a microfluidic device or “chip”. Fluid around the islet is sampled by electroosmotic flow and reagents for a competitive immunoassay added to the sample stream. The resulting stream is analyzed at 5-10 s intervals by using electrophoresis to separate antibody bound and free insulin. In this work, this system was improved by adding more automated control of the islet environment, adapting to measure other peptides, and performing co-culture experiments to elucidate how adipocytes affect insulin secretion.

To provide further automation, two computer-controlled syringe pumps were used to deliver programmed glucose gradients to the islet. Automatic online calibration to improve quantification was also added. The device performed an electrophoresis-based competitive immunoassay every 8 s and operated for 24 h, resulting in the completion of 14,000 assays. It was applied to several insulin secretion studies including an investigation of glucose pretreatment on glucose sensitivity. A modification of the chip was applied to measure the secretory kinetics of C-peptide. The kinetics were compared with insulin and used to validate C-peptide as indicator of insulin secretion. The chip was

further modified to enable study of the impact of adipocytes on islet insulin secretion by co-culture both cells on the same chip. Adipocytes are fat-storing cells that secrete glycerol, non-esterified fatty acids and adipokines. The adipocytes strongly potentiated insulin secretion from islets. The effect appeared to be due to multiple chemicals released by the adipocytes illustrating the potential for observing complex interactions.

A second microfluidic chip was developed to perform intracellular [Ca^{2+}] measurements. The chip was used to investigate the role of X-Box Binding Protein 1 in insulin regulated pancreatic α-cell function. The results suggested that [Ca^{2+}] alterations did not underlie the dysregulation of glucagon secretion in XBP1 deficient α-cells.

CHAPTER 1

Introduction

The development of microfluidic devices has led to enhanced capability to study cell physiology. Microfluidic systems have been developed with sophisticated cell culture capability and on-line chemical analysis of cells based on advances in perfusion, surface chemistry, 3D-structure, and analytical instrument integration. This dissertation describes the development and applications of microfluidic systems to monitor hormone secretion from and intracellular Ca^{2+} concentration in living cells, such as pancreas β-cells and α-cells. Important developments include automatic control of perfusate, 24 h long-term on chip culture and chemical monitoring, and co-culture for cell-cell interaction studies. The goal of the research is to provide more insight into the mechanism of insulin secretion to aid in the understanding diseases such as diabetes mellitus and obesity.

Microfluidics and Micro Total Analysis System

Microfluidics encompasses microfabricated devices or systems utilizing small amount of fluids and have channels or chamber structures in the dimension from tens to hundreds of micrometers. The first microfluidic system was a miniature gas chromatographic analysis system[1], including an injecting valve and a 1.5 m long separation column on a single silicon wafer and a separately fabricated thermal conductivity detector clamped on the column wafer. This system received little interest

from the scientific community at that time. A microfabricated capillary electrophoresis (CE) device[2] developed in 1992 drew more attention to microfluidics and fueled explosive developments over the past 2-3 decades leading to the concepts of “micro total analysis systems (μTAS)” and “lab on a chip”.[3] One goal of μTAS is to incorporate one or several analytical features-including sampling, sample preparation and pre-treatment, separations or extractions, chemical reactions, detection, and data analysis onto the same device as an integrated miniaturized system to enable routine complex analysis such as clinical diagnostics (see reference 4 and 5 for reviews).

Comparing to conventional bulk scale or bench-top scale instruments, μTAS has many potential advantages, primarily due to the size effect. μTAS requires less bench-top space and reagent consumption, which saves cost on reagent purchasing, storage and disposal. Smaller size increases the feasibility to design portable devices, which has the potential to totally change the process of field testing and monitoring (having potable systems in individual fields for *in situ* or online monitoring can greatly increase efficiency, compared to sending samples to one or a few labs and waiting for the results to make decisions). It also allows less mass and heat transfer distance, mixing and reaction time with precise control of small amounts of fluids. Additionally, the ability to automate many analytical steps and be multiplexed with well designed and fabricated patterns allow increased throughput, reproducibility and cost savings.

Despite numerous advantages, implementing μTAS also has drawbacks. μTAS usually require special and extremely cautious operation and maintenance, because they are prone to clogging, contamination and fouling. Issues that are not remarkable in macroscale systems such as gas bubbles, leakage or entering of small particles can

render microfluidic devices unusable. In practical terms, the small scale also brings more challenge to identify and diagnose failures (almost always require assistance of a microscope) and trouble-shoot (depending on the severity and location, some issues like clogging or contamination can be difficult to resolve). Coupling macroscale elements with μTAS for sample and reagent introduction, or coupling large scale or commercial detectors can also be challenging. Lastly, microfabrication usually requires a clean room and specialized equipment, which can be expensive to access or maintain.

Microfluidics for Cell Studies

Traditionally, cell culture is performed in bulk using petri dishes or flasks. Although useful, they usually fail to reconstitute realistic volume-to-cell ratio and lack fluid dynamics and mass transport, both are important features in mimicking *in vivo* environment. They also do not lend themselves to dynamic control over the cellular environment or integration with chemical measurements. Microfluidics is an excellent candidate for cell studies because the size dimension is compatible with cell sizes and microfluidic channels can mimic the vascular capillaries, providing dynamic nutrient supply, waste removal and drug presentation or other stimulus administration. Other crucial parameters around cells such as the ambient temperature and gas content can also be precisely controlled. The small dimension also enables small amounts of tissue and media consumption, implementation of high-throughput experiments, and integration with detection techniques for chemical monitoring.

Many applications of microfluidic cell culture have been reported (see reference 6 and 7 for reviews). One area for use of microfluidics that has emerged is to create *in*

vitro conditions that better mimic an *in vivo* environment with multiple cell types. These tools are often called “organs-on-a-chip” or “human-on-a-chip” to emphasize the creation of an *in vivo* like environment in the controlled confines of a microfluidic device. These systems were first developed to mimic *in vivo* pharmacokinetics and pharmacodynamics (PK/PD) on a chip.[8–10] The devices have interconnected compartments containing lung, liver, fat and other tissues in a circulatory system so that drugs introduced to the cells are metabolized like *in vivo*. Subsequent improvements include creation of 3-dimensional environments and long-term culture.[11–14] The concept has grown beyond drug metabolism so that now microfluidics has been further used for other types of cell-cell interaction such as studies on the adhesion of platelets to endothelial tissue[15] and neovascularlization[16]. In these “organ-on-chip” studies, the experimental output was typically a microscopic inspection of the cells. For the drug metabolism studies, the resulting metabolites were measured by collecting products and analyzing resulting samples off-line.

Microfluidics also enables integration of cellular manipulation and cellular analysis. One approach has been to combine flow cytometry[17,18], cell sorting[19,20] and cell lysis followed by extraction of intracellular contents[21,22] and *in vitro* cellular measurements (see reference 23 for a review of recent developments). More relevant to the work in this dissertation, previous work by the Kennedy group demonstrated the potential of monitoring the dynamics of hormone secretion with high temporal resolution by microfluidics combined with an on-line electrophoretic immunoassay.[24]

Microfluidic Capillary Electrophoresis Immunoassay

In this work, extensive use is made of a microchip based immunoassay to monitor insulin secretion. Radioimmunoassays (RIA)[25] or enzyme-linked immunosorbent assays (ELISA)[26] are common methods for hormone detection such as insulin. Immunoassays can be classified as non-competitive or competitive. Non-competitive assays rely on the binding of excess amount of radioactively or fluorescently labeled antibody (Ab*) to the antigen (Ag) of interest; competitive assays encompass unlabeled antibody (Ab), the target antigen (Ag) and a labeled analog of the antigen (Ag*) where the two forms of antigen compete for binding sites on antibody. Determination of the distribution of bound and free species containing a labeled component (detectable) is applied for quantification, where separation of bound and free species is essential.

$$\textit{Non-competitive: } Ab^* + Ag \leftrightarrow Ab^* : Ag$$
$$\textit{Competitive: } Ab + Ag + Ag^* \leftrightarrow Ab:Ag + Ab:Ag^*$$

The Kennedy group previously developed a capillary system for monitoring of insulin secretion using an on-line capillary electrophoresis (CE) competitive immunoassay based on rapid separation of free Ag* and Ab:Ag* complex.[24,27] It was later implemented on a microfluidic device.[28,29] The microfluidic device demonstrated the potential of monitoring the dynamics of insulin secretion from single islets of Langerhans with up to 8 s temporal resolution by perfusing cells and analyzing the perfusate using rapid, on-line electrophoretic immunoassay.

Compared to the capillary system, the microchip device demonstrated several advantages. Cell loading was much easier, and the transparent glass base and open

top design allowed morphological monitoring to assess islet health and other monitoring such as cellular fluorescence measurements or implanted electrodes. It can be easily implemented to allow high throughput measurements and such devices have been developed.[30,31] The high-throughput device[31] was capable of generating more than 3,600 immunoassays in 40 min and can be applied to compare multiple cells (e.g. healthy and diseased cells) in real time and generate much useful information. Another direction of cellular studies is to extend the monitoring period to generate more complex information to study cellular functions. A significant source of instability of CE hampering such application is the buffer, which may become depleted and degraded over several hours. Periodically replenishing electrophoresis buffer is one approach to solve that, but can be labor-intensive and not automatable on the capillary system or any other conventional system. However, several perfusion channels can be easily fabricated on a microchip and continuously perfused with fresh buffer, thus allow long-term stability.[32] The original microfluidic chip with cell perfusion, high throughput chip and long-term chip are illustrated in **Figure 1.1**.

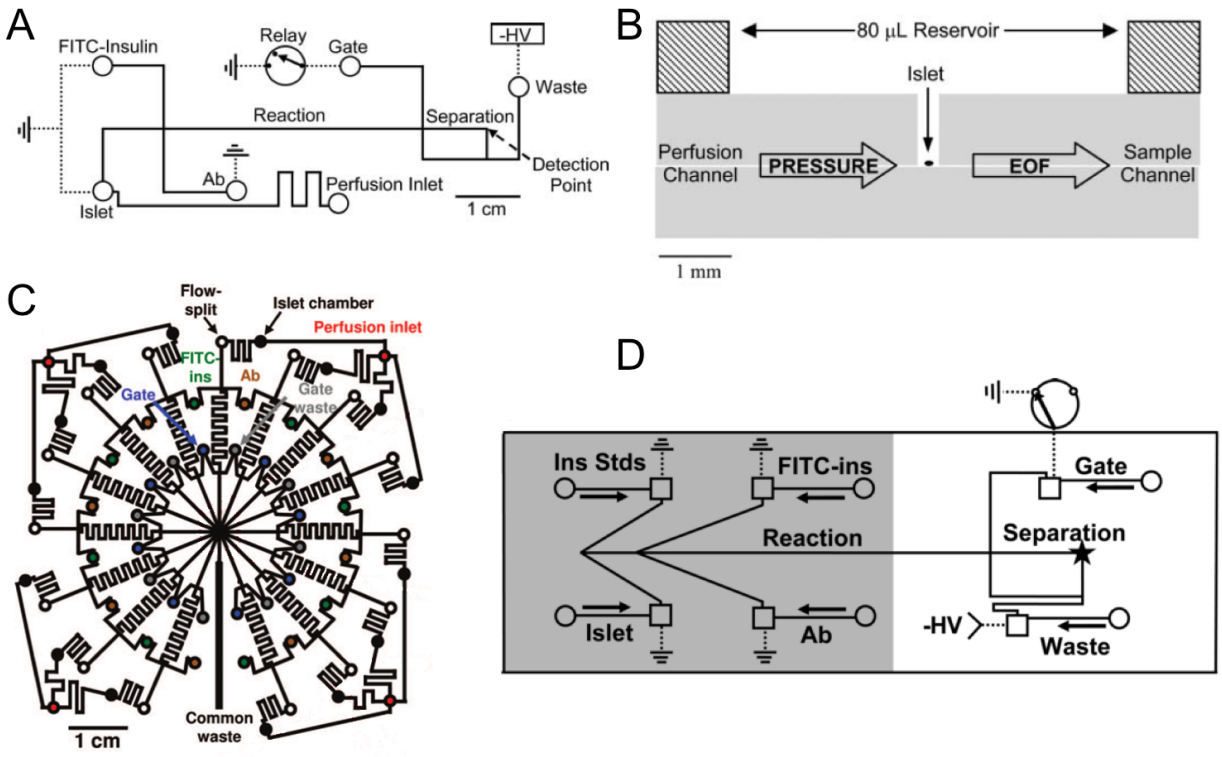

Figure 1.1. Microchip electrophoresis developed for insulin monitoring. (A) Fluidic layouts of the single islet perfusion chip. (B) The side view of the islet culture portion. (C) The 15-islet parallel CE chip and (D) long-term chip. In chip layouts, black lines represent channels; circles and squares indicate reservoirs. Reproduced from References 29,31 and 32.

In this dissertation, several developments based on the previous work to allow better glucose or other stimulus control, automated long-term monitoring and calibration, intracellular [Ca^{2+}] imaging, C-peptide monitoring, and cell-cell interaction studies are completed.

Diabetes Background

This work focuses on analyzing islet cell function. A justification for studying islets is the role of these cells in diabetes. The growing prevalence of diabetes has drawn a lot of research interest. From 1980 through 2014, the number of Americans with diagnosed diabetes has increased fourfold.[33] In 2012, approximately 29.1 million Americans, or 9.3% of the population, had diabetes and 86 million American age 20 and

older had prediabetes, a condition when fasting blood glucose level is not high enough for a diagnosis of diabetes, but enough to increase the risk of type 2 diabetes, heart disease, and stroke.[34] Diabetes was mentioned as a cause of death in more than 234,000 cases in 2010 (it is very likely underreported since many people with diabetes who died did not have diabetes listed as cause of death), making it the seventh leading cause of death. The total cost of diagnosed diabetes in the United States was $245 billion in 2012, including direct medical costs and reduced productivity.

The two main types of diabetes are type 1 and type 2 diabetes.[35] Type 1 diabetes, also called insulin-dependent diabetes, happens when β-cells are destroyed by autoimmunity leading to a deficiency of insulin. Type 2, or non-insulin dependent diabetes, usually starts from insulin resistance of adipose, muscle, and liver tissues, when they do not use insulin efficiently, which leads to more insulin secretion from pancreas to keep up with the added demand. Meanwhile, gradually declined β-cell function-as a hallmark of type 2 diabetes-begins as early as 12 years before diagnosis. Development of type 2 diabetes results from the failure of the β-cells to adequately compensate for insulin resistance.[36] Type 2 diabetes accounts for 90-95% of diabetes cases in the US, though the pathogenesis of type 2 diabetes is not well-understood. Factors like genetic predisposition and obesity are implicated in the development of T2D.

Islets and Glucose-Stimulated Insulin Secretion

In our work, we focus on tools to better study insulin secretion from the islets of Langerhans since defects in this process are a hallmark of type 2 diabetes.[37,38] Islets are 75-200 μm diameter spheroid cell clusters located in the pancreas that contains

2000-4000 cells each. An adult human pancreas has approximately 1 million islets, comprising 1-2 % of the volume of the pancreas. **Figure 1.2** depicts a typical mouse islet (left) and an image of several isolated mouse islets (right)[39].

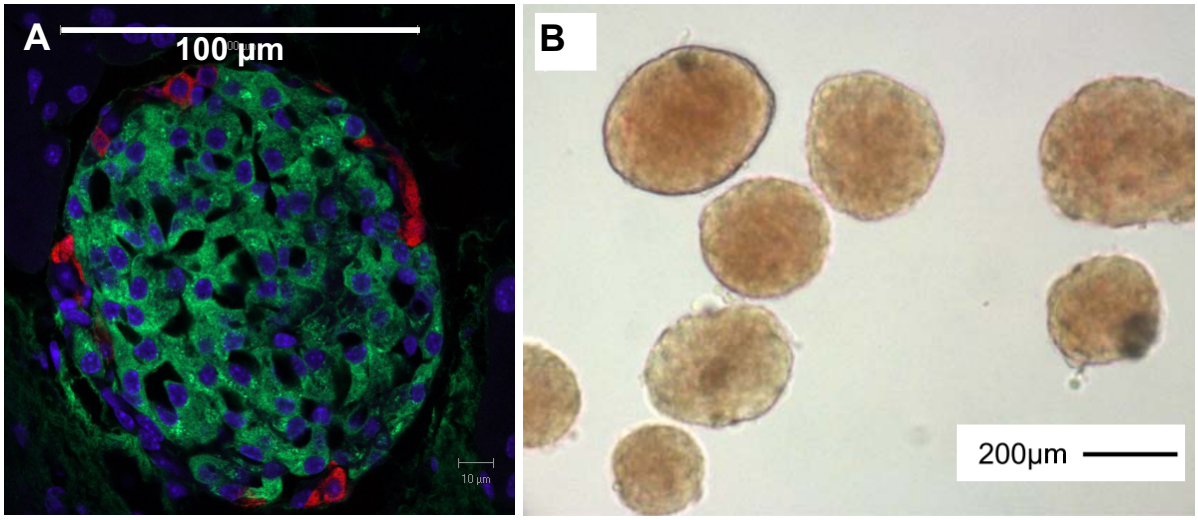

Figure 1.2. Images of islets of Langerhans. (A) A single islet with insulin (green), glucagon (red) and nuclei (blue) labeled (*Image credit: "Mouse islet LM Solimena Lab" by Chistin Süß, Jakob Suckale, Michele Solimena*). (B) A photomicrograph image of several isolated islets.

Islets are composed of five cell types: α-cells (~20 %) secrete glucagon; β-cells (~70-80 %) secrete insulin; delta-cells (<10 %) secrete somatostatin; PP-cells (<5%) secrete Pancreatic Polypeptide; a small amount of epsilon-cells (<1 %), which were found more recently, secrete ghrelin.[40]

Insulin is secreted from β-cells at elevated blood glucose concentration, and then carried by the bloodstream throughout the body. Released insulin is crucial for maintaining glucose homeostasis.[41] Insulin secretion is stimulated by glucose, with both triggering and amplifying effects. The triggering pathway is initiated when glucose is rapidly transported into the β-cells via GLUT2 and metabolized by oxidative glycolysis to produce ATP. The rise in ATP/ADP leads to the closure of ATP-sensitive K^+ (K_{ATP}) channels, membrane depolarization, opening of voltage-operated Ca^{2+} channels

allowing Ca^{2+} to enter the cell. The rise in cytoplasmic free Ca^{2+} concentration then leads to subsequent triggering of insulin secretion via exocytosis.[41]

The amplifying pathway is more complex. As suggested by previous studies, it is independent of K_{ATP} channels (it is also referred as K_{ATP} channel independent insulin secretion in some reports) yet relies on glucose metabolism.[42,43] Low concentrations of glucose (1-6 mM) can influence insulin secretion by the amplifying pathway, but it normally remains silent if $[Ca^{2+}]_i$ has not been raised first by the triggering pathway.[41] **Figure 1.3** illustrates a schematic representation of the triggering and amplifying pathways.[41]

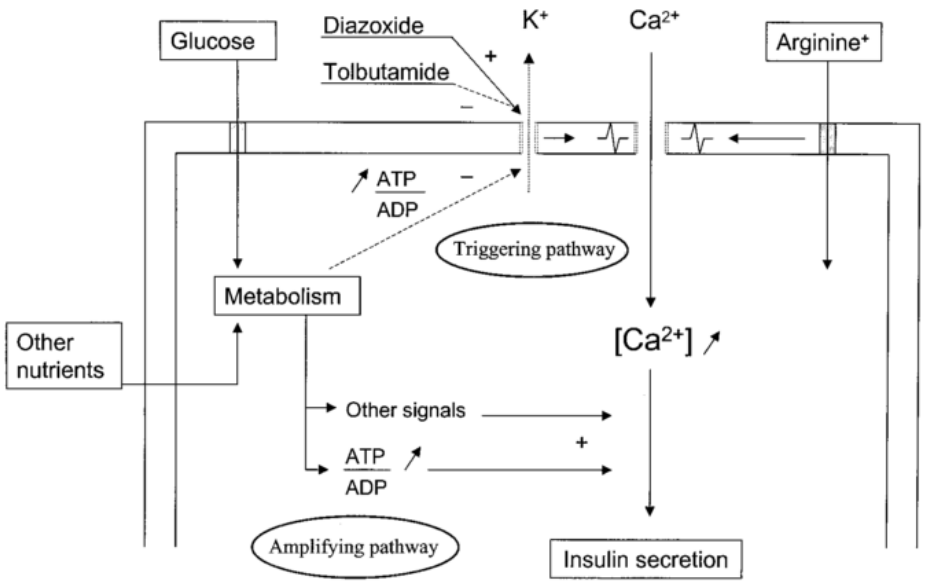

Figure 1.3. Simplified schematic of the triggering and amplifying pathways of GSIS (+, stimulation; -, inhibition). Triggering pathway happens when glucose enters the cell and subsequent metabolism results in an increase in ATP, which causes the K_{ATP} channels to open. The resulting membrane depolarization causes the voltage-sensitive Ca^{2+} to open and ultimately results in exocytosis of insulin. Several drugs affecting K_{ATP} and Ca^{2+} channels are illustrated. Amplifying pathway is independent of K_{ATP} channels and relies more on metabolism of glucose. Reproduced from reference 41.

Insulin Secretion Dynamics

Insulin secretion has complex dynamics including a biphasic and pulsatile pattern.[44] The 1st phase consists of a sharp burst in insulin secretion that typically occurs within 2-5 min of glucose stimulation (typically presented as a step from 3 mM to 11 mM). The 2nd phase is characterized by a gradual rise in insulin release that is sustained for several minutes and is often pulsatile. The lengths and profile of the 2nd phase varies from species to species. For example, in rodent models, rats and humans usually have stronger 2nd phase insulin secretion than mice.[45]

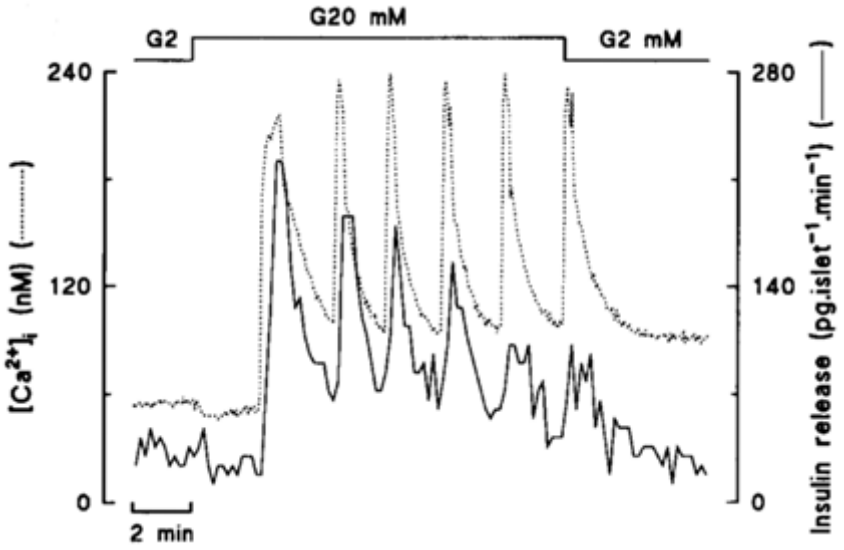

Figure 1.4. Biphasic and pulsatile insulin secretion. Glucose causes a 1st phase spike of insulin secretion followed by a 2nd phase of insulin secretion. The 2nd phase usually gradually rise and is often pulsatile. Reproduced from reference 46.

In vivo insulin secretion has a 5-15 min oscillation period.[47,48] Several studies suggest the oscillatory secretion patterns are important for optimal insulin action[49–51] and insulin secretion[52–54]. Loss of such oscillatory patterns is implicated in the development of type 2 diabetes[51,55–58], and may be one early sign of type 2 diabetes in relatives of type 2 diabetics or obese non-diabetics[59,60]. A comparison demonstrating the oscillations in healthy and diabetic individuals is illustrated in **Figure 1.5**. A period of

10 min insulin secretion and well contained glucose level were observed in healthy individuals and irregular insulin secretion and elevated glucose level were found in diabetics.

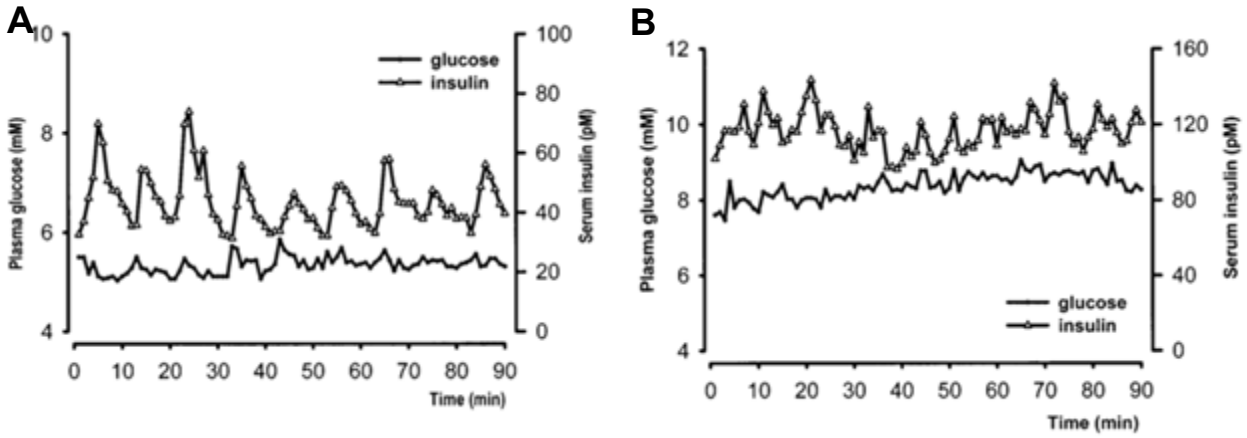

Figure 1.5. Plasma glucose and serum insulin level in normal (A) and diabetic subjects (B) when infused with 6 mg kg^{-1} glucose for 1 min every 10 min. The diabetic subjects exhibited irregular insulin secretion and elevated glucose level. Reprinted from reference 37.

Long-term Oscillatory Patterns of Insulin Secretion

In additional to the short-term trends, some studies also suggest longer period of insulin secretion with frequency of 50-120 min, termed as ultradian rhythm[61] or even longer than a few hours, termed as a circadian rhythm[62–64]. Alterations in the ultradian rhythms have been reported in patients with type 2 diabetes.[65–67]

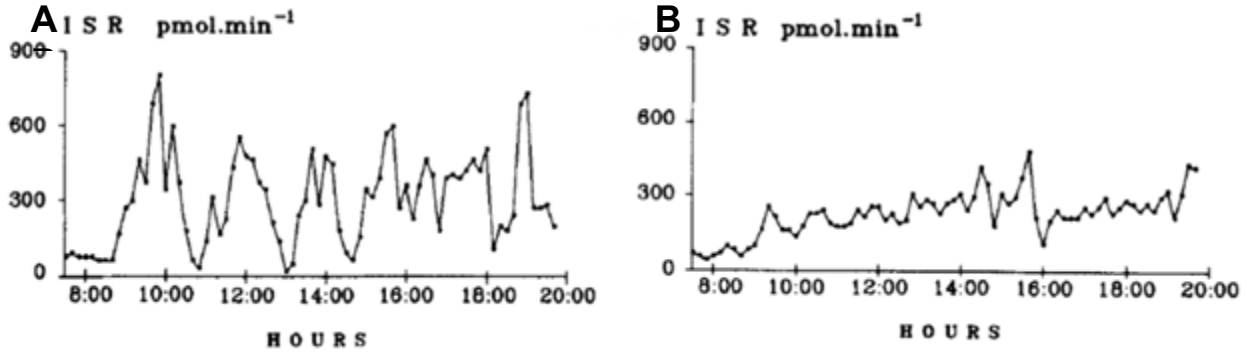

Figure 1.6. Insulin secretion rate (ISR) profiles from a control (A) and a type 2 diabetic patient (B) during continuous enteral nutrition. The ISR pulses in the diabetic subject were significantly less defined and lower in amplitude than the control subject. Reproduced from reference 38.

Gradual Glucose Control and Glucose Sensitivity Studies

In vitro studies of glucose stimulated insulin secretion traditionally use a step change from low to high glucose (e.g., 3 to 11 mM or 3 to 17 mM). However, *in vivo* blood glucose changes in mammals have patterns of gradual rises and falls. **Figure 1.7** illustrates such gradual glucose change in humans[68] and rodents[69]. Despite the success of using step changes in glucose to study insulin secretion, it fails to mimic *in vivo* physiological glucose dynamics. A system that allows islets to be exposed to controlled gradients of glucose would greatly expand the capabilities of *in vitro* studies.

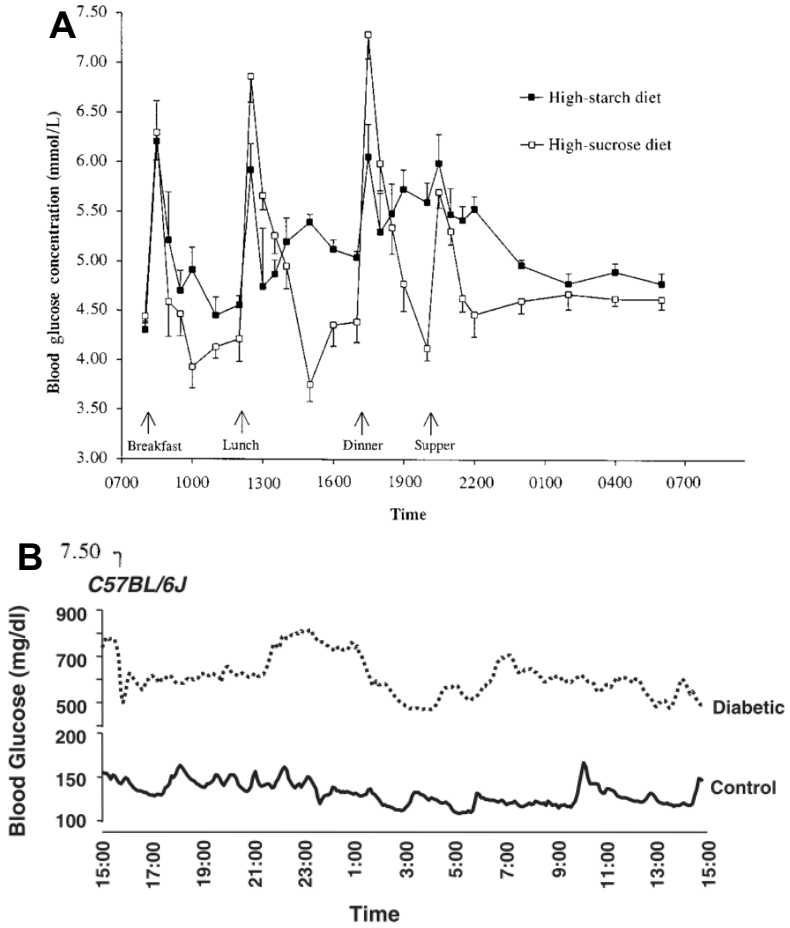

Figure 1.7. Blood glucose profile of human (A) and mouse (B). In human glucose level rises after meals and falls after a few hours, while it is more irregular in rodents because they do not have regular meals. Reproduced from reference 68 and 69.

One application where precise control of the glucose concentration gradient is used is to measure β-cell glucose sensitivity, defined by the threshold glucose level where β-cells start to secret insulin. β-cells normally secrete insulin when plasma glucose exceeds 7 mM; however, they will respond to increasing insulin demand, such as during hyperglycaemia, by increasing their mass, secretory function, and glucose sensitivity.[70,71] Ultimately β-cells' capacity to adapt to glucose response and expand mass may be disrupted and lead to the onset of type 2 diabetes.[59,72,73] A previous study[74] demonstrated that after undergoing 90% pancreatectomy, the remaining rat islets became more sensitive to glucose, apparently to compensate for the loss. It has been known that β-cell mass compensation is usually slow to respond effectively to decreased insulin sensitivity.[75,76] Increase of β-cell glucose sensitivity or metabolic/hormonal amplification of secretion are two candidates of hypothesized faster functional compensation. In this dissertation, a collaborative effort has been placed on investigating the hypothesis that chronic glucose causes rapid functional compensation and shifts islet glucose sensitivity.

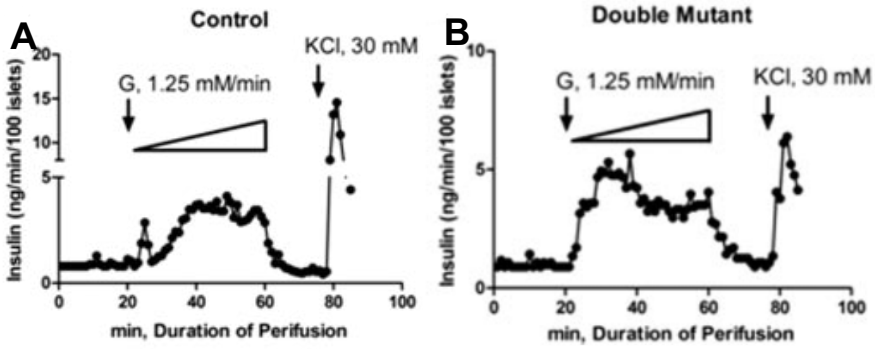

Figure 1.8. Using glucose ramp to measure glucose sensitivity. Control (A) and Foxa1/a2 mutant (B) islets were perfused by a glucose ramp (0-50 mM) flowing at a rate of 1.25 mM/min, followed by 20 min Krebs buffer wash and 30 mM KCl stimulation as positive control. Control islets produced a rapid and sharp 1st phase insulin secretion between 5-10 mM, while mutant islets were elicited by 3.75 mM glucose, failed to produce a distinct peak, and had more total insulin output. Reproduced from reference 77.

Glucose ramp has been proved useful to measure *in vitro* glucose sensitivity.[77] As illustrated in **Figure 1.8**, islets were exposed to a glucose ramp (0-50 mM, 1.25 mM/min) and insulin secretion was sampled every few minutes. Left or right shift of the threshold glucose level, the existence of distinct first phase insulin peak, and total insulin output are key parameters used to assess glucose sensitivity. Microfluidics offers the opportunity to perform such experiments with better secretory monitoring and more efficient use of islets.

Methods for Islet Function Characterization

Several cellular parameters have been used to characterize islet function, particularly focused on pancreas β-cells and α-cells. This dissertation is focused on several analytical methods developed to measure insulin, C-peptide and intracellular [Ca^{2+}].

1) Insulin detection

Insulin is the most commonly studied pancreatic hormone and widely used for β-cell functions characterization, as illustrated in several examples discussed above. Insulin secretion patterns have been investigated *in vivo*[78], in perfused pancreas[79], and with isolated islets[46]. *In vitro* experiments help elucidate insulin secretion mechanisms with simplified biological system compared to *in vivo*. Furthermore, to observe the fast oscillatory (2-5 min) dynamics, single isolated islets experiments are usually required to prevent destructive interference of out of phase oscillations from multiple islets in a large batch[80]; high temporal resolution sampling is also required. A comparison between a perfused pancreas and isolated islets is illustrated in **Figure 1.9**. Only the biphasic

nature of insulin secretion is observed with the perfused pancreas while the 2nd phase oscillatory dynamics are observed with single islet.

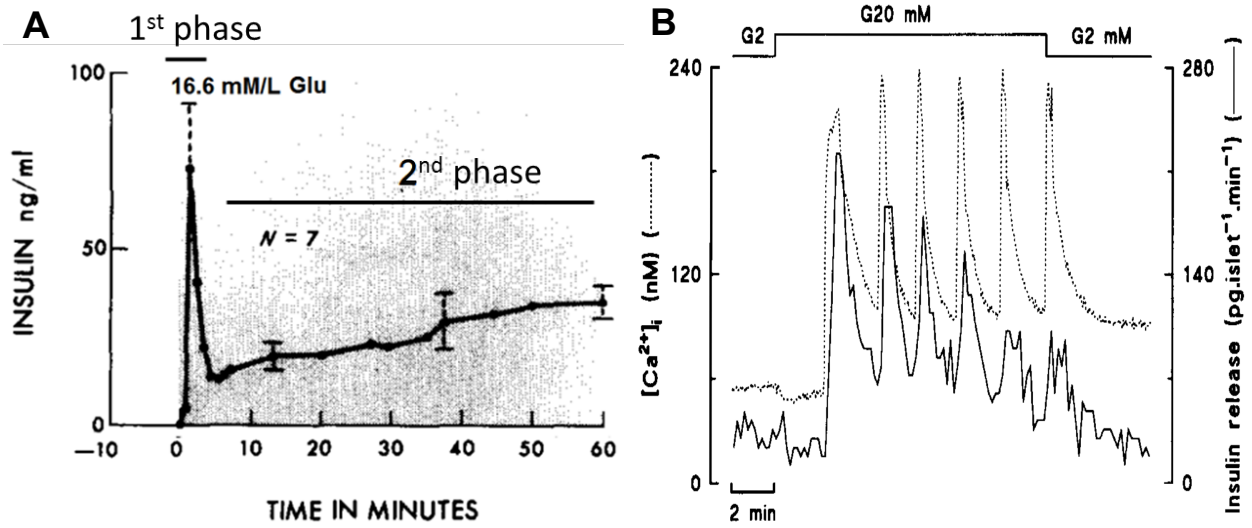

Figure 1.9. Insulin release from a perfused pancreas (A) and a perfused single islet (B). Much more oscillatory dynamics are observed from the single islet while only the biphasic nature of insulin release from the perfused pancreas is observed. Adapted from reference 81 and reproduced from reference 46.

Immunoassay has remained the primary and classical method for assaying hormone release with high sensitivity. Either *in vivo* or *in vitro* experiment involves blood drawing or fraction collection for offline immunoassay measurements, which are highly labor and time intensive. Another disadvantage of offline monitoring is temporal resolution, which is usually on the order of minutes. Increasing the frequency of fraction sampling is one way to compensate it, but would bring extreme increase of time and labor.

As illustrated in previous section, microfluidic capillary electrophoresis immunoassay is a good candidate for automatic and high temporally resolved insulin monitoring. In this dissertation, we demonstrate a microfluidic device which we improved upon previous designs by incorporating a new method to control glucose

concentration (or that of any drug) applied to the cells and by incorporating a method for automated calibration at defined times. For the control of glucose, the system incorporates two independent syringe pumps loaded with low and high concentration glucose. Flow rates of both are controlled by a home-made LabView program. By mixing 2 syringe pumps' contents at different flow rates through a tee fabricated on the electrophoresis chip, arbitrary glucose gradients can be generated.

Insulin secreted from the islets is measured at 5-10 s intervals by an electrophoretic competitive immunoassay. Single islets are perfused with different concentration of glucose. Processes of sampling of insulin secreted by the islet, insulin and FITC-insulin mixing and their competitively reacting with insulin antibody are achieved by electroosmotic flow (EOF). A high-voltage relay controls continuous injection of the sample plug to the separation channel, where free FITC-insulin and FITC-insulin bound to antibody are separated. The integrated system can perform 14,000 electrophoresis assays in 24 h and automatically control culture conditions, thus allowing continuous monitoring of insulin under well-controlled conditions.

2) C-peptide detection

C-peptide is a short 31-amino-acid peptide connecting insulin's A-chain and B-chain in proinsulin, which is subsequently removed from the A-chain and B-chain to produce mature insulin. A diagram of preproinsulin process is illustrated in **Figure 1.10**. 1:1 mole of C-peptide and insulin are then stored in secretory granules of the β-cells and both are released eventually. An alternative way to indirectly measure insulin secretion is to measure C-peptide levels.[82]

Moreover, visual assessment of pancreatic insulin content would be a useful approach to study the loss of β-cell insulin content, which can be a possible cause of pancreatic exhaustion.[83] However, imaging of insulin in the living animal or humans has not yet been achieved. A human proinsulin with C-peptide-bearing Superfolder Green Fluorescent Protein (CpepSfGFP) has been expressed in transgenic mice and the goal is to use it as a dynamic reporter of insulin storage and secretion *in situ*. Although *in vivo* fluorescence imaging of the pancreatic surface allowing assessment of pancreatic islet insulin content is important and the ultimate goal of this method, it is also necessary to validate that the kinetics of the release of insulin and CpepSfGFP are identical. *In vitro* measurement using isolated single islets is a good approach to compare CpepSfGFP and insulin release. In this dissertation, we developed a microfluidic device to monitor CpepSfGFP secretion from isolated single islets and compared the resulting secretion pattern with insulin.

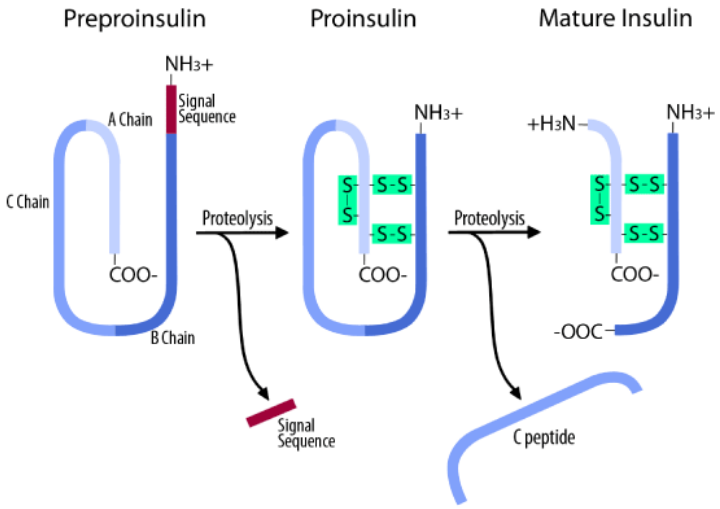

Figure 1.10. Preproinsulin Process. The signal peptide sequence is removed from the N-terminus of preproinsulin by proteases, forming proinsulin with 3 disulphide bonds. Further proteolytic cleavage removes the C-peptide producing insulin. Reproduced from reference 84.

3) Intracellular [Ca2+] Imaging

Ca^{2+} influx has been known as the trigger of exocytosis of hormones including insulin and glucagon. Fluorescence imaging is a promising and widely used technique for studying living cells. Intracellular [Ca^{2+}] measurements were revolutionized after the advent of cell-permeant Fura-2, a Ca^{2+} sensitive fluorescent dye.[85] Its excitation wavelength shifts from 380 nm to 340 nm upon Ca^{2+} binding, and the ratio of the integrated intensities of the fluorescence emission at 510 nm from 340 and 380 nm excitation allows for quantitation of intracellular Ca^{2+} following calibration.

Conventional Ca^{2+} measurements are usually performed with cell affixed on a coverslip, sealed into a chamber with approximately 3 mL volume. The chamber is perfused with a peristaltic pump. Although it has been applied in many applications, the drawbacks include large volume of media consumed and difficulty in precisely controlling the cell culture environment. The instrumentation itself includes several parts which are relatively hard and expensive to maintain. The microfluidic chip for Ca^{2+} imaging may allow rapid and precise introduction of fresh media to the cells. Several microfluidic devices have been implemented for intracellular Ca^{2+} imaging recently.[86–88] Our research group also have developed microfluidic devices for Ca^{2+} imaging in pancreas islets.[89]

In this dissertation, a PDMS/glass hybrid microfluidic device for Ca^{2+} imaging studies was developed. This device can accommodate a 5 mm × 5 mm square coverslip-where the cells are attached to, and continuously perfused during measurements. Excess buffer is removed from the top of the cell chamber and the temperature is well controlled.

The device was applied to study the role of X-box binding protein 1 (XBP1) in insulin regulation of pancreas α-cell function. Endoplasmic reticulum (ER) stress has been suggested to contribute to reduced β-cell mass[90,91], but its role in α-cell biology is less known. XBP1 is a transcription factor that plays a critical role in mediating the unfolded protein response (UPR), which is an important process towards ER stress. Recent study suggested that β-cell specific XBP1-deficient mice exhibit β-cell dysfunction.[92]

Hyperglucagonemia caused by α-cell dysfunction is a feature of type 2 diabetes, but the mechanism contributing to this hypersecretion is not fully understood. In addition to glucose[93], it has been suggested insulin signaling in α-cells is critical to the regulation of glucagon secretion[94,95]. To investigate the role of XBP1 in α-cells, *in vivo* and *in vitro* models were created by a collaborating lab. In our work, stable XBP1 knockdown and overexpression α-cell lines' intracellular Ca^{2+} were measured and compared with the control groups. The data we collected help explain the mechanism of XBP1 deficiency in altered insulin signaling and glucagon secretory dysfunction.

Obesity and Adipocytes Background

Obesity

In this work, we used microfluidics to investigate how adipocytes alters islet function. This work was motivated by the connections between obesity and type 2 diabetes. Obesity is a growing epidemic in the United States. As of 2014, more than one-third (34.9% or 78.6 million) of US adults were obese. Not a single US state had a prevalence of obesity less than 20%.[96] Obesity is a medical condition when excess body fat has accumulated to the extent that may have a negative effect on health, and is

usually accessed by measuring body mass index (BMI, mass height^{-2}). BMI values between 19-25 kg m^{-2} are normal, 25-30 are overweight, and >30 are considered obese. Obesity is related to conditions include heart disease, stroke, type 2 diabetes and certain types of cancer. The estimated annual cost of obesity in the US was $147 billion in 2008.

Obesity is characterized by an increased mass of adipose tissue both in the number and size of adipocytes, occurs when the intake of food exceeds the energy need of the body for a sustained period of time.[97] Blood fatty acid levels tend to be elevated in obese individuals. Short-term treatment of β-cell with fatty acids stimulates insulin secretion, while chronic fatty acid impairs insulin secretion.[98,99] Adipocytes also secrete other hormones which have been proven affecting β-cell function and survival.[99–101] Understanding the endocrine and metabolic interactions between adipocytes and islets would be essential to help us better understand the link between obesity and impaired insulin secretion in type 2 diabetes.

Adipocytes

Adipocytes are the cells that primarily compose adipose tissue, specialized in storing energy as fat. They play a key role in energy metabolism within an organism and are at the center of obesity and type 2 diabetes research, making it important to understand the physiology of adipocytes.

Typically, white adipose tissue is found subcutaneously in the abdominal region and skeletal muscle. The vast majority of stored energy in the body is in the form of triglycerides (TG)-comprised of one moiety of glycerol and three of fatty acids, which

account for ~95% of adipose tissue volume.[102,103] Triglycerides are converted into individual moieties of one glycerol and three fatty acids through lipolysis.[103]

Non-esterified fatty acids (NEFAs) are oxidized to provide a fuel source in hypoglycemic states, such as in fasting or starvation. NEFAs can also activate insulin secretion.[102,104] But it has been demonstrated that plasma NEFA concentrations are elevated in obese individuals[103,105] and have harmful effects on peripheral tissues[106–108]. Elevated NEFAs concentration have been implicated contributing to the development of impairment of insulin response in peripheral tissues such as muscle and liver which may lead to insulin resistance, and they also have been implicated in the development of β-cell dysfunction.

NEFAs have been shown to have bimodal effects on insulin secretion so that short term they enhance secretion[109] but with chronic exposure suppresses insulin secretion[108], suggesting a possible mechanism for dysfunctional insulin secretion in diabetes. It was reported that insulin secretion enhanced 65 fold after acute exposure to 0.5 mM stearate.[109] As of the chronic treatment, it is worth mentioning that previous work suggested that fatty-acid induced impairment of GSIS does not occur unless the islets are cultured with >8 mM glucose. This phenomenon is termed as glucolipotoxicity.[100,110]

Besides NEFAs, adipocytes also produce adipokines (a group of hormones and cytokines) which have been shown to affect pancreatic β-cell function and survival.[100,101] These molecules have been found affecting glucose stimulated insulin secretion, insulin sensitivity and β-cell apoptosis and proliferation. For example, leptin inhibits insulin secretion[111] and protects β-cells from apoptosis[112]. Adiponectin increases insulin

secretion[113], insulin sensitivity[114] and β-cell proliferation[115], and low levels of adiponectin were found in obesity and type 2 diabetes. Other molecules and proteins, including tumour necrosis factor α (TNFα), resistin, dipeptidyl peptidase IV (DPP-IV) and apelin, also have been found affecting β-cell and their functions are reviewed in reference 101 and 116. A summary of the main adipokines with demonstrated effects is given in **Table 1**.

Table 1. Summary of adipokines with demonstrated effects on pancreatic β-cells. Reproduced from reference 101.

Adipokine	Effect	References
Adiponectin	Increases GSIS	Gu *et al.* (2006)
	Increases proliferation	Brown *et al.* (2010*a*)
Apelin	Inhibits insulin secretion	Guo *et al.* (2009)
DPP-IV	Inhibits GLP1	Lamers *et al.* (2011)
FGF	Increases β-cell proliferation	Kilkenny & Rocheleau (2008)
	Increases insulin transcription	Wente *et al.* (2006)
IGF1	Increases β-cell mass	Dickson *et al.* (2001)
Interleukin-1β	Increases nitric oxide	Corbett *et al.* (1992)
	Cytotoxic	Mandrup-Poulsen *et al.* (1986)
Interleukin-6	Increases GSIS	Shimizu *et al.* (2000) and Suzuki *et al.* (2011)
Leptin	Inhibits GSIS	Brown *et al.* (2002)
	Decreases pre-proinsulin levels	Pallett *et al.* (1997)
	Protects from apoptosis	Brown & Dunmore (2007)
MCP1	Increased amylin expression	Cai *et al.* (2011*a*)
Non-esterified fatty acids	Increases GSIS (acute)	Thams & Capito (2001)
	Inhibits GSIS (chronic)	Newsholme *et al.* (2007)
	Decreases insulin transcription	Jacqueminet *et al.* (2000)
	Induces apoptosis	Kharroubi *et al.* (2004)
Resistin	Decreases insulin receptor and increases cell viability	Brown *et al.* (2007)
TGFβ	Regulates insulin transcription	Lin *et al.* (2009*b*)
TNFα	Inhibits GSIS	Zhang & Kim (1995)
	Decreases insulin transcription	Tsiotra *et al.* (2001)
	Induces apoptosis	Ortis *et al.* (2008)
	Increases amylin but not pro-insulin gene expression	Cai *et al.* (2011*b*)
Visfatin	Increases insulin secretion	Brown *et al.* (2010*b*)

Even though many adipokines have substantial effects β-cells as illustrated above, most of the reported studies have been done using individual adipokines applied in isolation. To implement models that mimic the *in vivo* case, where the β-cells are exposed to a full range of adipokines would provide a more integrated perspective to study their effects. One study[115] investigated the interactions between adiponectin and leptin and suggested that the ratio of adiponectin to leptin may possibly be a significant

factor to assess the overall effects. Actually, it is known that many adipokines act used by the pathways that intersect-including many signaling pathways and insulin receptor itself. Meanwhile, the reported changes in circulating adipokine concentrations observed in metabolic diseases (see reference 117 for a review) are complex and many questions are still unanswered. Further studies that focus on the effects of combinations of adipokines are needed.

One approach to study the complex effects is to co-culture adipocytes and β-cells to provide an integrated profile of adipokines to stimulate the islets. This field is understudied, although existing work suggests that adipocytes induce dysfunction in β-cell[118] and molecules like α-lipoic acid protect β-cells[119]. In this dissertation, we demonstrate with a microfluidic system that adipocytes impact insulin secretion that cannot be explained by the NEFA results alone. The results show that better mimicking the *in vivo* microenvironment, where the β-cell is exposed to full range of adipokines, provides a new perspective to study adipokines' effects on the β-cell different from the previous studies with individual adipokines.

The murine 3T3-L1 cell line is a model system for adipocytes. The work presented in this dissertation used cultured 3T3-L1 adipocytes. Preadipocytes can be differentiated into adipocyte-like cells that accumulate lipids[120], and it has been extensively studied and well-characterized.[121–123] Although some differences exist between cultured cells and primary adipocytes from animals (e.g. secreted leptin levels[124]), use of cell line allows long term culture while isolated adipocytes are only viable for a short time (< 24 h) after isolation. Ear mesenchymal stem cells (EMSCs) can be differentiated into a variety of cell types including adipocytes.[125–128] Although

they are still being characterized, they have the potential to be used to derive adipocytes in the future.

Dissertation Overview

Overall, the objective of this research was to design and develop novel analytical techniques to study insulin secretion from islets of Langerhans. The design, development, and characterization of a microfluidic device combining automatic glucose (or other stimulus) gradient control and calibration for monitoring insulin secretion from single islets for 24 h is presented in Chapter 2. It was used to study insulin secretion dynamics from islets for 24 h with a temporal resolution of 8 s. This work was published in *Methods in Molecular Biology*. The automatic glucose gradient control allowed studies of glucose sensitivity, and the data and results were published in *Endocrinology* in collaboration with Dr. Leslie Satin of the Brehm Diabetes Center at the University of Michigan Medical School.

The microfluidic device was further developed to a microchip electrophoresis device capable of co-culture two cell types and chemical monitoring. The data and results were illustrated in Chapter 3. We were able to study the effects of adipocytes on islets' insulin secretion and found augmented insulin secretion after short-term treatment. Data and results from Chapter 3 are in preparation for submission.

Chapter 4 presents a microchip electrophoresis device to monitor low concentration fluorescent labeled peptides. It was applied to measure the secretion kinetics of C-peptide-bearing Superfolder Green Fluorescent Protein (CpepSfGFP) from single islets, and compared with insulin secretion, to validate the capability of using CpepSfGFP imaging to measure insulin function *in vivo*. Results in Chapter 4 were

published in *Diabetes* in collaboration with Dr. Peter Arvan of the Brehm Diabetes Center at the University of Michigan Medical School.

A PDMS/glass hybrid microchip was developed for intracellular [Ca^{2+}] imaging with cell lines, allowing convenient fabrication, cell manipulation and chip operation. It was applied to study the role of X-Box Binding Protein 1 in insulin regulated pancreatic α-cell function. The intracellular Ca^{2+} concentration data were published in *Diabetes* in collaboration with Dr. Rohit Kulkarni of the Joslin Diabetes Center at Harvard Medical School.

References

(1) Terry, S. C.; Herman, J. H.; Angell, J. B. *IEEE Trans. Electron Devices* **1979**, *26*, 1880–1886.

(2) Harrison, D. J.; Manz, A.; Fan, Z.; Luedi, H.; Widmer, H. M. *Anal. Chem.* **1992**, *64*, 1926–1932.

(3) Manz, A.; Miyahara, Y.; Miura, J.; Watanabe, Y.; Miyagi, H.; Sato, K. *Sensors Actuators B. Chem.* **1990**, *1*, 249–255.

(4) Vilkner, T.; Janasek, D.; Manz, A. *Anal. Chem.* **2004**, *76*, 3373–3386.

(5) Patabadige, D. E. W.; Jia, S.; Sibbitts, J.; Sadeghi, J.; Sellens, K.; Culbertson, C. T. *Anal. Chem.* **2016**, *88*, 320–338.

(6) Young, E. W. K.; Beebe, D. J. *Chem. Soc. Rev.* **2010**, *39*, 1036–1048.

(7) Halldorsson, S.; Lucumi, E.; Gómez-Sjöberg, R.; Fleming, R. M. T. *Biosens. Bioelectron.* **2015**, *63*, 218–231.

(8) Huh, D.; Hamilton, G. A.; Ingber, D. E. *Trends Cell Biol.* **2011**, *21*, 745–754.

(9) Esch, M. B.; King, T. L.; Shuler, M. L. *Annu. Rev. Biomed. Eng* **2011**, *13*, 55–72.

(10) Viravaidya, K.; Sin, A.; Shuler, M. L. *Biotechnol. Prog.* **2004**, *20*, 316–323.

(11) Sung, J. H.; Shuler, M. L. *Lab Chip* **2009**, *9*, 1385–1394.

(12) Zhang, C.; Zhao, Z.; Abdul Rahim, N. A.; van Noort, D.; Yu, H. *Lab Chip* **2009**, *9*, 3185–3192.

(13) Maschmeyer, I.; Lorenz, A. K.; Schimek, K.; Hasenberg, T.; Ramme, A. P.; Hübner, J.; Lindner, M.; Drewell, C.; Bauer, S.; Thomas, A.; Sambo, N. S.; Sonntag, F.; Lauster, R.; Marx, U. *Lab Chip* **2015**, *15*, 2688–2699.

(14) van Midwoud, P. M.; Merema, M. T.; Verpoorte, E.; Groothuis, G. M. M. *Lab Chip* **2010**, *10*, 2778–2786.

(15) Ku, C. J.; Oblak, T. D. A.; Spence, D. M. *Anal. Chem.* **2008**, *80*, 7543–7548.

(16) Hsu, Y.-H.; Moya, M. L.; Hughes, C. C. W.; Georgea, S. C.; Lee, A. P. *Lab Chip* **2013**, *13*, 2990–2998.

(17) Schrum, D. P.; Culbertson, C. T.; Jacobson, S. C.; Ramsey, J. M. *Anal. Chem.* **1999**, *71*, 4173–4177.

(18) Zhao, M.; Schiro, P. G.; Kuo, J. S.; Koehler, K. M.; Sabath, D. E.; Popov, V.; Feng, Q.; Chiu, D. T. *Anal. Chem.* **2013**, *85*, 2465–2471.

(19) Fiedler, S.; Shirley, S. G.; Schnelle, T.; Fuhr, G. *Anal. Chem.* **1998**, *70*, 1909–1915.

(20) Fu, A. Y.; Spence, C.; Scherer, A.; Arnold, F. H.; Quake, S. R. *Nat. Biotechnol.* **1999**, *17*, 1109–1111.

(21) McClain, M. A.; Culbertson, C. T.; Jacobson, S. C.; Allbritton, N. L.; Sims, C. E.; Ramsey, J. M. *Anal. Chem.* **2003**, *75*, 5646–5655.

(22) Zare, R. N.; Kim, S. *Annu. Rev. Biomed. Eng.* **2010**, *12*, 187–201.

(23) Roper, M. G. *Anal. Chem.* **2016**, *88*, 381–394.

(24) Schultz, N. M.; Huang, L.; Kennedy, R. T. *Anal. Chem.* **1995**, *67*, 924–929.

(25) Yalow, R. S.; Berson, S. a. *Nature* **1959**, *184*, 1648–1649.

(26) Engvall, E.; Perlmann, P. *Immunochemistry* **1971**, *8*, 871–874.

(27) Tao, L.; Aspinwall, C. A.; Kennedy, R. T. *Electrophoresis* **1998**, *19*, 403–408.

(28) Roper, M. G.; Shackman, J. G.; Dahlgren, G. M.; Kennedy, R. T. *Anal. Chem.* **2003**, *75*, 4711–4717.

(29) Shackman, J. G.; Dahlgren, G. M.; Peters, J. L.; Kennedy, R. T. *Lab Chip* **2005**, *5*, 56–63.

(30) Dishinger, J. F.; Kennedy, R. T. *Anal. Chem* **2007**, *79*, 947–954.

(31) Dishinger, J. F.; Reid, K. R.; Kennedy, R. T. *Anal. Chem.* **2009**, *81*, 3119–3127.

(32) Reid, K. R.; Kennedy, R. T. *Anal. Chem.* **2009**, *81*, 6837–6842.

(33) CDC. Number of Persons Diagnosed Diabetes - Data & Trends http://www.cdc.gov/diabetes/statistics/prev/national/figpersons.htm (accessed Jan 20, 2017).

(34) American Diabetes Association. Diagnosing Diabetes and Learning About Prediabetes http://www.diabetes.org/diabetes-basics/diagnosis/ (accessed Jan 20, 2017).

(35) NIDDK. Types of Diabetes https://www.niddk.nih.gov/health-information/diabetes/types (accessed Oct 15, 2016).

(36) Fonseca, V. A. *Diabetes Care* **2009**, *32 Suppl 2*, S151–S156.

(37) Hollingdal, M.; Juhl, C. B.; Pincus, S. M.; Sturis, J.; Veldhuis, J. D.; Polonsky, K. S.; Pørksen, N.; Schmitz, O. *Diabetes* **2000**, *49*, 1334–1340.

(38) Sturis, J.; Polonsky, K. S.; Shapiro, E. T.; Blackman, J. D.; O'Meara, N. M.; Van Cauter, E. *Diabetologia* **1992**, *35*, 681–689.

(39) Carter, J. D.; Dula, S. B.; Corbin, K. L.; Wu, R.; Nunemaker, C. S. *Biol. Proced. Online* **2009**, *11*, 3–31.

(40) Kulkarni, R. N. *Int. J. Biochem. Cell Biol.* **2004**, *36*, 365–371.

(41) Henquin, J. C. *Diabetes* **2000**, *49*, 1751–1760.

(42) Gembal, M.; Gilon, P.; Henquin, J. C. *J. Clin. Invest.* **1992**, *89*, 1288–1295.

(43) Sato, Y.; Aizawa, T.; Komatsu, M.; Okada, N.; Yamada, T. *Diabetes* **1992**, *41*, 438–443.

(44) Nunemaker, C. S.; Wasserman, D. H.; McGuinness, O. P.; Sweet, I. R.; Teague, J. C.; Satin, L. S. *Am. J. Physiol. Endocrinol. Metab.* **2006**, *290*, E523–E529.

(45) Ma, Y. H.; Wang, J.; Rodd, G. G.; Bolaffi, J. L.; Grodsky, G. M. *Eur. J. Endocrinol.*

1995, *132*, 370–376.

(46) Gilon, P.; Shepherd, R. M.; Henquin, J. C. *J. Biol. Chem.* **1993**, *268*, 22265–22268.

(47) Lang, D. A.; Matthews, D. R.; Peto, J.; Turner, R. C. *N. Engl. J. Med.* **1979**, *301*, 1023–1027.

(48) Hansen, B. C.; Jen, K. C.; Belbez Pek, S.; Wolfe, R. A. *J. Clin. Endocrinol. Metab.* **1982**, *54*, 785–792.

(49) Schmitz, O.; Arnfred, J.; Nielsen, O. H.; Beck-Nielsen, H.; Orskov, H. *Acta Endocrinol. (Copenh).* **1986**, *113*, 559–563.

(50) Schmitz, O.; Juhl, C. B.; Hollingdal, M.; Veldhuis, J. D.; Porksen, N.; Pincus, S. M. *Metabolism.* **2001**, *50*, 41–46.

(51) Lang, D. A.; Matthews, D. R.; Burnett, M.; Turner, R. C. *Diabetes* **1981**, *30*, 435–439.

(52) Pedersen, M. G.; Sherman, A. *Proc. Natl. Acad. Sci. U. S. A.* **2009**, *106*, 7432–7436.

(53) Pørksen, N.; Munn, S.; Steers, J.; Vore, S.; Veldhuis, J.; Butler, P. *Am. J. Physiol.* **1995**, *269*, E478-88.

(54) Pørksen, N.; Munn, S.; Steers, J.; Veldhuis, J. D.; Butler, P. C. *Diabetes* **1996**, *45*, 1317–1323.

(55) Hunter, S. J.; Atkinson, A. B.; Ennis, C. N.; Sheridan, B.; Bell, P. M. *Diabetes* **1996**, *45*, 683–686.

(56) Meier, J. J.; Pennartz, C.; Schenker, N.; Menge, B. A.; Schmidt, W. E.; Heise, T.; Kapitza, C.; Veldhuis, J. D. *Diabetes, Obes. Metab.* **2013**, *15*, 258–263.

(57) Lin, J. M.; Fabregat, M. E.; Gomis, R.; Bergsten, P. *Diabetes* **2002**, *51*, 988–993.

(58) Satin, L. S.; Butler, P. C.; Ha, J.; Sherman, A. S. *Mol. Aspects Med.* **2015**, *42*, 61–77.

(59) O'Rahilly, S.; Turner, R. C.; Matthews, D. R. *N. Engl. J. Med.* **1988**, *318*, 1225–1230.

(60) Schmitz, O.; Porksen, N.; Nyholm, B.; Skjaerbaek, C.; Butler, P. C.; Veldhuis, J. D.; Pincus, S. M. *Am. J. Physiol.* **1997**, *272*, E218-26.

(61) Simon, C.; Brandenberger, G. *Diabetes* **2002**, *51*, S258-61.

(62) Peschke, E.; Peschke, D. *Diabetologia* **1998**, *41*, 1085–1092.

(63) Picinato, M. C.; Haber, E. P.; Carpinelli, A. R.; Cipolla-Neto, J. *J. Pineal Res.* **2002**, *33*, 172–177.

(64) Merl, V.; Peters, A.; Oltmanns, K. M.; Kern, W.; Hubold, C.; Hallschmid, M.; Born, J.; Fehm, H. L.; Schultes, B. *Metabolism.* **2004**, *53*, 1449–1453.

(65) Polonsky, K. S.; Given, B. D.; Hirsch, L. J.; Tillil, H.; Shapiro, E. T.; Beebe, C.; Frank, B. H.; Galloway, J. A.; Van Cauter, E. *N. Engl. J. Med.* **1988**, *318*, 1231–

1239.

(66) O'Meara, N. M.; Sturis, J.; Van Cauter, E.; Polonsky, K. S. *J. Clin. Invest.* **1993**, *92*, 262–271.

(67) O'Meara, N. M.; Sturis, J.; Herold, K. C.; Ostrega, D. M.; Polonsky, K. S. *Diabetes Care* **1995**, *18*, 568–571.

(68) Daly, M. E.; Vale, C.; Walker, M.; Littlefield, A.; George, K.; Alberti, M. M.; Mathers, J. C. *Am. J. Clin. Nutr.* **1998**, *67*, 1186–1196.

(69) Han, B. G.; Hao, C.-M.; Tchekneva, E. E.; Wang, Y.-Y.; Lee, C. A.; Ebrahim, B.; Harris, R. C.; Kern, T. S.; Wasserman, D. H.; Breyer, M. D.; Qi, Z. *Am. J. Physiol. Endocrinol. Metab.* **2008**, *295*, E981–E986.

(70) Alejandro, E. U.; Gregg, B.; Blandino-Rosano, M.; Cras-Méneur, C.; Bernal-Mizrachi, E. *Mol. Aspects Med.* **2015**, *42*, 19–41.

(71) Chan, C. B.; MacPhail, R. M.; Sheu, L.; Wheeler, M. B.; Gaisano, H. Y. *Diabetes* **1999**, *48*, 997–1005.

(72) Rhodes, C. J. *Science.* **2005**, *307*, 380–384.

(73) Polonsky, K. S. *Exp. Clin. Endocrinol. Diabetes* **1999**, *107 Suppl*, S124–S127.

(74) Leahy, J. L.; Bumbalo, L. M.; Chen, C. *Diabetologia* **1993**, *36*, 1238–1244.

(75) Ha, J.; Satin, L. S.; Sherman, A. S. *Endocrinology* **2016**, *157*, 624–635.

(76) Topp, B. G.; Atkinson, L. L.; Finegood, D. T. *Am. J. Physiol. Endocrinol. Metab.* **2007**, *293*, E1730-5.

(77) Gao, N.; Le Lay, J.; Qin, W.; Doliba, N.; Schug, J.; Fox, A. J.; Smirnova, O.; Matschinsky, F. M.; Kaestner, K. H. *Mol. Endocrinol. (Baltimore, Md)* **2010**, *24*, 1594–1604.

(78) Pørksen, N.; Nyholm, B.; Veldhuis, J. D.; Butler, P. C.; Schmitz, O. *Am. J. Physiol.* **1997**, *273*, E908–E914.

(79) Lenzen, S.; Joost, H. G.; Hasselblatt, A. *Diabetologia* **1976**, *12*, 495–500.

(80) Bergsten, P. *Am.J Physiol* **1998**, *274*, E796–E800.

(81) Grodsky, G. M.; Fanska, R. E. *Methods Enzymol.* **1975**, *39*, 364–372.

(82) Eaton, R. P.; Allen, R. C.; Schade, D. S.; Erickson, K. M.; Standefer, J. *J. Clin. Endocrinol. Metab.* **1980**, *51*, 520–528.

(83) Alarcon, C.; Boland, B. B.; Uchizono, Y.; Moore, P. C.; Peterson, B.; Rajan, S.; Rhodes, O. S.; Noske, A. B.; Haataja, L.; Arvan, P.; Marsh, B. J.; Austin, J.; Rhodes, C. J. *Diabetes* **2016**, *65*, 438–450.

(84) Thompson, A.; Kanamarlapudi, V. *Clin. Exp. Pharmacol.* **2013**, *3*, 138.

(85) Tsien, R. Y.; Rink, T. J.; Poenie, M. *Cell Calcium* **1985**, *6*, 145–157.

(86) Mohammed, J. S.; Wang, Y.; Harvat, T. A.; Oberholzer, J.; Eddington, D. T. *Lab Chip* **2009**, *9*, 97–106.

(87) Tran, L.; Farinas, J.; Ruslim-Litrus, L.; Conley, P. B.; Muir, C.; Munnelly, K.; Sedlock, D. M.; Cherbavaz, D. B. *Anal. Biochem.* **2005**, *341*, 361–368.

(88) Chao, P.-H. G.; West, A. C.; Hung, C. T. *Am. J. Physiol. Cell Physiol.* **2006**, *291*, C718–C725.

(89) Morioka, T.; Dishinger, J. F.; Reid, K. R.; Liew, C. W.; Zhang, T.; Inaba, M.; Kennedy, R. T.; Kulkarni, R. N. *Mol. Endocrinol.* **2012**, *26*, 967–976.

(90) Marchetti, P.; Bugliani, M.; Lupi, R.; Marselli, L.; Masini, M.; Boggi, U.; Filipponi, F.; Weir, G. C.; Eizirik, D. L.; Cnop, M. *Diabetologia* **2007**, *50*, 2486–2494.

(91) Eizirik, D. L.; Cardozo, A. K.; Cnop, M. *Endocrine Reviews*. 2008, pp 42–61.

(92) Lee, A.-H.; Heidtman, K.; Hotamisligil, G. S.; Glimcher, L. H. *Proc. Natl. Acad. Sci. U. S. A.* **2011**, *108*, 8885–8890.

(93) Ravier, M. A.; Rutter, G. A. *Diabetes* **2005**, *54*, 1789–1797.

(94) Moses, A. C.; Cohen, K. L.; Johnsonbaugh, R.; Peter Nissley, S. *J. Clin. Endocrinol. Metab.* **1978**, *46*, 937–946.

(95) Kawamori, D.; Kurpad, A. J.; Hu, J.; Liew, C. W.; Shih, J. L.; Ford, E. L.; Herrera, P. L.; Polonsky, K. S.; McGuinness, O. P.; Kulkarni, R. N. *Cell Metab.* **2009**, *9*, 350–361.

(96) CDC. Adult Obesity Prevalence Maps https://www.cdc.gov/obesity/data/prevalence-maps.html (accessed Jan 20, 2017).

(97) Niesler, C. U.; Siddle, K.; Prins, J. B. *Diabetes* **1998**, *47*, 1365–1368.

(98) Paolisso, G.; Gambardella, A.; Amato, L.; Tortoriello, R.; D'Amore, A.; Varricchio, M.; D'Onofrio, F. *Diabetologia* **1995**, *38*, 1295–1299.

(99) Bays, H.; Mandarino, L.; DeFronzo, R. A. *J. Clin. Endocrinol. Metab.* **2004**, *89*, 463–478.

(100) Muoio, D. M.; Newgard, C. B. *Nat Rev Mol Cell Biol* **2008**, *9*, 193–205.

(101) Dunmore, S. J.; Brown, J. E. P. *J. Endocrinol.* **2013**, *216*, T37–T45.

(102) Carmen, G. Y.; Víctor, S. M. *Cell. Signal.* **2006**, *18*, 401–408.

(103) Arner, P. *Best Pract. Res. Clin. Endocrinol. Metab.* **2005**, *19*, 471–482.

(104) Arner, P. *Diabetes, Obes. Metab.* **2001**, *3*, 11–19.

(105) Gordon, E. S. *Am. J. Clin. Nutr.* **1960**, *8*, 740–747.

(106) Chinen, I.; Shimabukuro, M.; Yamakawa, K.; Higa, N.; Matsuzaki, T.; Noguchi, K.; Ueda, S.; Sakanashi, M.; Takasu, N. *Endocrinology* **2007**, *148*, 160–165.

(107) Steinberg, H. O.; Chaker, H.; Leaming, R.; Johnson, A.; Brechtel, G.; Baron, A. D. *J. Clin. Invest.* **1996**, *97*, 2601–2610.

(108) Zhou, Y. P.; Grill, V. E. *J. Clin. Invest.* **1994**, *93*, 870–876.

(109) Stein, D. T.; Stevenson, B. E.; Chester, M. W.; Basit, M.; Daniels, M. B.; Turley, S. D.; McGarry, J. D. *J. Clin. Invest.* **1997**, *100*, 398–403.

(110) Poitout, V.; Robertson, R. P. *Endocrinology* **2002**, *143*, 339–342.

(111) Brown, J. E. P.; Thomas, S.; Digby, J. E.; Dunmore, S. J. *FEBS Lett.* **2002**, *513*, 189–192.

(112) Brown, J. E. P.; Onyango, D. J.; Dunmore, S. J. *FEBS Lett.* **2007**, *581*, 3273–3276.

(113) Gu, W.; Li, X.; Liu, C.; Yang, J.; Ye, L.; Tang, J.; Gu, Y.; Yang, Y.; Hong, J.; Zhang, Y.; Chen, M.; Ning, G. *Endocrine* **2006**, *30*, 217–221.

(114) Pajvani, U. B.; Du, X.; Combs, T. P.; Berg, A. H.; Rajala, M. W.; Schulthess, T.; Engel, J.; Brownlee, M.; Scherer, P. E. *J. Biol. Chem.* **2003**, *278*, 9073–9085.

(115) Brown, J. E. P.; Conner, A. C.; Digby, J. E.; Ward, K. L.; Ramanjaneya, M.; Randeva, H. S.; Dunmore, S. J. *Peptides* **2010**, *31*, 944–949.

(116) Deng, Y.; Scherer, P. E. *Ann. N. Y. Acad. Sci.* **2010**, *1212*, E1–E19.

(117) Wellen, K. E.; Hotamisligil, G. S. *J. Clin. Invest.* **2005**, *115*, 1111–1119.

(118) Zhao, Y. F.; Feng, D. D.; Hernandez, M.; Chen, C. *Endocrine* **2007**, *31*, 52–60.

(119) Wang, Y.; Dong, W.; Ding, X.; Wang, F.; Wang, Y.; Chen, X.; Yu, L.; Li, X.; Zhang, A.; Peng, Y. *Exp. Ther. Med.* **2012**, *4*, 469–474.

(120) Hausman, G. J.; Martin, R. J. *Biology of the adipocyte : research approaches*; New York : Van Nostrand Reinhold, 1987.

(121) Hwang, C. S.; Loftus, T. M.; Mandrup, S.; Lane, M. D. *Annu. Rev. Cell Dev. Biol.* **1997**, *13*, 231–259.

(122) Rosen, E. D.; Spiegelman, B. M. *Annu Rev Cell Dev Biol* **2000**, *16*, 145–171.

(123) Kawamura, M.; Jensen, D. F.; Wancewicz, E. V; Joy, L. L.; Khoo, J. C.; Steinberg, D. *Proc. Natl. Acad. Sci. U. S. A.* **1981**, *78*, 732–736.

(124) MacDougald, O. A.; Hwang, C. S.; Fan, H.; Lane, M. D. *Proc. Natl. Acad. Sci. U. S. A.* **1995**, *92*, 9034–9037.

(125) Rim, J.-S.; Mynatt, R. L.; Gawronska-Kozak, B. *FASEB J.* **2005**, *19*, 1205–1207.

(126) Sart, S.; Schneider, Y. J.; Agathos, S. N. *J. Biotechnol.* **2009**, *139*, 291–299.

(127) Staszkiewicz, J.; Frazier, T. P.; Rowan, B. G.; Bunnell, B. A.; Chiu, E. S.; Gimble, J. M.; Gawronska-Kozak, B. *Stem Cells Dev.* **2010**, *19*, 83–92.

(128) Gawronska-Kozak, B. *Methods Enzymol.* **2014**, *538*, 1–13.

CHAPTER 2

Microchip Electrophoresis Devices for Chemical Gradient Generation and 24 h Operation and Application to Perfusion and Chemical Monitoring of Living Cells

Introduction

Pancreatic β-cells, accounting for 70-80% of total cells in pancreatic islets, secrete insulin to help maintain glucose homeostasis.[1] Glucose stimulated insulin secretion involves several sequential cell signaling steps including rise of ATP/ADP ratio induced by glucose metabolism, closure of ATP sensitive K^+ channels, membrane depolarization, and opening of voltage-operated Ca^{2+} channels that allow Ca^{2+} to enter. The rise in cytoplasmic free Ca^{2+} concentration leads to subsequent triggering of insulin secretion.[2] β-cells dysfunction is fundamental to the pathophysiology of type 2 diabetes.[3]

Immunoassays such as RIA and ELISA are the most commonly used method to monitor insulin secretion from cells. Although the sensitivity is high, conventional immunoassays are usually labor and time intensive, making high temporal resolution measurements challenging. Microchip electrophoresis has been demonstrated useful to perform online immunoassay[4] with high speed, high efficiency and small sample volume requirement[5]. Microfluidics can also be used for cell culture[6,7], allowing it to be an excellent platform for simultaneous cell culture and chemical monitoring. Applications of cell culture combining flow cytometry[8,9], cell sorting[10,11], cell lysis followed by extraction

of intracellular contents[12,13] and *in vitro* cellular measurements (see reference 14 for a review of recent developments) have been reported.

Our research group developed a microchip electrophoresis (MCE) system for cell culture and insulin monitoring with competitive immunoassay.[15,16] Living islets were cultured on the microfluidic chip and continuously perfused.[16] Secreted insulin was sampled by electroosmotic flow (EOF) and monitored with 6 s temporal resolution by repetitive immunoassay using MCE.

These systems were capable of operating continuously for 2 h; however, at longer times the electropherogram signal became unstable and decreased. This effect was primarily due to degradation or depletion of buffers. It would be desiable to extend the running time of the microfluidic device allowing automated chemical monitoring over longer periods of secretion. Such measurements could be used to measure longer term trends in insulin secretion such as ultradian[17] and circadian rhythm[18–20]. Alterations in the ultradian rhythms have been reported in patients with type 2 diabetes.[21–23] Such rhythms have been difficult to observe *in vitro* due the challenge of monitoring islets over such long times.

Several studies have explored performing long term cell culture and analysis with microfluidic systems.[24–26] Although demonstrated useful for monitoring dynamic cellular activities, measurements were performed with relatively low temporal resolution (every 30 min-1 h) in these works. Our lab previously developed a microfluidic cell culture device capable of long-term electrophoresis operation.[27] To improve the stability of the electrophoresis, buffers were continuously replenished with perfusion channels built into the device. The electrophoretic immunoassay performance was calibrated every few

hours to measure any drift in calibration over the course of the 24 h monitoring period. Although it was the first system to demonstrate stable 24 h electrophoresis operation, it still required manual interventions, e.g. to perform calibrations. It would be desirable to have a system to automatically check the calibration to approach unattended monitoring.

Meanwhile, *in vitro* glucose stimulated insulin secretion model is traditionally built on direct change from low to high glucose (e.g., 3 to 11 mM or 3 to 17 mM). However, *in vivo* blood glucose change within mammalian animals usually have patterns of gradual rise and fall. Despite the success of using step changes in glucose to study insulin secretion, it fails to mimic such *in vivo* glucose dynamics. A system that allows islets to be exposed to controlled glucose gradient would greatly expand capabilities of *in vitro* studies.

In this chapter, we demonstrate a microfluidic device that is improved upon previous designs by incorporating a method to automatically generate arbitrary glucose (or any drug) profiles applied to the cells and by incorporating a method for automated calibration at defined times. For control of glucose, the system incorporates two independent syringe pumps loaded with low and high concentration glucose. Flow rates of both are controlled by a locally written LabView program. By mixing 2 syringe pumps' contents at different flow rates through a tee fabricated on the electrophoresis chip, arbitrary glucose gradients can be generated.

Insulin secreted from the islets is measured at 5-10 s intervals by an electrophoretic competitive immunoassay. Every few hours, a single pole double throw (SPDT) relay briefly moves the electrical connection from the islet reservoir to the

parallel insulin standard reservoir, allowing the electrophoretic sampling of insulin standards while maintaining the islet under perfusion. Single islets are perfused with different concentration of glucose. Processes of sampling of insulin secreted by the islet, insulin and FITC-insulin mixing and their competitively reacting with insulin antibody are achieved by electroosmotic flow (EOF). A high-voltage relay will control continuous injection of sample plug to the separation channel, where free FITC-insulin and FITC-insulin bound to antibody are separated. The integrated system can perform 14,000 electrophoresis assays in 24 h and automatically control culture condition, thus allowing continuous monitoring of insulin under well-controlled conditions.

This system is applied to measure glucose sensitivity of islets exposed to various glucose concentrations overnight *in vitro* with gradient glucose profile.[28] The concentrations of glucose that were able to trigger measureable insulin secretion were progressively reduced by 3 mM, 11 mM or 11 mM + Diazoxide (an insulin secretion inhibition drug) overnight treatment, suggesting an increase in glucose sensitivity.

Experimental Section

Chemicals and reagents

Cell culture reagents were purchased from Invitrogen (Carlsbad, CA). Monoclonal antibody (Ab) to human insulin was purchased from Meridian Life Science (Memphis, TN). Tricine, electrophoresis grade was obtained from MP Biomedicals (Aurora, OH). Collagenase P was obtained from Roche Diagnostic (Indianapolis, IN). Fluorescein isothiocyanate--labeled insulin (FITC-insulin) Tween 20, ethylenediaminetetraacetic acid (EDTA), insulin and fatty acid free bovine serum albumin (BSA) were obtained from Sigma-Aldrich (St. Louis, MO). All other chemicals

were from Fisher (Pittsburgh, PA). All solutions were prepared with Milli-Q (Millipore, Bedford, MA) 18 MΩ deionized water and filtered with 0.2 μm nylon syringe filters (Fisher) before using. Stock antibody solution was stored at 4 °C in the manufacturer provided phosphate buffer saline. Stock FITC-insulin was diluted to 166 μM in immunoassay reagent buffer and stored at -20 °C.

Balance salt solution (BSS) contained 125 mM NaCl, 5.9 mM KCl, 1.2 mM $MgCl_2$, 2.4 mM $CaCl_2$, 25 mM Tricine, and 0.7 mg mL^{-1} BSA. Immunoassay reagent buffer contained 60 mM NaCl, 1 mM EDTA, 20 mM tricine, 0.1% (w/v) Tween 20 and 0.7 mg mL^{-1} BSA. Electrophoresis buffer was 20 mM NaCl and 150 mM tricine. All buffers were adjusted to pH 7.4.

Microfluidic Chip Fabrication and Preparation

The microfluidic devices were fabricated using a method previously described.[15,29] Briefly, 1 mm thick Borofloat photomask blanks (3.8 cm × 7.6 cm) coated with a 120 nm layer of chrome and AZ1518 positive photoresist (Telic Company, Valencia, CA) are exposed to UV light for 6 s through a patterned photomask (Fineline Imaging Inc., Colorado Springs, CO). The exposed photomasks were developed in AZ 726 MIF developer (Clariant Corp., SummerVille, NJ) and the exposed chrome was developed in CEP-200 chrome etchant (Microchrome Technologies, Inc., San Jose, CA). The exposed glass was etched in 17:24:79 (v/v/v) HNO_3/HF/H_2O for 25 min to create 25 μm deep channels on the top wafer. Fluidic access holes were drilled with 360 μm diameter drilling bits (Kyocera Tycom, Costa Mesa, CA). The remaining photoresist was removed with acetone and the remaining chrome was removed with the CEP-200 chrome etchant. Glass wafers were washed for 20 min in piranha solution (3:1, v/v,

H_2SO_4/H_2O_2) and then heated RCA solution (5:1:1, v/v/v, $H_2O/NH_4/H_2O_2$) for 40 min. ***Caution!****: piranha solution is aggressive and explosive. Never mix piranha waste with solvents. Check the safety precautions before using it.* The wafers were rinsed with water, aligned and annealed at 610 °C for 8 h. Reservoirs and access ports (IDEX Health and Science, Oak Harbor, WA) were glued to the device over drilled access holes with epoxy glue.

Computational modeling

Perfusion of the mixing Tee (gradient generator) was modeled using COMSOL Muitiphysics (COMSOL, Inc., Burlington, MA). The "laminar flow" and transport of diluted species" models were used to monitor the mixing process. All simulations assumed water perfusion through the chip, with a density of 998 kg m^{-3} and a viscosity of 1.002 × 10^{-3} Pa ·s' (20 °C). The microfluidic channels were modeled in 2D with the shallow channel set to 36 μm tall. The sum of the flow rate was set at 0.6 μL min^{-1}, while both arms' flow rates were adjusted accordingly to simulate different mixing conditions.

Figure 2.1. (Next page) Overview of the microfluidic platform for monitoring insulin secretion from single islets. (A) The channel layout of the microfluidic device. Microfluidic channels are indicated by solid lines; Electrical connections are indicated by dotted lines. Circles indicate perfusion inlets and squares indicate reservoirs that are sampled by electroosmotic flow (EOF). Arrows indicate directions of perfusion flow. Gradient mixer indicates the Tee fabricated on chip to generate arbitrary glucose gradients. The shaded portion is heated at 37°C with a thin film heater. The star indicates laser-induced fluorescence occurred 1 cm past injection point. -HV are where high voltage is applied. (B) Side-view of an islet perfusion chamber. Islet is loaded into a 0.1 μL chamber and perfused with pressure-driven flow. After which the fluid flows into a 100 μL fluidic reservoir. Islet is loaded into a 0.1 μL chamber and perfused with pressure-driven flow, after which the fluid flows into a 100 μL fluidic reservoir. Solution with insulin from the chamber is sampled by EOF through the sampling channel at a rate of approximately 2 nL min−1. (C) Scheme for perfusing reservoirs. Perfusion buffer supply is pushed by syringe pumps or pressurized and fluid flows into the chip to constantly supply buffer that is sampled by EOF.

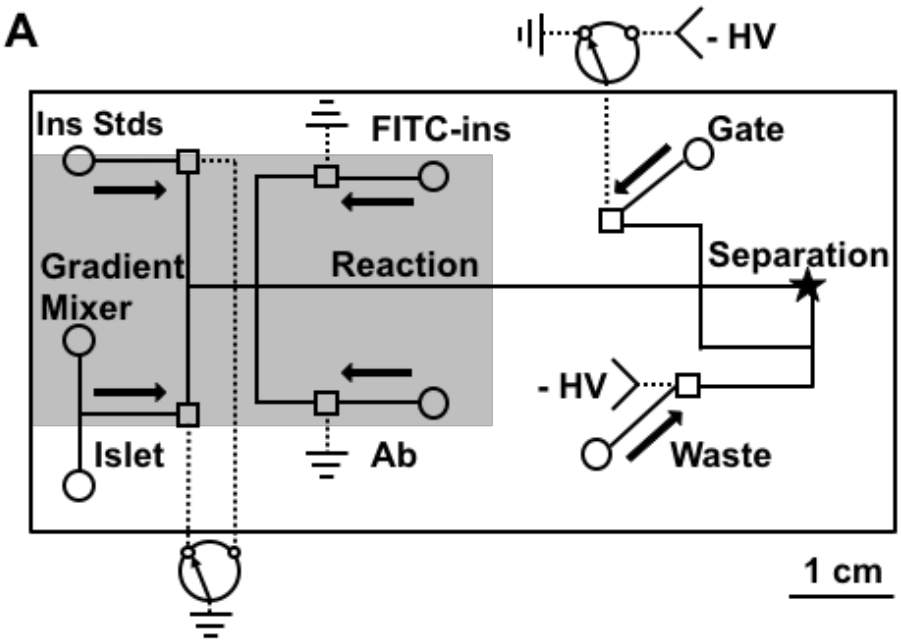
A
- HV
Ins Stds
FITC-ins
Gate
Gradient
Mixer
Reaction
Separation
- HV
Islet
Ab
Waste
1 cm

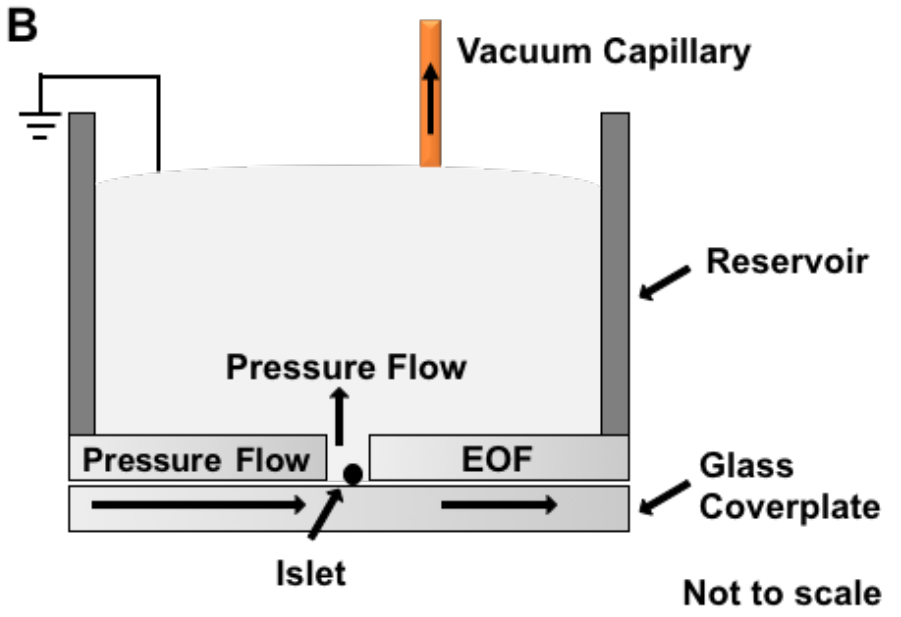
B
Vacuum Capillary
Reservoir
Pressure Flow
Pressure Flow
EOF
Glass
Coverplate
Islet
Not to scale

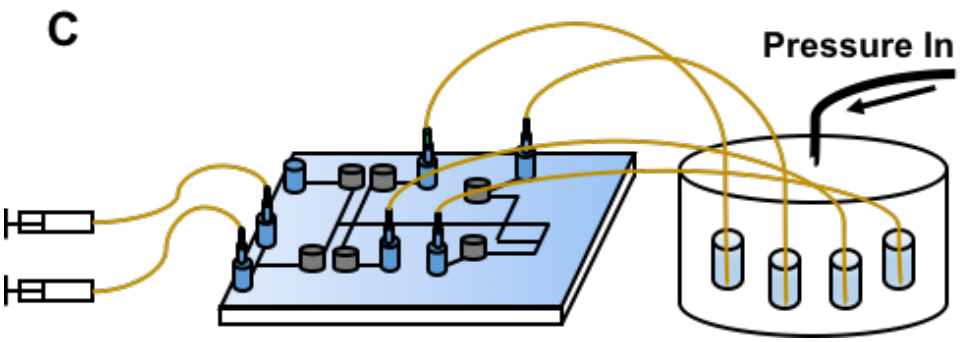
C
Pressure In

Microfluidic Chip Operation

The layout of the microfluidic chip is shown in **Figure 2.1**. All solutions were daily filtered from a stock solution to prevent introduction of particulates to the chip or degradation. Prior to experiments, the chip was conditioned with 0.1 M NaOH through the channels, followed by deionized water and then experimental buffers. During chip operation, the islet chamber was perfused with fresh BSS buffer pumped by 2 syringe pumps through fused-silica capillaries inserted into vials. All the other reservoirs were continuously pumped with fresh solutions pressured with 5-30 psi of Helium. During a long-term operation, all solutions excessing 100 μL were removed with a capillary connected to a vacuum pump to prevent overflow in the reservoirs. A high voltage (HV) of -6 kV was applied at the waste reservoir of the device. With all the other reservoirs grounded, Solutions containing insulin secreted by islet and 100 nM FITC-insulin are mixed and reacted competitively with 50 nM Ab on a heated reaction channel. Both FITC-insulin and Ab are dissolved in immunoassay reagent buffer. The electrophoresis buffer was placed in the gate and waste reservoirs. A SPDT high voltage relay (Kilovac, Santa Barbara, CA) was connected to the gate reservoir. When the gate was opened for a short period of time, the gate reservoir was connected to a -5 kV HV and a sample plug was allowed to flow into the 1.5 cm separation channel. Separation occurred in this channel resulting in a zone of FITC-insulin bound to antibody (B) followed by a zone of free FITC-insulin (F). Laser-induced fluorescence (LIF) detection occurred 1 cm from the injection cross and the ratio of the peak area of B/Fs were used to quantify insulin with calibration.

Islets were perfused with BSS and different concentrations of glucose at 0.6 μL min^{-1}. For islet experiments, a single islet was placed in the grounded islet reservoir. Perfusate from the islet was sampled via electroosmotic flow. For calibration, grounding was alternated from the islet reservoir to the insulin standards reservoir, allowing the electrophoretic sampling of insulin standards without interfering islets, which was still continuously perfused with normal glucose. During long-term experiments, a home-made LabView program controlled a SPDT relay to switch between islet reservoir and insulin standard reservoir to calibrate the immunoassay.

For control of glucose, the system incorporates two independent syringe pumps loaded with low and high concentrations of glucose. Flow rates of both are controlled by a home-made LabView program. By mixing 2 syringe pumps' contents at different flow rates through the Tee fabricated on the electrophoresis chip, arbitrary glucose gradients can be generated. We used fluorescein to mimic glucose, programmed step change (with frequency of 5 min) and ramping change (with frequency of 1 min), and detected it at the end of the mixing channel to assess the gradients.

Instruments and LIF Detection

LIF detection was performed with a Zeiss Axiovert 35 M inverted microscope equipped with a Photon Technology International 814 photometer (Birmingham, NJ). The 488 nm Excitation light of a 20 mW optically pumped semiconductor Sapphire laser (Coherent, Santa Clara, CA) is directed onto a 500 nm long-pass dichroic mirror and through a 40×, 0.6 numerical aperture, long working distance objective (Carl Zeiss, Inc., Thornwood, NY). After passing through the dichroic mirror, the emission light is further filtered through a 530 ± 30 nm band-pass filter. The fluorescence emission is further

spatially filtered by an iris diaphragm on the photometer. Instrument control and data collection are performed using LabVIEW software written in house (National Instruments, Austin, TX). High-throughput analysis of collected electropherograms is performed using Cutter software.[30]

Islet Isolation and Culture

Pancreatic islets were obtained from 20-30 g male CD-1 mice as previously described.[31] Briefly, mice were sacrificed by cervical dislocation, and collagenase P was injected into the pancreas through the main pancreatic duct. The pancreas was removed and incubated in 5 mL of collagenase solution at 37 °C for ~16 min. A Ficoll gradient was used to separate exocrine tissue from endocrine tissue, and islets were picked up by hand under a stereomicroscope. Islets with oblong to spherical shape, 100-200 μm diameter and intact membrane (showing smooth surface) are selected for experiments. The islets are placed in RPMI-1640 cell culture media supplemented with 10% fetal bovine serum, 100 unit mL^{-1} penicillin, and 100 μg mL^{-1} streptomycin at 37 °C, 5% CO_2, pH 7.4. Islets were used 2-5 days following isolation.

Islets Pretreatments

To measure glucose sensitivity change, isolated islets were divided into control and experimental groups. Control islets were cultured overnight (16-18 h) in RPMI 1640 media containing 11 mM glucose, whereas experimental islets were pretreated in RPMI 1640 containing 2.8 mM, and 11 mM + 100 μM diazoxide (DMSO < 0.1 % by volume).

Results and Discussion

Microfluidic Device and Operation Overview

The microfluidic chip is illustrated in **Figure 2.1**. This design allowed all buffers and reagents to be continuously perfused into the chip via syringe pumps and pressure-driven flow to keep buffers pulled into the electrophoretic channels fresh. Suggested by previous study[27], continuous perfusions keep immunoassay and electrophoresis stable for as long as 24 h. A single islet was placed in a chamber on the chip and continuously perfused with BSS, a physiological saline solution.

Before loading the cells, standard operations to sterilize instruments contacting islets or perfusion buffer were performed. Glass vials, pipet tips and fused silica capillaries were autoclaved and kept in biosafety cabinet. Syringes, microfluidic channels and islet chamber were rinsed with ethanol and DI water before loaded with buffer.

Calibration of Immunoassay and Limit of Detection of Insulin

The insulin immunoassay calibration data (see an example in **Figure 2.2**) allow calculation of detection limits and evaluation of sensitivity. The detection limit was 0.5 nM, calculated as the concentration required to give a B/F that was at least 3 standard deviations less than the B/F for 0 nM insulin. The assay was most sensitive in the range of 10-150 nM insulin, matching the majority of insulin concentrations that are detected from islets. The sensitivity range can be adjusted by changing the antibody and tracer concentrations.[32] It is desired to have a 1:1 ratio at the low end of required dynamic range for best sensitivity. Sample electropherograms at low and high concentrations of

insulin are demonstrated in **Figure 2.2**. Calibration was performed daily to minimize variation.

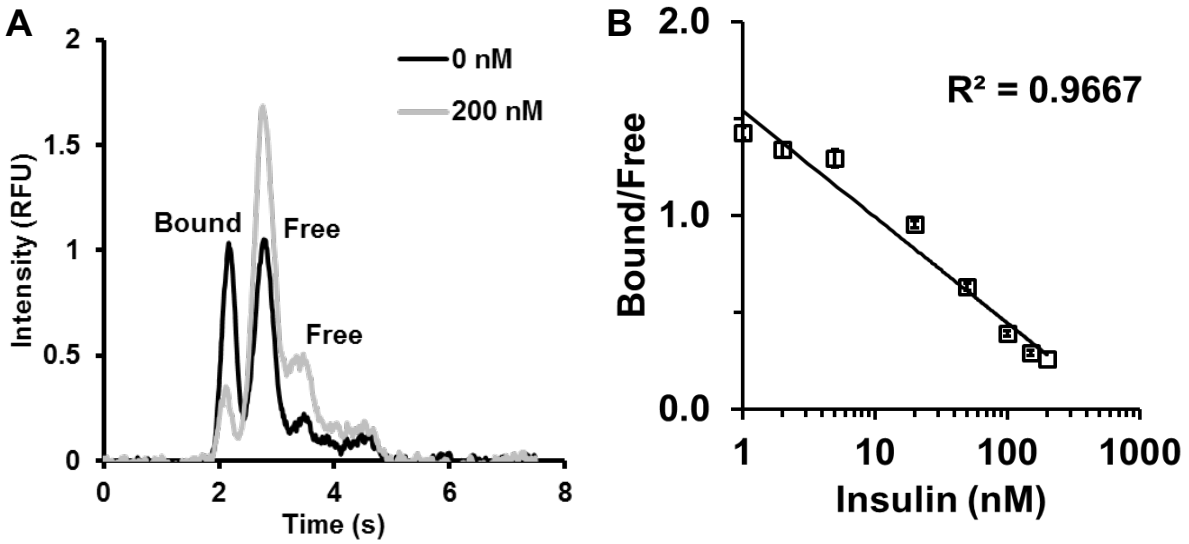

Figure 2.2. Sample electropherograms and a sample calibration curve. (A) Sample electropherograms at 0 nM and 200 nM insulin standards. Bound and free indicate Ab:Ag* complex and free Ag*, respectively. There are 2 free peaks because FITC-insulin are mono- and double-labeled. We use the first free peak area for B/F calculation. B/F is approximately one at 0 nM insulin. (B) A sample calibration curve. Error bars indicate ±1 standard deviation. The mean and standard deviation were calculated based on 10-15 electropherograms for each data point.

Long-term Islet Culture

To stably maintain islets on chip for 24 h is necessary for long-term monitoring. Previous work[27] from our group suggested perfusion with fresh media is the key to keep islets healthy. Moreover, we found it is also important to keep the inner-environment of the islet chamber sterile. Islet morphology is a straightforward indicator of the viability of the islets in their microfluidic environment. We confirmed this observation by comparing islets cultured in sterile and unsterile cell chamber and used islet morphology as an indicator. As illustrated in **Figure 2.3**, one islet cultured in unsterile cell chamber suffered disrupted membrane and did not appear healthy while the one in sterile

chamber remained intact membrane. Fraction of healthily cultured islets increased from 1/7 to 27/33 after taking the steps of sterilization.

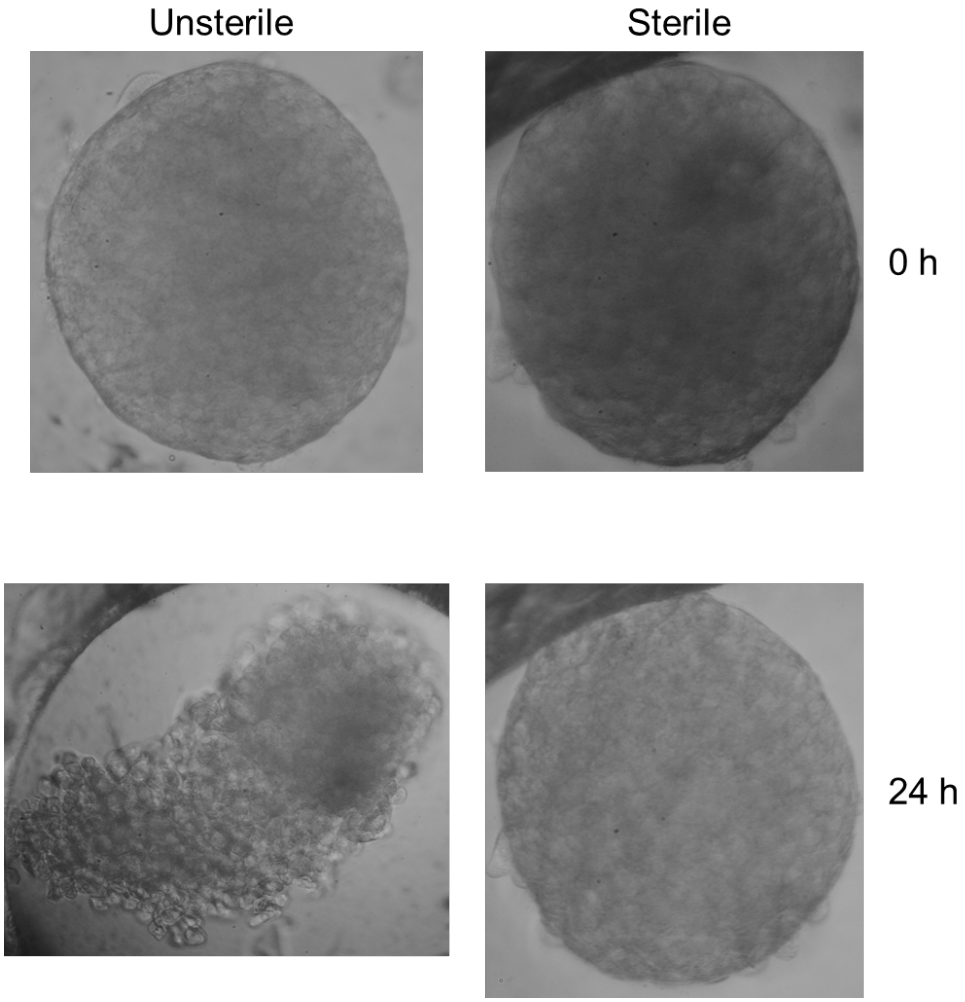

Figure 2.3. Islet morphology comparison. Two islets were placed in 11 mM glucose in a 360 μm diameter cell chamber on a heated long-term microfluidic device for 24 h. One culture condition was sterilized with ethanol prior to experiments as described in the experimental section and the other was not. Both were perfused with 11 mM glucose. The unsterile one appeared disrupted membrane and the cells were leaking out from the core, thus did not appear healthy. In contrast, the other one kept in sterile condition remained intact islet capsule.

Long-term Insulin Secretion Monitoring

To illustrate the potential of the system for long-term cell monitoring, we used it to record insulin secretion from single islets treated with 3 to 11 mM step changed glucose with up to 25 h stability. 7 islets were successfully monitored for 12 h or more, although

clogs in the chip caused quicker failure in other attempts. The average insulin secretion cut at 12 h is illustrated in **Figure 2.4**. It shows an initial burst of 1st phase insulin secretion followed by a lower plateau of 2nd phase. Calibrations were performed at the beginning and end of experiments.

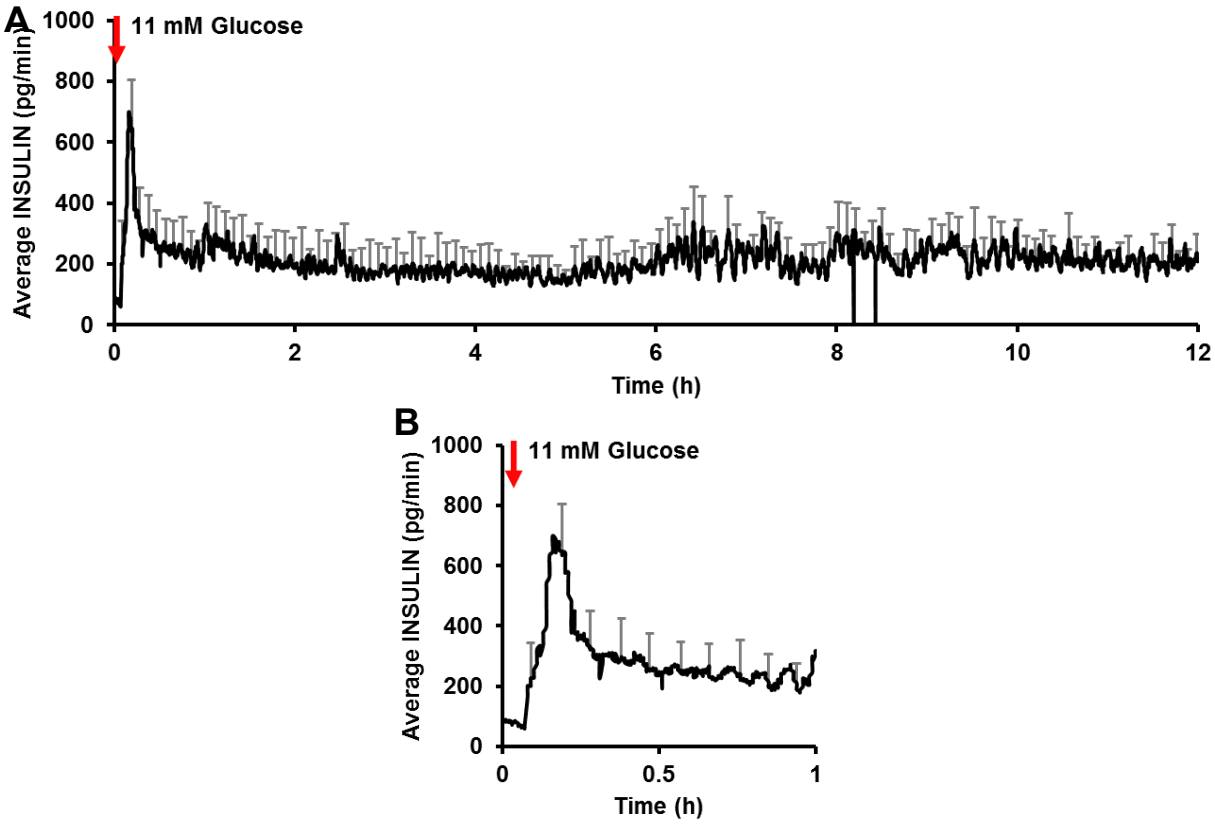

Figure 2.4. Average long-term insulin secretion. Average of insulin secretion from 7 islets (A) and an enlarged view of the 1st hour insulin secretion (B). The error bars indicate SEM of the mean. Time of glucose change from 3 mM to 11 mM is indicated by a red arrow.

To continuously assess stability performance of long-term running of electrophoresis, it is necessary to periodically calibrate the immunoassay while keeping the cells under stable perfusion. To achieve that with the islet present, an independent channel parallel with the islets was implemented for calibration. During long-term experiments, it was continuously perfused with constant concentration of insulin

standard and a SPDT controlled by a program periodically connected it to ground allowing sampling from this channel.

A single islet that was successfully monitored for 25 h as illustrated in **Figure 2.5**, combining automatic calibration every 5 h. The calibration was checked periodically by measuring the B/F of 100 nM insulin. The single point calibrations are also shown in **Figure 2.5**, confirming that the calibration of the immunoassay system was stable over the course of the long-term experiment. Several representative insulin secretion dynamics are enlarged in **Figure 2.5** for better view. For this particular islet, it secreted insulin with ~6 min period of strong oscillatory burst between approximately 10-15 h. The islet did not immediately begin to oscillate after the initial burst, which is a characteristic of *in vitro* perfused mouse islets that has been suggested by previous studies.[33,34] However, the oscillations afterwards and the transition between oscillatory and non-oscillatory periods were never observed before the long-term CE immunoassay.

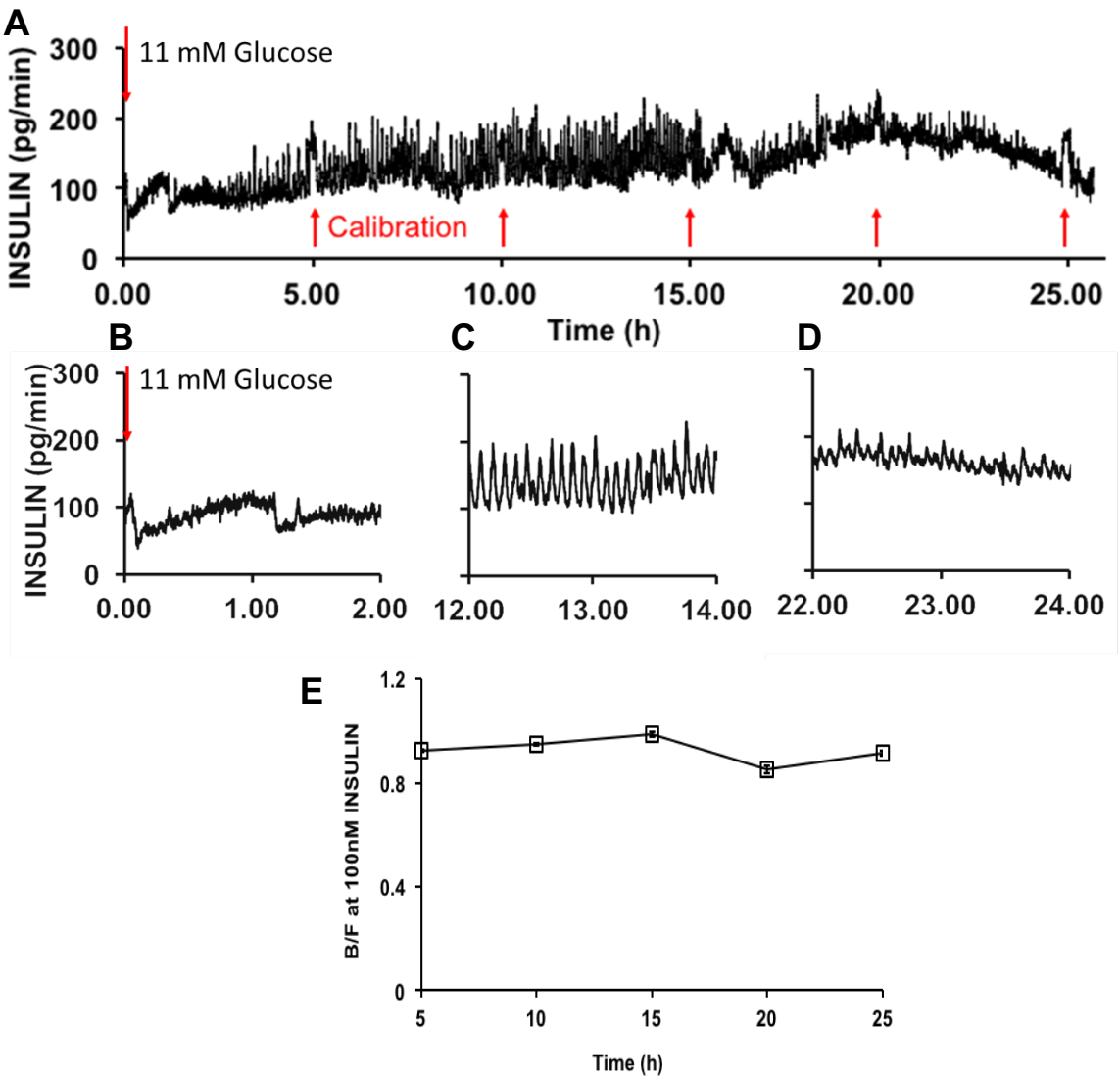

Figure 2.5. (A) 25 h islet insulin secretion. An example of 25 h insulin release from a single islet treated with 3 to 11 mM glucose step change. It was perfused with BSS and glucose at 0.6 µL min-1. (B)-(D) Several enlarged view of insulin secretion dynamics are shown. (E) Calibrations were performed every 5 h automatically with a SPDT relay to measure any drift over the course of 24 h period.

Glucose Gradient Characterization

Fluid mixing is the most important performance consideration for the gradient generator. To assist in determining the mixing, a COMSOL model was developed to simulate the mixing process. For easy demonstration, low and high concentrations were set as 0 mM and 1 mM. A line scan was set at the outlet of the mixing channel to track the average concentration change. Screenshot of mixing status of 6, 10 and 16 s and

the concentration at the mixing outlet is illustrated in **Figure 2.6**. We also attempted different flow rate combination to achieve different concentrations.

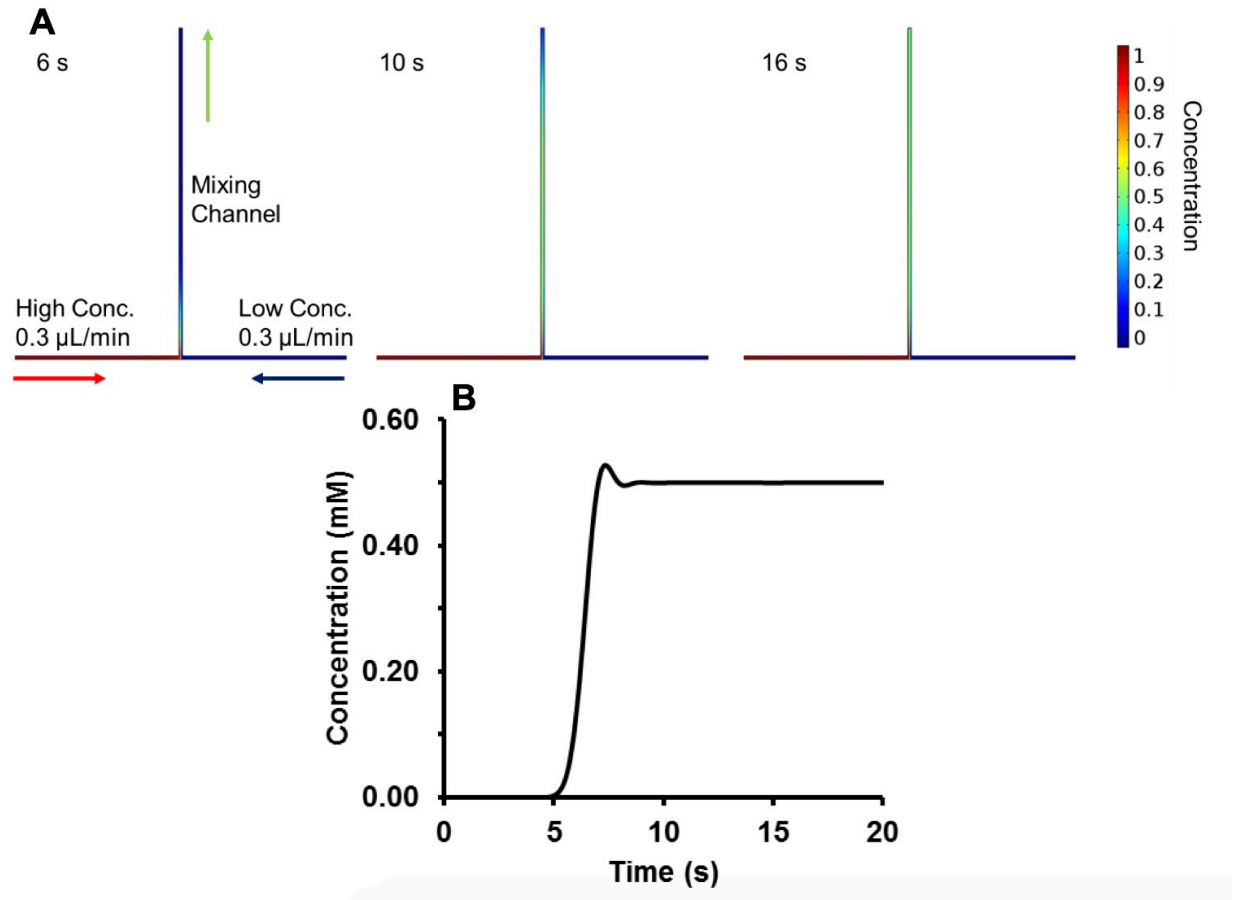

Figure 2.6. (A) A COMSOL model simulating on-chip mixing. In this specific set-up, flow rates of both arms of the Tee were set at 0.3 µL min^{-1} with concentrations of 0 and 1 mM. Snapshots of the process of mixing is demonstrated. (B) Average concentration at the outlet of the mixing channel is monitored. A 1:1 mixing reaches the concentration of 0.5 mM.

To validate the capability of the system to generate gradients, different profiles were programmed in the software for testing. Fluorescein was used to mimic glucose (or other stimulus) and measured at the end of the mixing channel. Low and high concentrations of fluorescein were loaded on 2 syringe pumps and perfused with different flow rates. The 2 profiles pre-setup in the program were illustrated in **Figure 2.7**. The delay time was 5 s and the rise time from 10% to 90% of intensity difference

between 2 concentrations was 10 s. The stable and smooth step and gradual change validated that glucose ramp can be generated with this system.

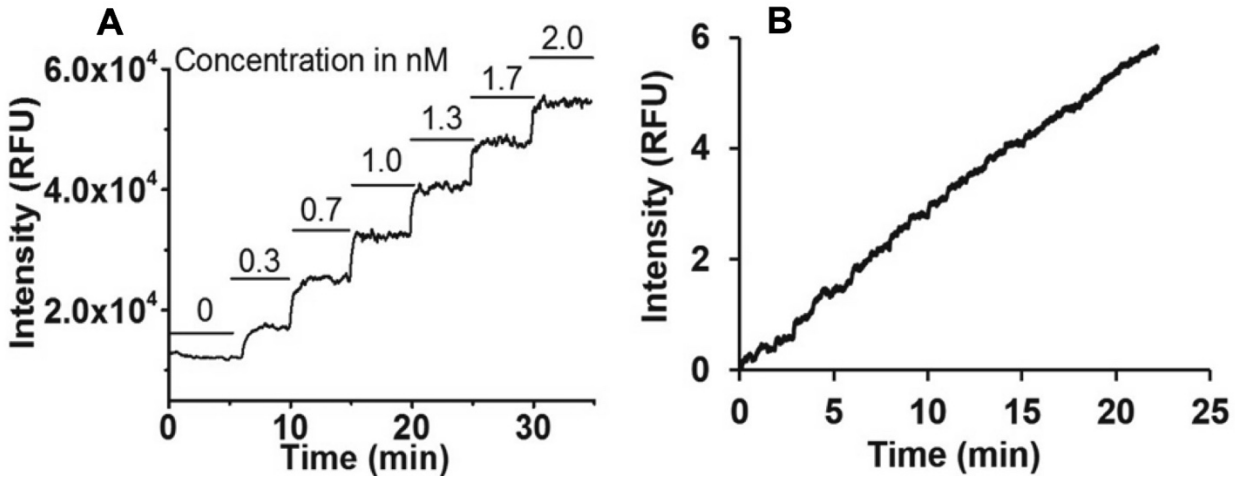

Figure 2.7. Programmed on-chip glucose changes with pumps mimicked by fluorescein. (A) Program controlled step changes from 0 nM to 2 nM fluorescein. (B) Continuous changing the syringe pumps flow rates slightly each minute to allow mixed concentration gradually increases in the total 22 min time.

Glucose Sensitivity Measurements with Glucose Ramp

This device was applied for glucose sensitivity studies. Islets pretreated with 3 mM, 11 mM and 11 mM + DZ for 16-18 h were assessed in response to ramping glucose from 1 mM to 24 mM in 1 mM increments (rate, 1 mM/min). As illustrated in **Figure 2.8**, islets exposed to 11G overnight responded to glucose ramps by rapidly secreting insulin once a threshold near 7 mM was reached and slowly subsiding. Abruptly reducing glucose at the end of the ramp resulted in a slow decline of secretion and subsequently stepping glucose up to 25 mM produced a secondary peak (not shown in **Figure 2.8**). Islets exposed overnight to 11G/Dz had earlier insulin release in the ramp, indicating a left shift; while overnight treatment with 3 mM glucose caused a right shift and less insulin output. The bar graphs in **Figure 2.8** quantify the threshold glucose shift with each condition.

β-cell threshold glucose concentration is one of the most important parameters to assess their sensitivity to glucose.[28] It is straightforward to reflect the lowest concentration of glucose to evoke insulin secretion. In our study, we have found that inhibiting insulin secretion with Dz left shifted (enhanced) glucose sensitivity and glucose concentration lower than 11 mM right shifted (reduced) it. In the collaborative work[35], measurements of Ca^{2+} and electrical oscillation with islets treated with the same condition had coincident results, suggesting insulin and low concentration of glucose have opposing actions on the islet glucose sensitivity.

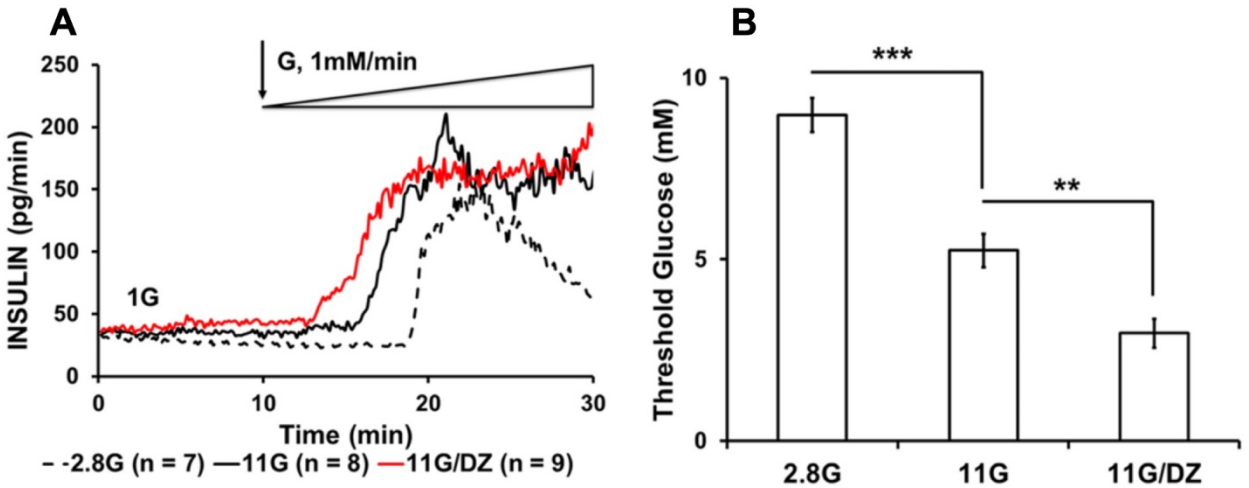

Figure 2.8. Insulin secretory dynamics in the 3 treatment groups. (A) Secretion from mouse islets chronically exposed to 11G (solid black line), 3mM glucose (dashed black line), or 11G + Dz (red line). The leftmost ordinate depicts average insulin secretion rate, in pg/min, of 7-9 single islets in each condition, whereas the wedge shown at upper right corresponds to ramped glucose levels. (B) Threshold glucose values of islets cultured overnight in 3mM, 11mM, or 11G + Dz. ***, P < .001; **, P < .01.

Conclusion

We have demonstrated a versatile microfluidic platform capable of long-term cell culture and chemical monitoring, combining automatic glucose (or other stimulus) gradient control and calibration. It has been demonstrated useful for several

applications to study insulin secretion dynamics from pancreatic islets, including monitoring glucose sensitivity and long-term insulin monitoring.

References

(1) Kulkarni, R. N. *Int. J. Biochem. Cell Biol.* **2004**, *36*, 365–371.

(2) Henquin, J. C. *Diabetes* **2000**, *49*, 1751–1760.

(3) Muoio, D. M.; Newgard, C. B. *Nat Rev Mol Cell Biol* **2008**, *9*, 193–205.

(4) Pagaduan, J. V.; Sahore, V.; Woolley, A. T. *Anal. Bioanal. Chem.* **2015**, *407*, 6911–6922.

(5) Kennedy, R. T. *Anal. Chim. Acta* **1999**, *400*, 163–180.

(6) Young, E. W. K.; Beebe, D. J. *Chem. Soc. Rev.* **2010**, *39*, 1036–1048.

(7) Mehling, M.; Tay, S. *Curr. Opin. Biotechnol.* **2014**, *25*, 95–102.

(8) Schrum, D. P.; Culbertson, C. T.; Jacobson, S. C.; Ramsey, J. M. *Anal. Chem.* **1999**, *71*, 4173–4177.

(9) Zhao, M.; Schiro, P. G.; Kuo, J. S.; Koehler, K. M.; Sabath, D. E.; Popov, V.; Feng, Q.; Chiu, D. T. *Anal. Chem.* **2013**, *85*, 2465–2471.

(10) Fiedler, S.; Shirley, S. G.; Schnelle, T.; Fuhr, G. *Anal. Chem.* **1998**, *70*, 1909–1915.

(11) Fu, A. Y.; Spence, C.; Scherer, A.; Arnold, F. H.; Quake, S. R. *Nat. Biotechnol.* **1999**, *17*, 1109–1111.

(12) McClain, M. A.; Culbertson, C. T.; Jacobson, S. C.; Allbritton, N. L.; Sims, C. E.; Ramsey, J. M. *Anal. Chem.* **2003**, *75*, 5646–5655.

(13) Zare, R. N.; Kim, S. *Annu. Rev. Biomed. Eng.* **2010**, *12*, 187–201.

(14) Roper, M. G. *Anal. Chem.* **2016**, *88*, 381–394.

(15) Roper, M. G.; Shackman, J. G.; Dahlgren, G. M.; Kennedy, R. T. *Anal. Chem.* **2003**, *75*, 4711–4717.

(16) Shackman, J. G.; Dahlgren, G. M.; Peters, J. L.; Kennedy, R. T. *Lab Chip* **2005**, *5*, 56–63.

(17) Simon, C.; Brandenberger, G. *Diabetes* **2002**, *51*, S258-61.

(18) Peschke, E.; Peschke, D. *Diabetologia* **1998**, *41*, 1085–1092.

(19) Picinato, M. C.; Haber, E. P.; Carpinelli, A. R.; Cipolla-Neto, J. *J. Pineal Res.* **2002**, *33*, 172–177.

(20) Merl, V.; Peters, A.; Oltmanns, K. M.; Kern, W.; Hubold, C.; Hallschmid, M.; Born, J.; Fehm, H. L.; Schultes, B. *Metabolism.* **2004**, *53*, 1449–1453.

(21) Polonsky, K. S.; Given, B. D.; Hirsch, L. J.; Tillil, H.; Shapiro, E. T.; Beebe, C.; Frank, B. H.; Galloway, J. A.; Van Cauter, E. *N. Engl. J. Med.* **1988**, *318*, 1231–1239.

(22) O'Meara, N. M.; Sturis, J.; Van Cauter, E.; Polonsky, K. S. *J. Clin. Invest.* **1993**, *92*, 262–271.

(23) O'Meara, N. M.; Sturis, J.; Herold, K. C.; Ostrega, D. M.; Polonsky, K. S. *Diabetes Care* **1995**, *18*, 568–571.

(24) Luke, C. S.; Selimkhanov, J.; Baumgart, L.; Cohen, S. E.; Golden, S. S.; Cookson, N. A.; Hasty, J. *ACS Synth. Biol.* **2016**, *5*, 8–14.

(25) Kimura, H.; Yamamoto, T.; Sakai, H.; Sakai, Y.; Fujii, T. *Lab Chip* **2008**, *8*, 741–746.

(26) Davidsson, R.; Boketoft, Å.; Bristulf, J.; Kotarsky, K.; Olde, B.; Owman, C.; Bengtsson, M.; Laurell, T.; Emnéus, J. *Anal. Chem.* **2004**, *76*, 4715–4720.

(27) Reid, K. R.; Kennedy, R. T. *Anal. Chem.* **2009**, *81*, 6837–6842.

(28) Gao, N.; Le Lay, J.; Qin, W.; Doliba, N.; Schug, J.; Fox, A. J.; Smirnova, O.; Matschinsky, F. M.; Kaestner, K. H. *Mol. Endocrinol. (Baltimore, Md)* **2010**, *24*, 1594–1604.

(29) Manz, A.; Harrison, D. J.; Verpoorte, E. M. J.; Fettinger, J. C.; Paulus, A.; Lüdi, H.; Widmer, H. M. *J. Chromatogr. A* **1992**, *593*, 253–258.

(30) Shackman, J. G.; Watson, C. J.; Kennedy, R. T. *J. Chromatogr. A* **2004**, *1040*, 273–282.

(31) Pralong, W. F.; Bartley, C.; Wollheim, C. B. *EMBO J.* **1990**, *9*, 53–60.

(32) Taylor, J.; Picelli, G.; Harrison, D. J. *Electrophoresis* **2001**, *22*, 3699–3708.

(33) Ma, Y. H.; Wang, J.; Rodd, G. G.; Bolaffi, J. L.; Grodsky, G. M. *Eur. J. Endocrinol.* **1995**, *132*, 370–376.

(34) Nunemaker, C. S.; Wasserman, D. H.; McGuinness, O. P.; Sweet, I. R.; Teague, J. C.; Satin, L. S. *Am. J. Physiol. Endocrinol. Metab.* **2006**, *290*, E523–E529.

(35) Glynn, E.; Thompson, B.; Vadrevu, S.; Lu, S.; Kennedy, R. T.; Ha, J.; Sherman, A.; Satin, L. S. *Endocrinology* **2016**, *157*, 611–623.

CHAPTER 3

A Microfluidic System to Study Cell-cell Interaction

Introduction

Cell-cell interactions are vital to normal operation of cells.[1–3] Indeed, it is well-known that isolated cells in culture may differ in function from the same cells in vivo due to the loss of normal cellular milieu that is comprised of structure and secretions from other cell types. Studying cells in vivo however can be challenging experimentally and ethically. Furthermore, it is difficult to manipulate the interaction of specific cells in vivo. In vitro models that mimic the in vivo microenvironment better than isolated cells are effective alternatives. A simple method to study cell-cell interaction is to co-culture 2 cell types in both sides of a transwell[4] or a single compartment[5]. Although useful, these methods have unrealistic volume-to-cell ratio and lack fluid dynamics and mass transport that are part of the in vivo environment. They also do not lend themselves to dynamic control over the cellular environment and integration with chemical measurements. In this work, we describe a microfluidic system that allows secretions from one cell type to interact with a second while using an integrated immunoassay to monitor protein release from the target cells. The system is used to investigate adipocyte effects on insulin secretion from islet cells.

Microfluidics has emerged as a powerful tool to create in vitro cell conditions that better mimic an in vivo environment. These tools are often called “organs-on-a-chip” or

"human-on-a-chip" to emphasize the creation of an in vivo like environment in the controlled confines of a microfluidic device. These systems were first developed to mimic in vivo pharmacokinetics and pharmacodynamics (PK/PD) on a chip.[3,6,7] The devices have interconnected compartments containing lung, liver, fat and other tissues in a circulatory system so that drugs introduced to the cells are metabolized similar to in vivo. Subsequent improvements include creation of 3-dimensional environments and long-term culture.[8–11] The concept has grown beyond drug metabolism so that now microfluidics has been further used for other types of cell-cell interaction such as studies on adhesion of platelets to endothelial tissue[12] and neovascularlization[13]. These systems have revealed many advantages such as precise control of cell culture environment, consumption of small amounts of tissue and media, and high-throughput.[7–14] In these "organ-on-chip" studies, the experimental output was typically a microscopic inspection of the cells. For the drug metabolism studies, the resulting metabolites were measured by collecting products and analyzing resulting samples off-line.

Microfluidics also enables integration of cellular manipulation and cellular analysis. One approach has been to combine flow cytometry[15,16], cell sorting[17,18] and cell lysis followed by extraction of intracellular contents[19,20] and in vitro cellular measurements (see reference 21 for a review of recent developments). Another approach has been to measure cell function by monitoring chemical secretions from cells incubated on microfluidic devices.[22–29] In our own work in this area we have coupled chips to mass spectrometry providing a powerful way to identify and quantify multiple secretions from cells. More relevant to the current work, we have also

demonstrated the potential of monitoring the dynamics of insulin secretion from single islets of Langerhans with up to 8 s temporal resolution by perfusing cells and analyzing the perfusate using rapid, on-line electrophoretic immunoassay.[30]

Islets are 75-200 μm diameter spheroid cell clusters located in the pancreas that contain 2000-4000 cells each, 70-80% of which are insulin secreting β-cells.[31] β-cells are stimulated to secrete insulin at elevated blood glucose concentration[32], which is crucial for maintaining glucose homeostasis[33]. Insulin secretion has complex dynamics. In vitro step increases in glucose concentration (typically from 3 mM to 11 mM) usually result in an initial burst (first phase) and oscillations with periods of 3-5 min (second phase) insulin secretions.[34]

Many studies of insulin secretion from islets in vitro have been reported with the goal of better understanding the mechanism of secretion. It is known that the extracellular environment in vivo contains many factors that modulate insulin secretion. One cell type that is of interest for its effects on islet cells is the adipocyte. Adipocytes are fat-storing cells that secrete glycerol and non-esterified fatty acids (NEFAs) as a result of the catabolism of triglycerides through lipolysis.[35] NEFAs have been shown to have bimodal effects on insulin secretion so that short term they enhance secretion but with chronic exposure they may suppress insulin secretion, suggesting a possible mechanism for dysfunctional insulin secretion in diabetes. Adipocytes also produce adipokines (a group of hormones and cytokines) which have been shown to affect pancreatic β-cells.[33,36]

It is well-known that obesity is a risk factor for diabetes which is characterized by impaired insulin secretion. This observation suggests the possibility that adipocytes

secretions might play a role in degrading islet cell function. Previous studies have suggested that dysregulation of several adipokines' secretion observed in obesity may promote insulin resistance, change insulin sensitivity and regulate insulin secretion (see reference 37 for a review), representing a potential pathophysiological link between obesity and type 2 diabetes. Investigations of adipocyte secretory products on insulin secretions have mostly relied on exposing islets to isolated components, such as NEFAs or individual adipokines; although, some studies[38] have focused on adipokine interactions. In this study, we demonstrate with a microfluidic system that adipocytes have impact on insulin secretion that cannot be explained by NEFA results alone. The results show that better mimicking the in vivo microenvironment, where the β-cell is exposed to full range of adipokines, provides a more integrated perspective to study adipokines' effects on the β-cell.

Experimental Section

Chemicals and reagents

Cell culture reagents, Amplex UltraRed Reagent, and Hank's buffered salt solution (HBSS) (Cat.No. 14175) were purchased from Life Technologies (Carlsbad, CA). Monoclonal antibody (Ab) to human insulin was purchased from Meridian Life Science (Memphis, TN). Tricine, electrophoresis grade was obtained from MP Biomedicals (Aurora, OH). Collagenase P was obtained from Roche Diagnostic. Fluorescein isothiocyanate-labeled insulin (FITC-insulin) Tween 20, ethylenediaminetetraacetic acid (EDTA), insulin and fatty acid free bovine serum albumin (BSA) were obtained from Sigma-Aldrich (St. Louis, MO). The fatty acid assay reagents and standard solution were purchased in a kit of HR Series NEFA-HR (2),

from Wako Chemicals USA, Inc. (Richmond, VA). All other chemicals were from Fisher (Pittsburgh, PA). All solutions were prepared with Milli-Q (Millipore, Bedford, MA) 18 MΩ deionized water and filtered with 0.2 μm nylon syringe filters (Fisher) before using. Stock antibody solution was stored at 4 °C in the manufacturer provided phosphate buffer saline. Stock FITC-insulin was diluted to 166 μM in immunoassay reagent buffer and stored at -20 °C.

Balance salt solution (BSS) contained 125 mM NaCl, 5.9 mM KCl, 1.2 mM $MgCl_2$, 2.4 mM $CaCl_2$, 25 mM Tricine, and 0.7 mg mL^{-1} BSA. Immunoassay reagent buffer contained 60 mM NaCl, 1 mM EDTA, 20 mM tricine, 0.1% (w/v) Tween 20 and 0.7 mg mL^{-1} BSA. Electrophoresis buffer was 20 mM NaCl and 150 mM tricine. All buffers were adjusted to pH 7.4.

Glass Microfluidic Chip Fabrication and Preparation

The microfluidic devices were fabricated using a method previously described.[26,39] Briefly, the device consisted of 2 etched glass wafers: a bottom wafer for the bottom portion of the adipocyte chamber and a top wafer for the fluidic channels and the top portion of the adipocyte cell chamber. 1 mm thick Borofloat photomask blanks (3.8 cm X 10.2 cm) coated with a 120 nm layer of chrome and AZ1518 positive photoresist (Telic Company, Valencia, CA) are exposed to UV light for 6 s through a patterned photomask (Fineline Imaging Inc., Colorado Springs, CO). The exposed photomasks were developed in AZ 726 MIF developer (Clariant Corp., SummerVille, NJ) and the exposed chrome was developed in CEP-200 chrome etchant (Microchrome Technologies, Inc., San Jose, CA). The exposed glass was etched in 17:96:7 (v/v/v) HNO_3/HF/H_2O for 57 min to create 250 μm deep cell chamber on the bottom wafer and

17:24:79 (v/v/v) HNO_3/HF/H_2O for 25 min to create 25 μm deep channels on the top wafer. Fluidic access holes and top portion of the adipocyte cell chamber were drilled in the top wafer with 360 μm diameter (Kyocera Tycom, Costa Mesa, CA) and 9.5 mm diameter (Starlite Industries, Rosemont PA) drilling bits, respectively. The remaining photoresist was removed with acetone and the remaining chrome was removed with the CEP-200 chrome etchant. Glass wafers were washed for 20 min in piranha solution (3:1, v/v, H_2SO_4/H_2O_2) and then heated RCA solution (5:1:1, v/v/v, H2O/NH4/H2O2) for 40 min. ***Caution!****: piranha solution is aggressive and explosive. Never mix piranha waste with solvents. Check the safety precautions before using it.* The wafers were rinsed with water, aligned and annealed at 610 °C for 8 h. Reservoirs and access ports (IDEX Health and Science, Oak Harbor, WA) were glued to the device over drilled access holes with epoxy glue.

Polydimethylsiloxane (PDMS) slice fabrication

All of the PDMS used in the chip fabrication was RTV-615 (Curbell plastics, Livonia, MI) and had base to curing agent ratio of 10:1. A mold was made by milling 9.1 mm diameter and 0.8 mm depth wells on plastic at desired positions. A 2 mm layer of PDMS was poured over the mold and heated to 80 °C for at least 30 min before been peeled away from the mold. It was cut to appropriate shape to use afterwards.

Computational modeling

Perfusion of the cell chambers was modeled using COMSOL Muitiphysics (COMSOL, Inc., Burlington, MA). The “laminar flow” and transport of diluted species” models were used to monitor the flow split and theoretical temporal resolution. All simulations assumed water perfusion through the chip, with a density of 998 kg m^{-3} and

a viscosity of 1.002 × 10^{-3} Pa ·s' (20 °C). The diffusion coefficient used for oleic acid was 5.26 × 10^{-10} m^2 s^{-1}. [40] The adipocyte and islet chamber were modeled separately due to size difference to reduce computation times with different mesh accuracy. Both cell chambers were modeled in a 3D geometry. The adipocyte chamber had dimensions of 9.5 mm diameter × 1 mm with a 9.1 mm diameter × 0.8 mm cylinder removed from top to mimic the PDMS plug on the cover piece. The islet chamber had dimensions of 0.36 mm diameter × 1 mm. The inlet and outlet channels for the cell chamber were modeled in 2D with the shallow channel set to 36 μm tall. The cell chamber inlet flow rate was set at 0.3 μL min^{-1}.

Microfluidic Chip Operation

The layout of the microfluidic chip is shown in **Figure 3.1**. All solutions were daily filtered from a stock solution to prevent introduction of particulates to the chip or degradation. The chip was conditioned prior to experiments by flowing 0.1 M NaOH through the channels, followed by deionized water and experimental solutions.

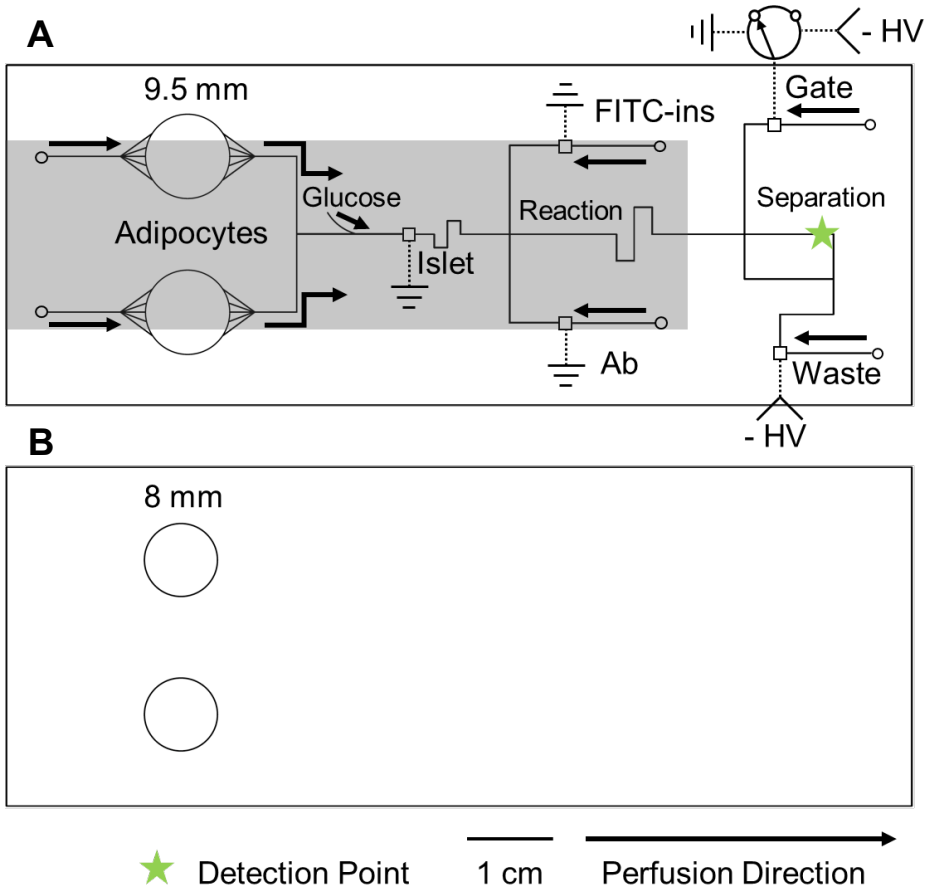

Figure 3.1. Microfluidic chip layout. In the top layer (A), microfluidic channels are indicated by solid lines; Electrical connections are indicated by dotted lines. Circles indicate perfusion inlets and squares indicate reservoirs that are sampled by electroosmotic flow (EOF). At the adipocyte chamber portion, 2 holes with diameter of 9.5 mm were drilled. On the bottom layer (B), 2 circles with diameter of 8 mm were etched to 250 μm deep and aligned with the top layer during bonding.

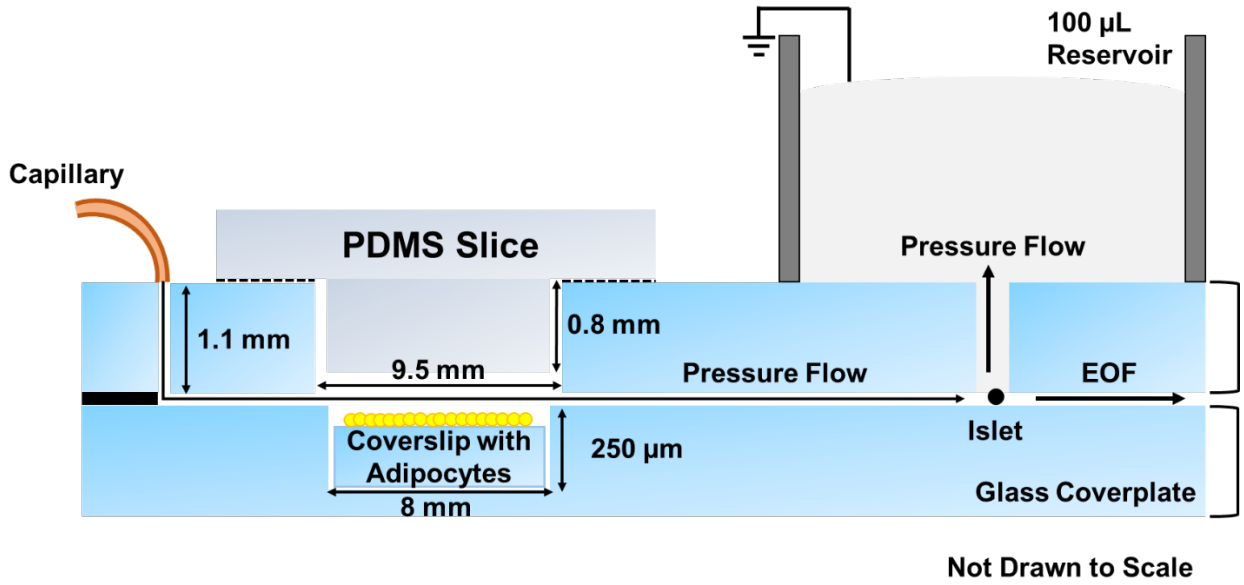

Figure 3.2. Side view of adipocytes and islet perfusion culture. Adipocytes and islet were loaded into cell chambers and perfused with pressure-driven flow, after which the fluid flowed into a 100 µL fluidic reservoir. The adipocyte chambers were sealed with a piece of PDMS slice. Solution with insulin from the chamber was sampled by EOF through the sampling channel at a rate of approximately 2 nL min^{-1}.

Cell culture

Adipocytes and islets were perfused with BSS containing glucose at 0.6 µL min^{-1}. For islet experiments, a single islet was placed in the grounded islet reservoir. The adipocytes chamber and PDMS cover piece were rinsed with 70% ethanol and dust was removed with Scotch tape. To load adipocytes, 2 coverslips with ~190,000 attached 3T3-L1 adipocytes were removed from the culture dish with sterile tweezers and placed in the lower cell chamber. Cells per coverslip were roughly estimated by the fraction of the plate area occupied by the coverslip on the culture plate times the total number of cells, assuming an even distribution of cells. Total number of cells was estimated from the number of seeded preadipocytes (measured by hemocytometer) and the replication rate during differentiation. About 50 µL of buffer was added to prevent trapping bubbles

during sealing. Blank coverslips were applied for control experiments. The PDMS slide was pressed with the rear end of a tweezer to make a conformal contact.

A compression frame to enclose the adipocyte portion was built in-house from 2 sheets of acrylic plastic. Holes were drilled through both sheets along the outer edge to allow screws to pass through to tighten the frame. **Figure 3.4** shows the assembled chip in the compression frame.

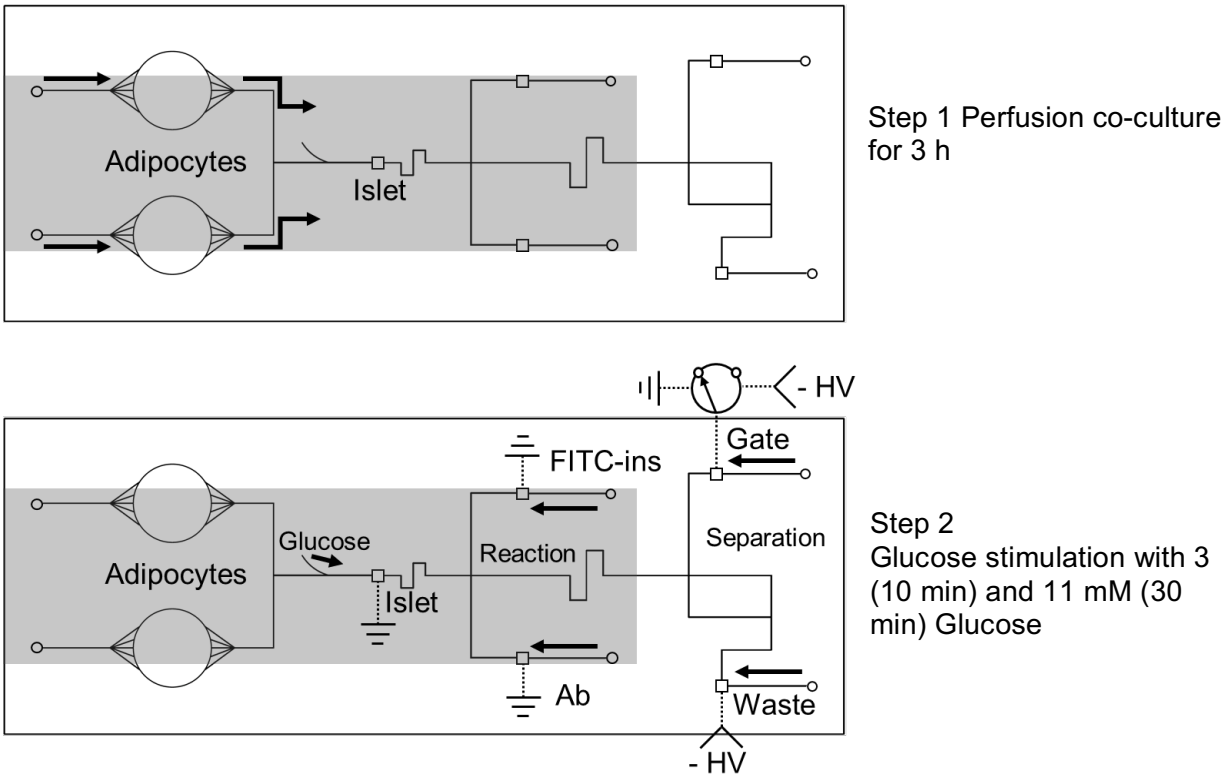

Figure 3.3. Workflow of Experiments. During step 1, islets were co-cultured with adipocytes for 3 h without chemical monitoring; during step 2, perfusion from adipocytes was stopped and glucose was delivered from the side channel to stimulate the islet.

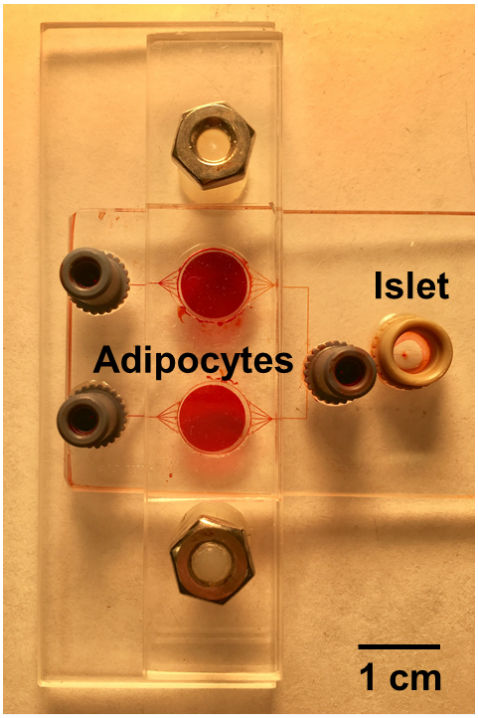

Figure 3.4. The assembled chip in compression frame with only the cell culture portion is shown. Red food dye was perfused into the channels for better visualization.

Perfusion and Chemical Monitoring

The workflow of experiments is illustrated in **Figure 3.3**. During co-culture, BSS buffer was pumped onto the chip through adipocytes and islets, via fused-silica capillaries pumped by external syringe pumps (Chemyx, Stafford, TX). During chemical monitoring, perfusion through adipocytes was stopped and buffer was perfused directly to islets through a side channel. Besides islet reservoir, to provide fresh buffer to all the other reservoirs, appropriate solutions were continuously pump onto the chip via fused-silica capillaries inserted into vials in a reservoir pressurized to 12 psi with helium.

Negative high voltage (-6 kV) was applied at the waste reservoir of the device. With all the other reservoir grounded, Solutions containing insulin secreted by islet and 100 nM FITC-insulin were mixed and reacted competitively with 50 nM Ab on a heated reaction channel. Both FITC-insulin and Ab were dissolved in immunoassay reagent

buffer. Electrophoresis buffer was pumped into gate and waste reservoirs. The gate reservoir is connected to ground via a high voltage relay. Injection is performed by opening the relay as described elsewhere.[41] When the relay is opened, sample is allowed to load onto the separation channel. The gate is then returned to ground and separation is performed. Another sample can be loaded after the previous separation is completed. Sample injection time is 0.5 s applied at 7.5 s intervals. Laser-induced fluorescence detection occurs 1 cm from the injection cross. Each separation results in a FITC-insulin bound to antibody (B) peak followed by a free FITC-insulin (F) peak. Concentration of insulin is quantified by comparing B/F peak areas ratios of each electrophoregrams to a calibration curve.

Instruments and LIF Detection

LIF detection was performed with a Zeiss Axiovert 35 M inverted microscope equipped with a Photon Technology International 814 photometer (Birmingham, NJ). The 488 nm Excitation light of a 20 mW optically pumped semiconductor Sapphire laser (Coherent, Santa Clara, CA) is directed onto a 500 nm long-pass dichroic mirror and through a 40×, 0.6 numerical aperture, long working distance objective (Carl Zeiss, Inc., Thornwood, NY). After passing through the dichroic mirror, the emission light is further filtered through a 530 ± 30 nm band-pass filter. The fluorescence emission is further spatially filtered by an iris diaphragm on the photometer. Instrument control and data collection are performed using LabVIEW software written in house (National Instruments, Austin, TX). High-throughput analysis of collected electropherograms is performed using Cutter software.[42]

Adipocyte culture

8 mm diameter glass coverslips (Warner Instruments, Hamden, CT) were sterilized in 70% ethanol for at least 1 h and were then dried in a sterile culture hood. Three to four coverslips were placed in each 35 mm petri dish using sterile tweezers prior to seeding preadipocytes. Murine 3T3-L1 preadipocytes were seeded into the 35 mm dishes (200,000 cells per dish), maintained in Dulbecco's modified Eagle's medium (Cat. No. 11965-092, Life Technologies) with 8% v/v bovine calf serum (Denville Scientific, South Plainfield, NJ), 100 units mL^{-1} penicillin, 100 µg/mL streptomycin, 2 mM L-glutamine, and 1 mM sodium pyruvate and were stored in an incubator with 10 % CO_2. Two days after the cells became confluent, differentiation (adipogenesis) was induced by adding 500 µM methylisobutylxanthine, 1 µM dexamethasone, and 5 µg/mL insulin. Medium was replaced with adipogenic medium was the same as the preadipocyte medium except that 10 % fetal bovine serum replaced the bovine calf serum two days post-differentiation. Every 2 days following, culture medium was refreshed with adipogenic medium that did not contain insulin. Adipocytes were matured to at least 14 days post-induction before on-chip experiments.

Islet Isolation and Culture

Pancreatic islets were obtained from 20-30 g male CD-1 mice as previously described.[43] Briefly, mice were sacrificed by cervical dislocation, and collagenase P was injected into the pancreas through the main pancreatic duct. The pancreas was removed and incubated in 5 mL of collagenase solution at 37 °C for ~16 min. A Ficoll gradient was used to separate exocrine tissue from endocrine tissue, and islets were picked up by hand under a stereomicroscope. Islets with oblong to spherical shape,

100-200 μm diameter and intact membrane (showing smooth surface) are selected for experiments. The islets are placed in RPMI-1640 (Thermo Fisher 11875, 11 mM glucose) cell culture media supplemented with 10% fetal bovine serum, 100 unit mL^{-1} penicillin, and 100 μg mL^{-1} streptomycin at 37 °C, 5% CO_2, pH 7.4. Islets were used 2-5 days following isolation.

Off-line NEFA Enzyme Assays

NEFAs concentration was determined by collecting perfusates on chip and performing enzyme assays on a multi-plate reader (Perkin Elmer Fusion) using a method described previously.[25,44] Briefly, the fatty acid reagents were reconstituted per manufacturer's instructions to create Color Reagent A (CR-A) and Color Reagent B (CR-B). 20 μL perfusate was mixed with 200 μL CR-A and incubated at 37 ˚C for 10 min. 9.3 μL of reconstituted Amplex UltraRed Reagent (33 M prior to mixing) and 400 μL CR-B were then added and incubated at 37 ˚C for another 10 min. The mixture was transferred into 96 well plates and measured in multi-plate reader. The fluorescent reagent was excited by 535 nm light and emitted 620 nm fluorescence.

Results and Discussion

Microfluidic Device and Operation Overview

The microfluidic chip developed for cell-cell interaction integrated with electrophoresis-based insulin secretion monitoring is illustrated in **Figure 3.1.** A side view of the cell culture portion is illustrated in **Figure 3.2**. This chip design builds on previous work aimed at measuring insulin secretion from islets[26,27] and NEFAs from adipocytes[24,25]. This prior work identified important principles of microfluidic cell culture such as minimizing the difficulty of loading cells into the chip, prevention of shear stress

on the cells during perfusion, and simple regeneration of chips which are used in this work. Our goal in this work was to produce a chip that exposes islets to adipocytes producing physiological concentrations of NEFA and observe the effect on glucose stimulated insulin secretion as a model of cell-cell interaction with integrated analysis.

The chip contains 3 cell chambers, 2 to hold adipocytes and 1 to hold a single islet. 2 coverslips containing adipocytes were placed at the bottom of the cell chambers, which were sealed by placing a PDMS “slice” in the open top chamber. The adipocyte chamber portion was pressed to make a conformal contact with a compression frame. This procedure allowed easy loading and re-use of a chip. Single islets were pipetted into the open islet chamber. Leaving the islet chamber open to atmosphere (**Figure 3.2**) allowed: 1) easy loading and unloading of the chamber; 2) perfusate from the adipocytes to flow out the top of the chamber without causing high flow into the electrophoresis channel; and 3) the potential for placing sensors or electrophysiological probes in the islet for other studies.

During operation, the adipocytes were perfused with BSS, a physiological saline solution at 0.3 μL min^{-1}. The perfusate passed into the islet chamber so that islets were exposed to adipocyte secretions. After perfusion for a desired period, the adipocyte flow was stopped and glucose solutions were perfused to the islet chamber (**Figure 3.3, Step 2**) to record glucose stimulated insulin secretion.

At 0.6 μL min^{-1} perfusion system rapidly replaced the solution in the islet chamber (approximately 100 nL volume) in a few seconds. The rapid wash-out allows high temporal resolution monitoring of insulin secretion from the islet. The islet chamber was continuously sampled at 2 nL min^{-1} by electroosmotic flow generated by applied voltage

from the chamber to the exit of the electrophoresis system (**Figure 3.3, Step 2**). The resulting sample stream was mixed with immunoassay reagents (Ab and FITC-insulin) in the reaction channel. This stream was injected every 8 s onto the electrophoresis channel where the bound and free FITC-insulin were separated (sample electropherograms shown in **Figure 3.5**). Using a calibration curve, these data enabled determination of insulin concentrations and secretion rates. To improve reliability of the continuous operation of the electrophoresis chip, a pressure-driven flow was used to replenish buffers and reagents into the chip. Continuous electrolysis in buffer reservoirs will degrade buffers, so that perfusion of buffers is effective to maintain long-term electrophoresis stability[28]. With these precautions, electrophoresis was stable for 3 h of measurement, although longer times are possible.[28] Keeping buffer refreshed also obviated the need to condition the chip for every electrophoresis measurement, which can be tedious and prone to fail after assembling the adipocyte culture portion.

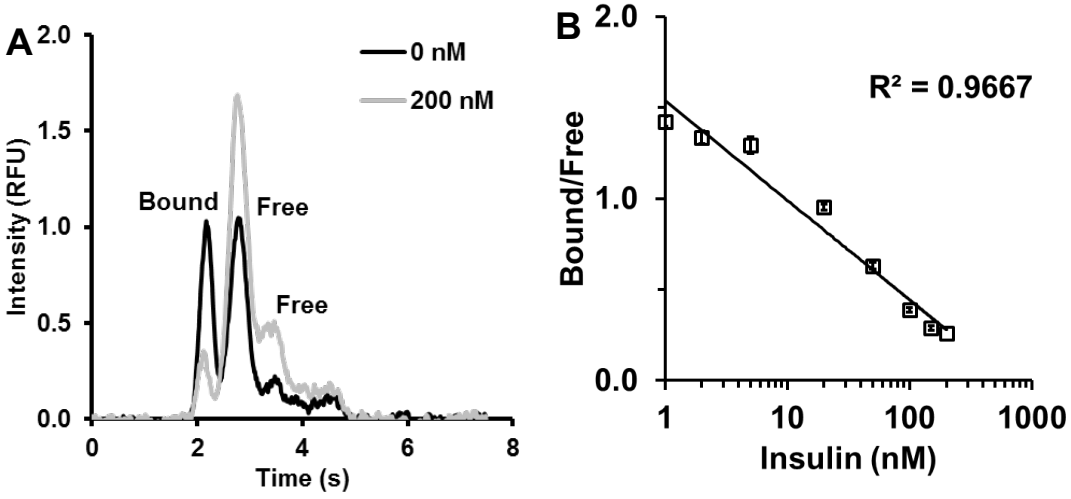

Figure 3.5. Sample electropherograms and a sample calibration curve. (A) Sample electropherograms at 0 nM and 200 nM insulin standards. Bound and free indicate Ab:Ag* complex and free Ag*, respectively. There are 2 free peaks because FITC-insulin are mono- and double-labeled. We use the first free peak area for B/F calculation. B/F is approximately one at 0 nM insulin. (B) A sample calibration curve. Error bars indicate ±1 standard deviation. The mean and standard deviation were calculated based on 10-15 electropherograms for each data point.

Fluid dynamics of adipocyte and islet chamber

Flow distribution and fluid dynamic response are important performance considerations for the chip. To assist in determining the flow conditions, several COMSOL models were developed. Adipocyte chamber and islet chamber flow profile, and cellular release were modeled separately (**Figure 3.6**). For simulations, the cell chamber inlet flow rate was set at 0.6 μL min^{-1}. Measurements showed that the actual flow rate varied by less than 10% from this value. The volume of the adipocyte chamber was 40 μL, and the islet chamber was 0.1 μL based on calculations from the geometry of the chip.

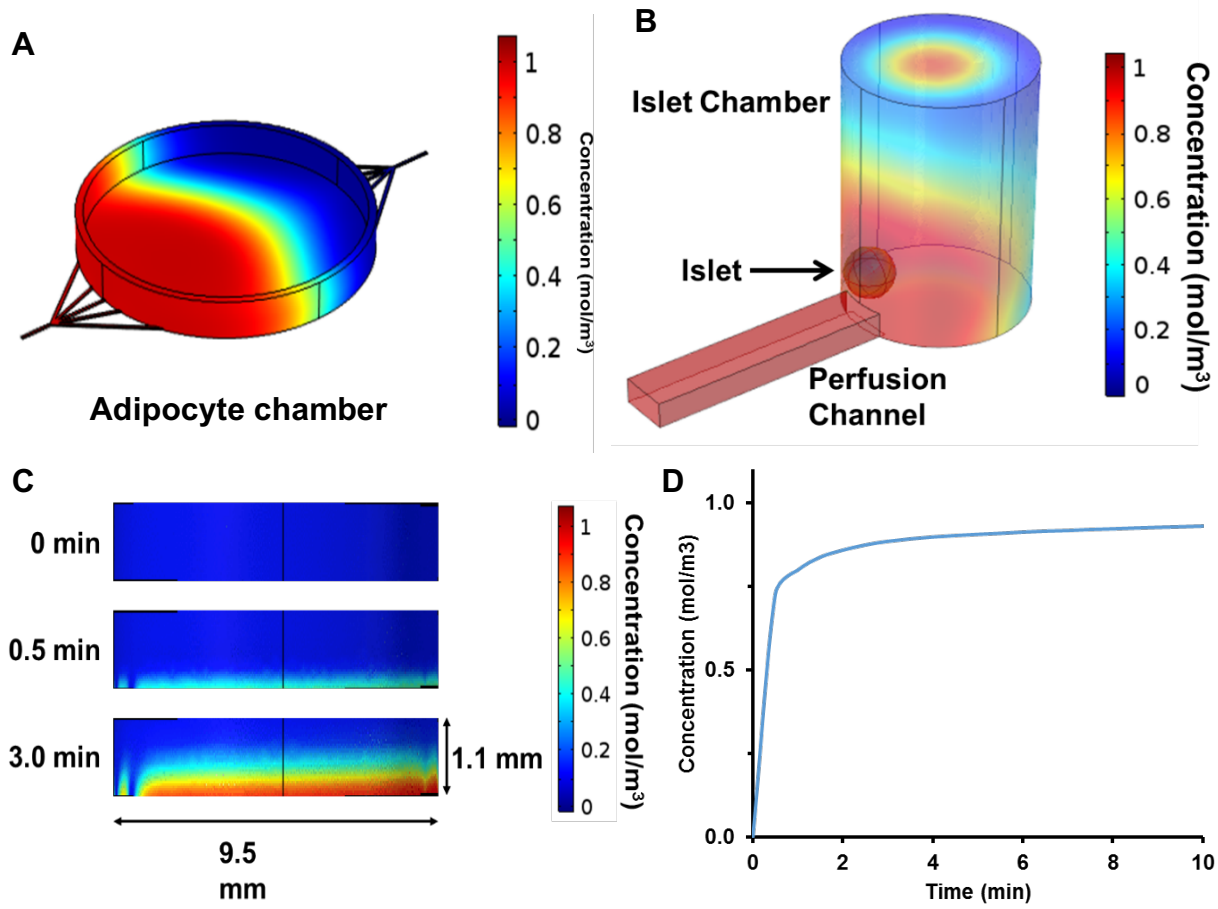

Figure 3.6. COMSOL model of adipocyte chamber, islet chamber and cellular release. (A) Fluid distribution in adipocyte chamber; (B) Islet chamber and perfusion channel with single islet in it. The average concentration changes of the sphere (mimicking islet) sides facing and back to the perfusion channel were probed. The back side reaches 90% increase at 12 s. (C) and (D) Side view of the adipocyte chamber showing a simulation of the concentration flowing from the bottom of chamber assuming a constant release of chemicals from the cells below. The concentration reaching the outlet of the chamber had a 10-90 % rise time of 4 min.

The flow through the adipocyte chamber and islet chamber are shown in **Figure 3.6A and B**. A simulation of a chemical species injection into the adipocyte chamber is illustrated in **Figure 3.6A**, allowing visualization of the flow profile of the cell chamber. The flow across the cell chamber is uniformly distributed. **Figure 3.6B** illustrates chemical species simulation in the islet chamber. A sphere is located in the bottom of the chamber to mimic the islet. The concentrations of the semi-spheres facing and back

to the perfusion channel are probed to demonstrate uniform distribution of the fluid around the islet.

Our goal was to expose islets to stable concentrations of adipocyte secretions. As shown in **Figure 3.2**, the adipocytes site in recessed chamber with flow passing over them. The recessed position protects the fragile cells from shear.[24,45] As a result of the positions, secretions must diffuse into the flow path to be brought to the islets. **Figure 3.6C** shows a simulation of the concentration flowing from the chamber assuming a constant release of chemicals from the cells below. The concentration reaching the outlet of the chamber had a 10-90 % rise time of 4 min as illustrated in **Figure 3.6D**. The model also shows that chemicals released from the adipocytes tend to stay near the bottom of the chamber as they flow downstream. This flow pattern favors rapid entry into the to the downstream channels towards the islet.

Fatty acid concentration validation

The NEFA concentration reaching the islet will depend on the number of adipocytes present in the chip and mass transport as modeled above. Based on previous results, we estimated that 190,000 adipocytes would produce approximately 80 μM NEFA at the islets. To confirm this expectation, fractions of perfusate were collected from the islet chamber and assayed for NEFA using a fluorescent enzyme assay. We also flowed standard concentrations of 50 μM and 100 μM palmitic acid through the chip to verify that suitable transport of known concentrations through the chip. As shown in **Figure 3.7**, standards gave the expected concentration indicating inconsequential NEFA loss through the chip. Adipocytes produced 80 μM putting it within the desired range.[25] Suggested by previous investigation[25], the concentration of

fatty acid produced by adipocytes highly relies on cell number and post induction day. Cells were counted and seeded to allow constant density batch by batch. They were applied for co-culture 14-20 days post-induction, when the NEFA secretion is stable.

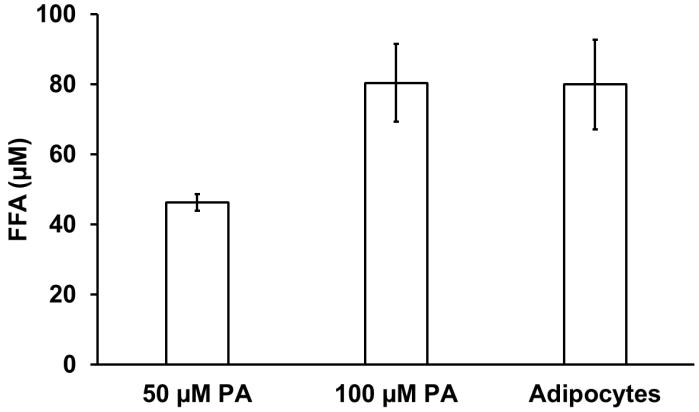

Figure 3.7. FFA concentration measured with off-line NEFA enzyme assay. Error bars indicate ± SEM. n = 3.

Calibration of insulin immunoassay

The insulin immunoassay calibration data (see an example in **Figure 3.5**) allow calculation of detection limits and evaluation of sensitivity. The detection limit was 0.5 nM, calculated as the concentration required to give a B/F that was at least 3 standard deviations less than the B/F for 0 nM insulin. The assay was most sensitive in the range of 10-150 nM insulin, matching the majority of insulin concentrations that are detected from islets. The sensitivity range can be adjusted by changing the antibody and tracer concentrations[46] and it is desired to have a 1:1 ratio at the low end of required dynamic range for best sensitivity. Calibration was performed daily to minimize variation.

Islet pretreatment, co-culture with adipocytes and insulin secretion monitoring

We used the system to co-culture adipocytes and islets and record insulin secretion from single islets following 3 to 11 mM glucose step change. Results from adipocytes were compared to perfusion with 50 and 100 µM palmitic acid for the same

period as a positive control. Palmitic acid was chosen because it is the most concentrated fatty acid in serum[47,48], and it is widely used to study the effect of fatty acid on insulin secretion in lab. As shown in **Figure 3.8**, the islet chip records a classical peak of insulin secretion (first phase) followed by a lower rate (second phase) for all conditions. Pretreatment with palmitic acid potentiated the first phase of GSIS in a concentration dependent fashion (**Figure 3.8 and Figure 3.9**). Adipocytes, which produced 80 μM NEFA, had an even greater potentiation of secretion. The peak insulin secretion rate and average insulin output rate of 1st phase are compared as illustrated in **Figure 3.9**.

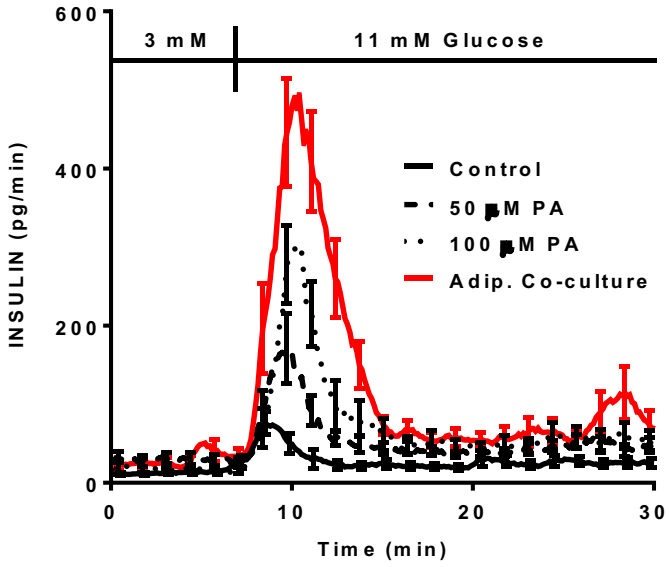

Figure 3.8. Summary of insulin secretion stimulated with 3h palmitate (PA) pretreatment and adipocytes co-culture. Individual islets were isolated from 3-5 individual mice in each condition. n = 5-19.

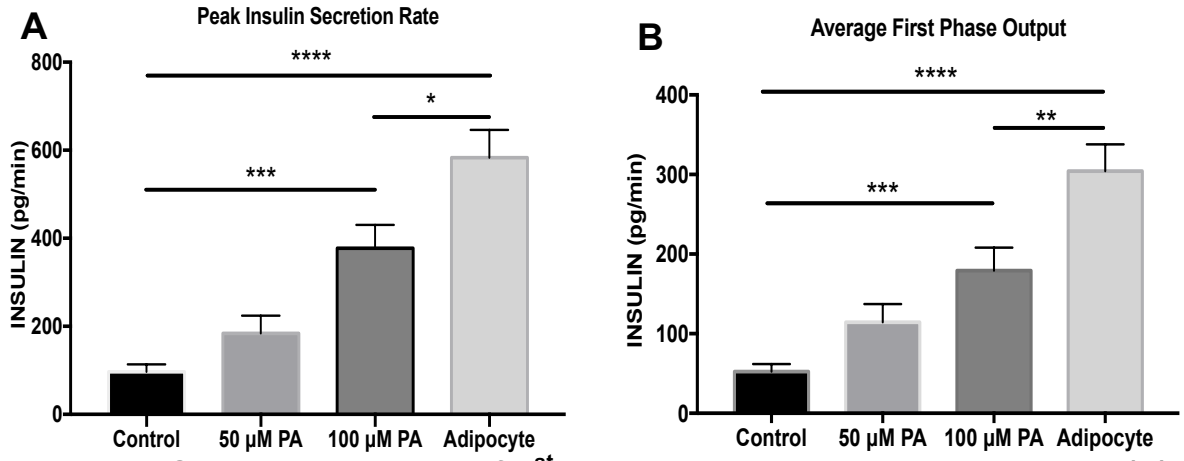

Figure 3.9. Statistical analysis of 1st phase insulin secretion peak value (A) and average secretion rate (B). **** p < 0.0001; *** p < 0.001; ** p < 0.01; * p < 0.05.

Second phase is typically low in mouse islets in vitro[49,50], but sometimes oscillations were observed. We first compared the average 2nd phase insulin secretion rate after 1st phase peak (**Figure 3.10**) and found 100 μM palmitic acid and adipocytes stimulated more 2nd phase insulin secretion. Considering not all cells have 2nd phase, we further investigated the ratio of islets with active 2nd phase oscillations, and found *10/19 (52.6 %), 9/14 (64.3%) and 9/12 (75.0%)* islets had active oscillation in control, 100 μM and adipocyte group, respectively (50 μM group is not included to compare with relatively smaller n-value). This data suggests that NEFAs and adipocytes may induce more 2nd phase insulin oscillation. Moreover, the 2nd phase oscillation frequency was counted, including all pulses between 1st phase peak till 30 min in each group (**Figure 3.10**). It is worth noting that several islets co-cultured with adipocytes had a "rest period" between 1st and 2nd phase, lowering the frequency, although the intensity of 2nd phase oscillation was stronger (**Figure 3.10**). This phenomenon also suggests that prolonged monitoring would be meaningful to explore more on the effects of fatty acid and adipocytes on insulin secretion. Sample representative individual islets secretion traces are illustrated in **Figure 3.11**.

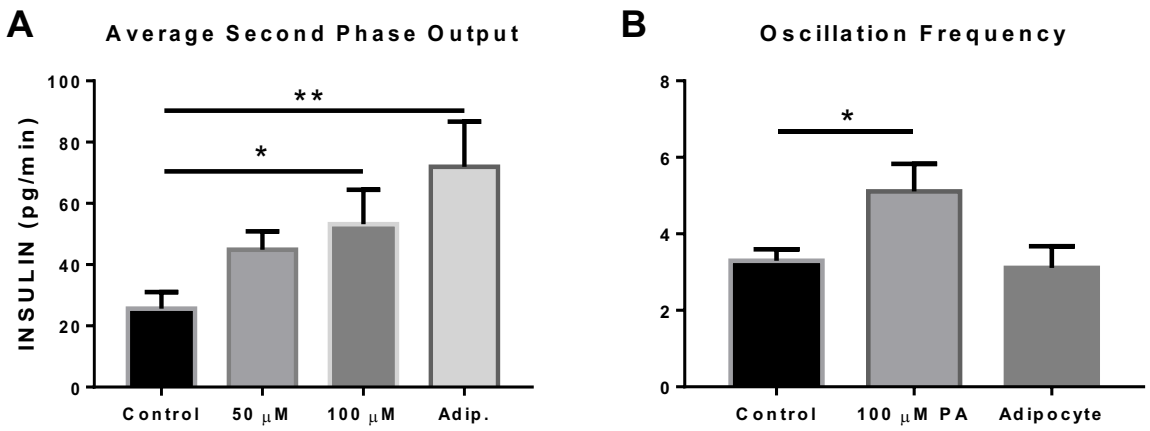

Figure 3.10. Statistical analysis of 2nd phase average insulin secretion rates (A) and oscillation frequency (B). ** $p < 0.01$; * $p < 0.05$.

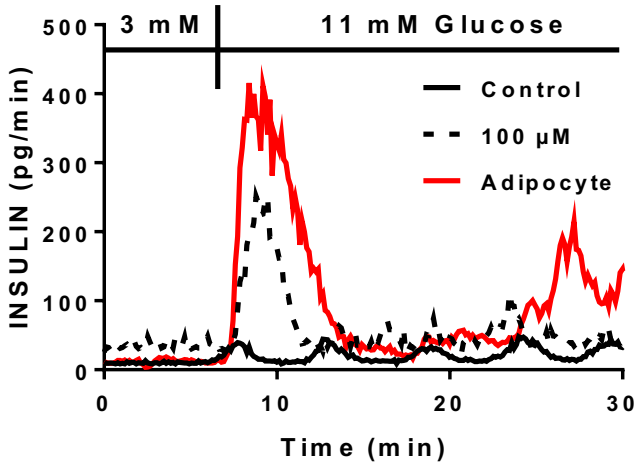

Figure 3.11. Representative insulin secretion from individual islets stimulated with 3h palmitate (PA) pretreatment and adipocytes co-culture.

These results suggest that the remarkable augmentation of secretion of insulin following exposure to adipocyte perfusate is due to more than NEFA. It may be due to either the mix of NEFAs that are released (although palmitic is a primary NEFA released from these cells[51]) or to other secretory products such as adipokines. **Figure 3.8** illustrates the averaged data from islets treated with different conditions. We observed enhanced 1st phase insulin secretion when islets were pretreated with 100 μM palmitic acid and halving the concentration of palmitic acid weakened the enhancement.

The enhanced insulin secretion with fatty acid pretreatment can be possibly explained with insulin releasable pool model.[52] β-cells have a readily releasable pool (contributing to 1st phase) and reserve pool(s) (contributing to 2nd phase). When the cells are pretreated with high glucose/fatty acid or other stimulus for a period of time, they are primed to prepare more insulin at the readily releasable pool thus provide augmented 1st phase insulin secretion. The effects of fatty acid on mouse islets' insulin secretion have been under debate for many years. Different attempts have been made by adding and removing fatty acid during low or high glucose and monitoring insulin and related hormone secretion[53–56], or applying a glucose ramp to study glucose sensitivity[57]. Contradictory conclusions were drawn on effects of short-term fatty acid treatments on β-cell functions and the mechanism is still under debate. Our work first demonstrates 3 h pretreatment enhances insulin secretion even with relatively low FFA concentration, suggesting short-term fatty acid pretreatment is a positive regulator of insulin secretion.

The 2 fold augmentation compared with equivalent fatty acid (100 μM) stimulated by adipocytes was even a little beyond our expectation. Although further validation may be required, the results here first demonstrates positive regulation of adipocytes, with potential amplified effects results from adipokines interplay.

Moreover, we also measured intracellular Ca^{2+} concentration ($[Ca^{2+}]$) of islets pretreated with 100 μM and blank buffer with a method described previously.[58] The results (**Figure 3.12**) did not demonstrated significant difference between the 2 groups. Ca^{2+} influx caused by K_{ATP} channel closure has been widely known as the pace maker of insulin secretion[32], while there are also K_{ATP} channel independent pathways exist.[59,60]

The lack of [Ca^{2+}] alteration suggests that it not likely underlie the augmentation of insulin secretion, although further investigation is needed to confirm. The [Ca^{2+}] data also suggests that insulin monitoring is meaningful to observe islets' functions.

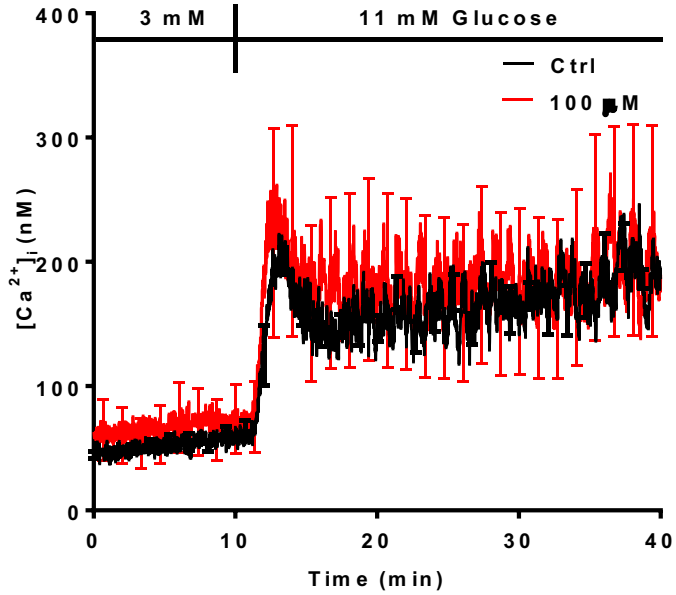

Figure 3.12. Intracellular Ca^{2+} concentration of control islets and islets pretreated with 100 μM palmitic acid for 3 h. n = 7.

Besides 1st phase, we also compared 2nd phase signal, and found co-cultured cells may have stronger 2nd phase oscillations. The short monitoring time limited our capability to find more evidence, which suggested longer-term measurement is necessary. Our group have extended the monitoring window to longer period of time[28], where oscillations with different frequency and intensity were observed. In the future it would be desired to extend the monitoring time to study the 2nd phase, where ultradian (2 h rhythms)[61] and circadian (24 h rhythms)[62] were observed and deficiencies in them have been linked to type 2 diabetes.

Meanwhile, the short-term positive regulation of adipocytes is potentially related to the pathogenesis of type 2 diabetes onset. Disregulated adipokine secretion may

cause insulin resistance and β-cell compensation and ultimately lead to β-cell failure.[37,63] Longer-term co-culture would help us investigate more on this.

Conclusion

We have developed a microfluidic chip capable of co-culture two cell types and chemical monitoring with capillary electrophoresis immunoassay. With this device we were able to study the effects of adipocytes on islets' insulin secretion and found augmented insulin secretion after short-term treatment. This device keeps the capability of running long-term monitoring. With modifications, it may be used for further investigation of potential pathophysiological link between obesity and type 2 diabetes. The results illustrate the importance of using live cell interaction to modulatory effects of one cell upon the other. Retaining this design would also allow further studies on more complex studies such as comparing of short-term and long-term effects of adipocytes on insulin secretion.

References

(1) Huh, D.; Torisawa, Y.; Hamilton, G. a.; Kim, H. J.; Ingber, D. E. *Lab Chip* **2012**, *12*, 2156.

(2) Sung, J. H.; Shuler, M. L. *Bioprocess Biosyst. Eng.* **2010**, *33*, 5–19.

(3) Huh, D.; Hamilton, G. A.; Ingber, D. E. *Trends Cell Biol.* **2011**, *21*, 745–754.

(4) Lau, Y. Y.; Chen, Y.-H. H.; Liu, T. T.; Li, C.; Cui, X.; White, R. E.; Cheng, K.-C. C. *Drug Metab. Dispos.* **2004**, *32*, 937–942.

(5) Li, A. P.; Bode, C.; Sakai, Y. *Chem. Biol. Interact.* **2004**, *150*, 129–136.

(6) Esch, M. B.; King, T. L.; Shuler, M. L. *Annu. Rev. Biomed. Eng* **2011**, *13*, 55–72.

(7) Viravaidya, K.; Sin, A.; Shuler, M. L. *Biotechnol. Prog.* **2004**, *20*, 316–323.

(8) Sung, J. H.; Shuler, M. L. *Lab Chip* **2009**, *9*, 1385–1394.

(9) Zhang, C.; Zhao, Z.; Abdul Rahim, N. A.; van Noort, D.; Yu, H. *Lab Chip* **2009**, *9*, 3185–3192.

(10) Maschmeyer, I.; Lorenz, A. K.; Schimek, K.; Hasenberg, T.; Ramme, A. P.; Hübner, J.; Lindner, M.; Drewell, C.; Bauer, S.; Thomas, A.; Sambo, N. S.; Sonntag, F.; Lauster, R.; Marx, U. *Lab Chip* **2015**, *15*, 2688–2699.

(11) van Midwoud, P. M.; Merema, M. T.; Verpoorte, E.; Groothuis, G. M. M. *Lab Chip* **2010**, *10*, 2778–2786.

(12) Ku, C. J.; Oblak, T. D. A.; Spence, D. M. *Anal. Chem.* **2008**, *80*, 7543–7548.

(13) Hsu, Y.-H.; Moya, M. L.; Hughes, C. C. W.; Georgea, S. C.; Lee, A. P. *Lab Chip* **2013**, *13*, 2990–2998.

(14) Frank, T.; Tay, S. *Lab Chip* **2015**, *15*, 2192–2200.

(15) Schrum, D. P.; Culbertson, C. T.; Jacobson, S. C.; Ramsey, J. M. *Anal. Chem.* **1999**, *71*, 4173–4177.

(16) Zhao, M.; Schiro, P. G.; Kuo, J. S.; Koehler, K. M.; Sabath, D. E.; Popov, V.; Feng, Q.; Chiu, D. T. *Anal. Chem.* **2013**, *85*, 2465–2471.

(17) Fiedler, S.; Shirley, S. G.; Schnelle, T.; Fuhr, G. *Anal. Chem.* **1998**, *70*, 1909–1915.

(18) Fu, A. Y.; Spence, C.; Scherer, A.; Arnold, F. H.; Quake, S. R. *Nat. Biotechnol.* **1999**, *17*, 1109–1111.

(19) McClain, M. A.; Culbertson, C. T.; Jacobson, S. C.; Allbritton, N. L.; Sims, C. E.; Ramsey, J. M. *Anal. Chem.* **2003**, *75*, 5646–5655.

(20) Zare, R. N.; Kim, S. *Annu. Rev. Biomed. Eng.* **2010**, *12*, 187–201.

(21) Roper, M. G. *Anal. Chem.* **2016**, *88*, 381–394.

(22) Huang, W. H.; Cheng, W.; Zhang, Z.; Pang, D. W.; Wang, Z. L.; Cheng, J. K.; Cui, D. F. *Anal. Chem.* **2004**, *76*, 483–488.

(23) Ma, C.; Fan, R.; Ahmad, H.; Shi, Q.; Comin-Anduix, B.; Chodon, T.; Koya, R. C.; Liu, C.-C.; Kwong, G. A.; Radu, C. G.; Ribas, A.; Heath, J. R. *Nat. Med.* **2011**, *17*, 738–743.

(24) Clark, A. M.; Sousa, K. M.; Jennings, C.; MacDougald, O. A.; Kennedy, R. T. *Anal. Chem.* **2009**, *81*, 2350–2356.

(25) Dugan, C. E.; Cawthorn, W. P.; MacDougald, O. a.; Kennedy, R. T. *Anal. Bioanal. Chem.* **2014**, *406*, 4851–4859.

(26) Roper, M. G.; Shackman, J. G.; Dahlgren, G. M.; Kennedy, R. T. *Anal. Chem.* **2003**, *75*, 4711–4717.

(27) Shackman, J. G.; Dahlgren, G. M.; Peters, J. L.; Kennedy, R. T. *Lab Chip* **2005**, *5*, 56–63.

(28) Reid, K. R.; Kennedy, R. T. *Anal. Chem.* **2009**, *81*, 6837–6842.

(29) Dishinger, J. F.; Reid, K. R.; Kennedy, R. T. *Anal. Chem.* **2009**, *81*, 3119–3127.

(30) Schultz, N. M.; Huang, L.; Kennedy, R. T. *Anal. Chem.* **1995**, *67*, 924–929.

(31) Kulkarni, R. N. *Int. J. Biochem. Cell Biol.* **2004**, *36*, 365–371.

(32) Henquin, J. C. *Diabetes* **2000**, *49*, 1751–1760.

(33) Muoio, D. M.; Newgard, C. B. *Nat Rev Mol Cell Biol* **2008**, *9*, 193–205.

(34) Kennedy, R. T.; Kauri, L. M.; Dahlgren, G. M.; Jung, S.-K. *Diabetes* **2002**, *51*, S152–S161.

(35) Reshef, L.; Olswang, Y.; Cassuto, H.; Blum, B.; Croniger, C. M.; Kalhan, S. C.; Tilghman, S. M.; Hanson, R. W. *J. Biol. Chem.* **2003**, *278*, 30413–30416.

(36) Dunmore, S. J.; Brown, J. E. P. *J. Endocrinol.* **2013**, *216*, T37–T45.

(37) Wellen, K. E.; Hotamisligil, G. S. *J. Clin. Invest.* **2005**, *115*, 1111–1119.

(38) Brown, J. E. P.; Conner, A. C.; Digby, J. E.; Ward, K. L.; Ramanjaneya, M.; Randeva, H. S.; Dunmore, S. J. *Peptides* **2010**, *31*, 944–949.

(39) Manz, A.; Harrison, D. J.; Verpoorte, E. M. J.; Fettinger, J. C.; Paulus, A.; Lüdi, H.; Widmer, H. M. *J. Chromatogr. A* **1992**, *593*, 253–258.

(40) Stewart, J. M.; Driedzic, W. R.; Berkelaar, J. A. *Biochem. J.* **1991**, *275*, 569–573.

(41) Jacobson, S. C.; Ermakov, S. V.; Ramsey, J. M. *Anal. Chem.* **1999**, *71*, 3273–3276.

(42) Shackman, J. G.; Watson, C. J.; Kennedy, R. T. *J. Chromatogr. A* **2004**, *1040*, 273–282.

(43) Pralong, W. F.; Bartley, C.; Wollheim, C. B. *EMBO J.* **1990**, *9*, 53–60.

(44) Clark, A. M.; Sousa, K. M.; Chisolm, C. N.; MacDougald, O. A.; Kennedy, R. T. *Anal. Bioanal. Chem.* **2010**, *397*, 2939–2947.

(45) Figallo, E.; Cannizzaro, C.; Gerecht, S.; Burdick, J. A.; Langer, R.; Elvassore, N.; Vunjak-Novakovic, G. *Lab Chip* **2007**, *7*, 710–719.

(46) Taylor, J.; Picelli, G.; Harrison, D. J. *Electrophoresis* **2001**, *22*, 3699–3708.

(47) Sera, R. K.; Mcbride, J. M.; Higgins, S. A.; Rodgerson, D. *J. Clin. Lab. Anal.* **1994**, *8*, 81–85.

(48) Abdelmagid, S. A.; Clarke, S. E.; Nielsen, D. E.; Badawi, A.; El-Sohemy, A.; Mutch, D. M.; Ma, D. W. L. *PLoS One* **2015**, *10*, e0116195.

(49) Ma, Y. H.; Wang, J.; Rodd, G. G.; Bolaffi, J. L.; Grodsky, G. M. *Eur. J. Endocrinol.* **1995**, *132*, 370–376.

(50) Nunemaker, C. S.; Wasserman, D. H.; McGuinness, O. P.; Sweet, I. R.; Teague, J. C.; Satin, L. S. *Am. J. Physiol. Endocrinol. Metab.* **2006**, *290*, E523–E529.

(51) Kontrová, K.; Zídková, J.; Bartoš, B.; Skop, V.; Sajdok, J.; Kazdová, L.; Mikulík, K.; Mlejnek, P.; Zídek, V.; Pravenec, M. *Physiol. Res.* **2007**, *56*, 493–496.

(52) Bratanova-Tochkova, T.; Cheng, H.; Daniel, S.; Gunawardana, S.; Liu, Y.; Mulvaney-Musma, J.; Schermerhorn, T.; Straub, S.; Yajima, H.; Sharp, G. *Diabetes* **2002**, *51*, S83–S90.

(53) Tian, G.; Maria Sol, E. R.; Xu, Y.; Shuai, H.; Tengholm, A.; Sol, E. M.; Xu, Y.; Shuai, H.; Tengholm, A. *Diabetes* **2015**, *64*, 904–915.

(54) Alstrup, K. K.; Gregersen, S.; Jensen, H. M.; Thomsen, J. L.; Hermansen, K. *Metabolism* **1999**, *48*, 22–29.

(55) Thams, P.; Capito, K. *Diabetologia* **2001**, *44*, 738–746.

(56) Warnotte, C.; Gilon, P.; Nenquin, M.; Henquin, J. C. *Diabetes* **1994**, *43*, 703–711.

(57) Doliba, N. M.; Qin, W.; Vinogradov, S. A.; Wilson, D. F.; Matschinsky, F. M. *Am. J. Physiol. Metab.* **2010**, *299*, E475–E485.

(58) Tsien, R. Y.; Rink, T. J.; Poenie, M. *Cell Calcium* **1985**, *6*, 145–157.

(59) Gembal, M.; Gilon, P.; Henquin, J. C. *J. Clin. Invest.* **1992**, *89*, 1288–1295.

(60) Sato, Y.; Aizawa, T.; Komatsu, M.; Okada, N.; Yamada, T. *Diabetes* **1992**, *41*, 438–443.

(61) Simon, C.; Brandenberger, G. *Diabetes* **2002**, *51*, S258-61.

(62) Peschke, E.; Peschke, D. *Diabetologia* **1998**, *41*, 1085–1092.

(63) Hirose, H.; Lee, Y. H.; Inman, L. R.; Nagasawa, Y.; Johnson, J. H.; Unger, R. H. *J. Biol. Chem.* **1996**, *271*, 5633–5637.

CHAPTER 4

Microchip for monitoring C-peptide-bearing Superfolder Green Fluorescent Protein (CpepSfGFP) secretion from living islets

Introduction

C-peptide is a short 31-amino-acid peptide connecting insulin A-chain and B-chain in proinsulin, which is subsequently cleaved from the A-chain and B-chain producing mature insulin. A 1:1 mole ratio of C-peptide and insulin is stored in secretory granules of the β-cells and both are released during exocytosis. Therefore, a way to indirectly measure insulin secretion is to measure C-peptide levels.[1]

A visual assessment of pancreatic insulin content would be a useful approach to study the loss of β-cell insulin content, which can be a possible cause of pancreatic exhaustion.[2] However, imaging of insulin in the living animal or humans has not yet been achieved. A potential approach to imaging islets *in vivo* is to image a surrogate of insulin such as C peptide. Our collaborators have developed human proinsulin with C-peptide-bearing Superfolder Green Fluorescent Protein (CpepSfGFP) as a potential dynamic reporter of insulin storage and secretion in situ. To use *in vivo* fluorescence imaging of CpepSfGFP in the pancreas to allow assessment of pancreatic islet insulin, it is necessary to validate the kinetics of the release of insulin and CpepSfGFP are identical. *In vitro* measurement with isolated single islets is a good approach to compare CpepSfGFP and insulin release.

In this chapter, we report on a microfluidic device to monitor C-peptide-bearing Superfolder Green Fluorescent Protein (CpepSfGFP) secretion from single islets. Its kinetics were compared with insulin secretion.

Experimental Section

The microfluidic chip was modified for better performance, as illustrated in **Figure 4.1**. The immunoassay channels were removed to increase sensitivity. Perfusion channels were also removed except the channel for islet perfusion. Chemicals and reagents, microfluidic chip fabrication and operation, detection, were the same as described in chapter 2 besides the following differences.

Islets isolation procedures were the same as chapter 2, except CpepSfGFP transgenic mice were used. Islets were preincubated for 1 h at 37 ˚C in Krebs-Ringer bicarbonate HEPES buffer (KRBH) (concentrations in mM: 4.7 KCl, 115 NaCl, 1.2 KH_2PO_4,1.2 $MgSO_4$, 2.56 $CaCl_2$, 20 $NaHCO_3$, and 16 HEPES; pH 7.2) supplemented with 2.8 mM glucose and 0.7% BSA, followed by 20 min of incubation in KRBH supplemented with 0.7% BSA in the presence of 25 mM glucose. The islets were also perfused with depolarizing KRBH solution (with 60 mM KCl) as positive control.

Results and discussion

Microfluidic Device Overview

The microfluidic device was modified to measure CpepSfGFP secretion from islets as illustrated in **Figure 4.1**. Originally the experiments were attempted with the same microfluidic chip for insulin monitoring (**Figure 2.1**), while the immunoassay channels for FITC-insulin and insulin Ab were not used. However, we observed very weak peak intensity, possibly due to the low fluorescence quantum yield of CpepSfGFP,

and more importantly, due to low abundance of fluorescent labeled C-peptide. To avoid the fluorescent label affecting metabolism, only ~0.04 % of total islet C-peptide were labeled.

Simply adding number of islets did not improve the intensity (for example loading 3 islets did not provide a 3-fold signal enhancement). According to previous investigation, EOF tends to sample solution closest to the inlet of the electrophoretic channels. Although more islets were loaded, the peptide secreted from them may not be well sampled.

Another source of dilution is from the unused immunoassay channels, which were loaded with water. To avoid the dilution, in the new design, immunoassay channels were removed, the cell culture portion was also simplified to a single perfusion channel. Other perfusion channels were also removed because long-term monitoring is not needed in this application.

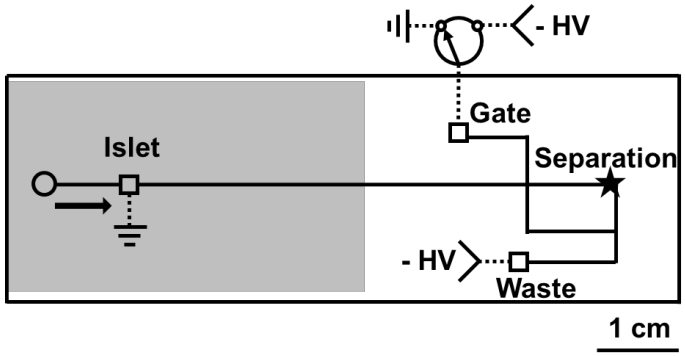

Figure 4.1. Microfluidic chip for monitoring C-peptide secretion from single islet modified from the previous design. In comparison with the microfluidic chip for insulin monitoring (as illustrated in Figure 2.1), the parallel insulin standard channel, immunoassay channels were removed. All the other perfusion channels except for the islet chamber were also removed.

Stably enhanced peak intensity was observed with these steps being taken and the modified chip was used for following experiments. The electropherograms of basal (2.8 mM glucose) and stimulated (25 mM) before and after the microchip modification

were illustrated in **Figure 4.2**, to demonstrate the signal enhancement achieved with the new chip. The results also demonstrated microfluidics techniques' advantage in high sensitivity detection.

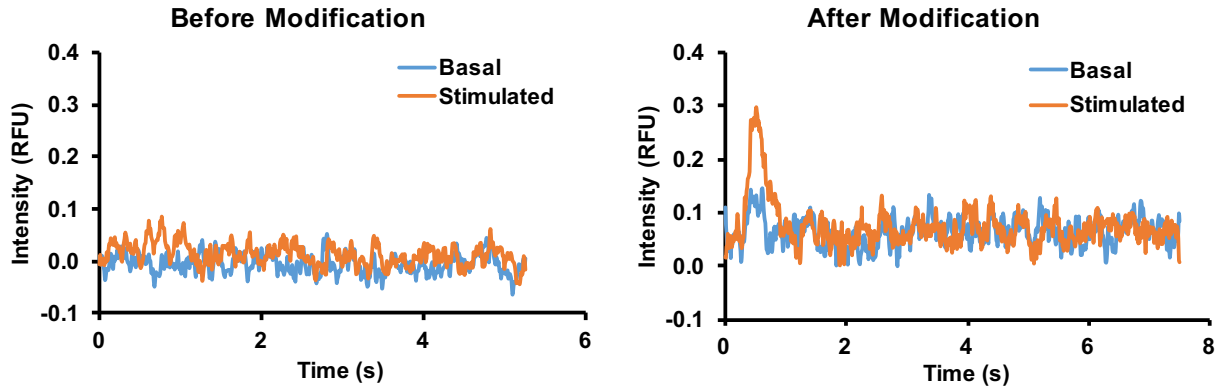

Figure 4.2. Electropherograms of CpepSfGFP before modifying the microchip (left) and after (right). Representative traces of basal (2.8 mM glucose) and stimulated (25 mM glucose) conditions are demonstrated. Overt signal enhancement on both basal and stimulated conditions is observed with the new chip.

C-peptide monitoring

C-peptide was monitored with this device as illustrated in **Figure 4.3**. The C-peptide data is overlaid with insulin data, monitored with capillary electrophoresis immunoassay independently using islets isolated from CD-1 mice (as illustrated in chapter 2 and 3). The results here demonstrate that the kinetics of C-peptide secretion are similar to insulin secretion collected from CD-1 mice islets.

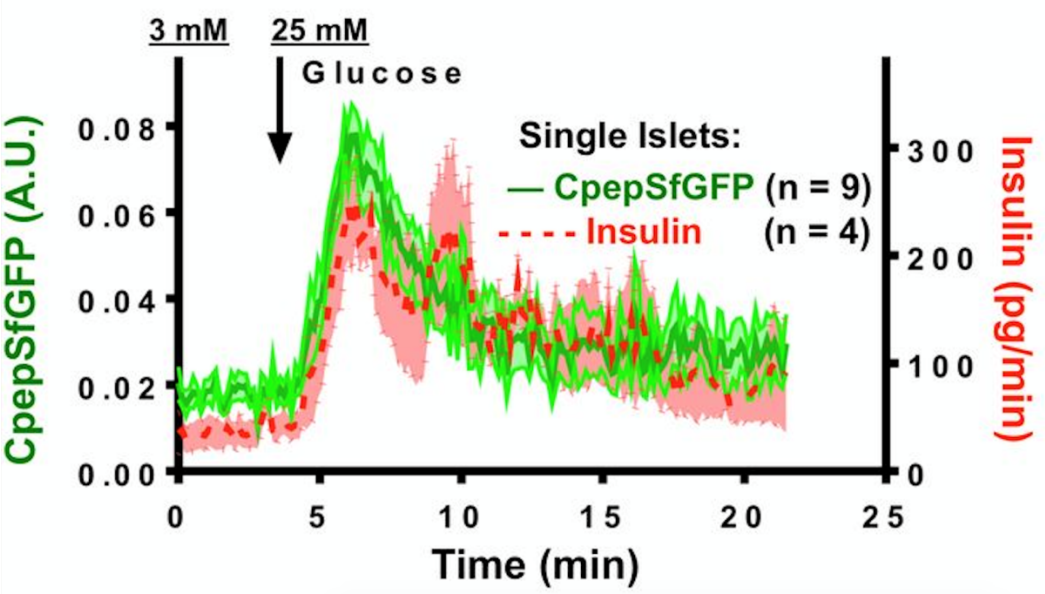

Figure 4.3. Kinetics of transgenic CpepSfGFP and mouse insulin from isolated CpepSfGFP islets. Single islets were perfused at 3 mM glucose and then switched to 25 mM glucose (arrow at top). Single-islet secretion was measured by the release of GFP fluorescence (averaging of nine single-islet traces is shown by the dark solid line, with the lighter surrounding area showing the SEM on these measurements) and by competitive immunoassay for insulin (averaging of four single-islet traces shown in dashed line, with lighter surrounding area showing the SEM of these measurements), both at 8 s intervals throughout a 22.5-min time course.

The islets were also stimulated with 60 mM K^+ as positive control. The results are demonstrated in **Figure 4.4**. Compared with glucose stimulated C-peptide, the profile secreted by K^+ demonstrated slightly steeper response and transient duration.

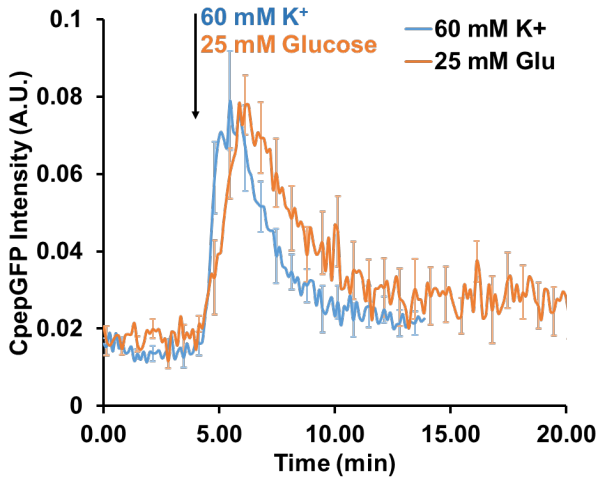

Figure 4.4. Comparison of CpepSfGFP secretion stimulated by 60 mM K^+ and 25 mM glucose. Single islets were pretreated with KRBH supplied with 2.8 mM glucose for 1 h and then switched to 25 mM glucose or 60 mM K^+ as indicated by the arrow. Error bars indicate ± SEM of 9 individual islets in both groups.

The above results show that CpepSfGFP and insulin have similar secretory responses as expected. This result supports the conclusion that monitoring CpepSfGFP is a useful surrogate for estimating insulin secretion. Our collaborators demonstrated the CpepSfGFP could be imaged *in vivo* at the pancreatic surface by fluorescence providing a way to assess pancreatic islet insulin content *in vivo*. In one application investigated in this work, when blood glucose reaches 15 mM, a small subset of islets showed rapid dispossession of a major fraction of their stored CpepSfGFP content, while most islets exhibit no demonstrable CpepSfGFP loss. It strongly suggested that there are "first responder" islets to an *in vivo* glycemic challenge.[3]

Although useful, the goal of this work was still to use CpepSfGFP to indicate insulin action, which made it necessary to prove the kinetics of CpepSfGFP release is identical to insulin. *In vitro*, single islet experiment is an excellent option to study such kinetics to prevent destructive interference of out of phase secretion from multiple islets in a large batch. Automatic high temporal resolved monitoring combining microchip electrophoresis

allowed easy recording of CpepSfGFP secretion profile using single islets, making the kinetics comparison more trustworthy.

Conclusion

A microfluidic chip was developed to monitor fluorescent labeled peptides from single cells. This device was applied to monitor CpepSfGFP secretion from single islets on chip. The results were compared with insulin secretion and suggested identical *in vitro* kinetics.

References

(1) Eaton, R. P.; Allen, R. C.; Schade, D. S.; Erickson, K. M.; Standefer, J. *J. Clin. Endocrinol. Metab.* **1980**, *51*, 520–528.

(2) Alarcon, C.; Boland, B. B.; Uchizono, Y.; Moore, P. C.; Peterson, B.; Rajan, S.; Rhodes, O. S.; Noske, A. B.; Haataja, L.; Arvan, P.; Marsh, B. J.; Austin, J.; Rhodes, C. J. *Diabetes* **2016**, *65*, 438–450.

(3) Stefan, Y.; Meda, P.; Neufeld, M.; Orci, L. *J. Clin. Invest.* **1987**, *80*, 175–183.

CHAPTER 5

Investigation of the Role of X-Box Binding Protein 1 in Insulin Regulated Pancreatic α-cell Function

Introduction

It has been known that hyperglucagonemia caused by α-cell dysfunction is a feature of overt type 2 diabetes;[1–3] but, the mechanism contributing to the hypersecretion is not fully understood. In addition to glucose[4], previous studies found that insulin signaling in α-cells is critical to the regulation of glucagon secretion.[5,6] Impaired insulin signaling in α-cells leads to enhanced glucagon secretion.[6,7]

Gradual loss of β-cell mass is a notable feature in type 2 diabetes patients, while α-cell's mass is maintained relatively intact.[8] Endoplasmic reticulum (ER) stress has been proposed as one factor contributing to reduced β-cell mass,[9,10] but its role in α-cell biology is less known. Unfolded protein response (UPR) is an important process in development of ER stress. XBP1 is a transcription factor that plays a critical role in mediating the UPR. A recent study reported that β-cell specific XBP1-deficient mice exhibit β-cell dysfunction.[11]

The goal of this collaborative work is to study the role of XBP1 in α-cells. In vivo (α-cell-specific XBP1 knockout mice) and *in vitro* (stable XBP1 knockdown and overexpression α-cell lines) models were prepared by collaborating labs. Ca^{2+} influx is

the trigger of exocytosis of hormones including insulin and glucagon. Cytoplasmic Ca^{2+} concentration ($[Ca^{2+}]$) is an important parameter to assess the mechanism of dysregulation of glucagon secretion in the cells. In our work, XBP1 knockdown and overexpression α-cell lines' $[Ca^{2+}]$ were measured *in vitro* and compared with the control groups.

Fluorescence imaging is a promising and widely used technique for studying living cells. Intracellular Ca^{2+} measurements were revolutionized after the advent of cell-permeant Fura-2, a Ca^{2+} sensitive fluorescent dye.[12] Its excitation wavelength shifts from 380 nm to 340 nm upon Ca^{2+} binding, and the ratio of the integrated intensities of the fluorescence emission from 340 and 380 nm excitation allows for quantitation of intracellular Ca^{2+} following calibration.

Conventional Ca^{2+} measurements are usually performed with cells affixed on a coverslip that is sealed into a chamber with approximately 3 mL volume. The chamber is perfused with a peristaltic pump. Although it has been applied in many applications, the drawbacks include large volume of media consumed and difficulty precisely controlling the cell culture environment. The microfluidic chip for Ca^{2+} imaging may allow rapid and precise introduction of fresh media to the cells. Several microfluidic devices have been implemented for intracellular $[Ca^{2+}]$ imaging recently.[13–15] Two such microfluidic devices are illustrated in **Figure 5.1**. Our research group also have developed microfluidic devices for Ca^{2+} imaging in pancreas islets.[16]

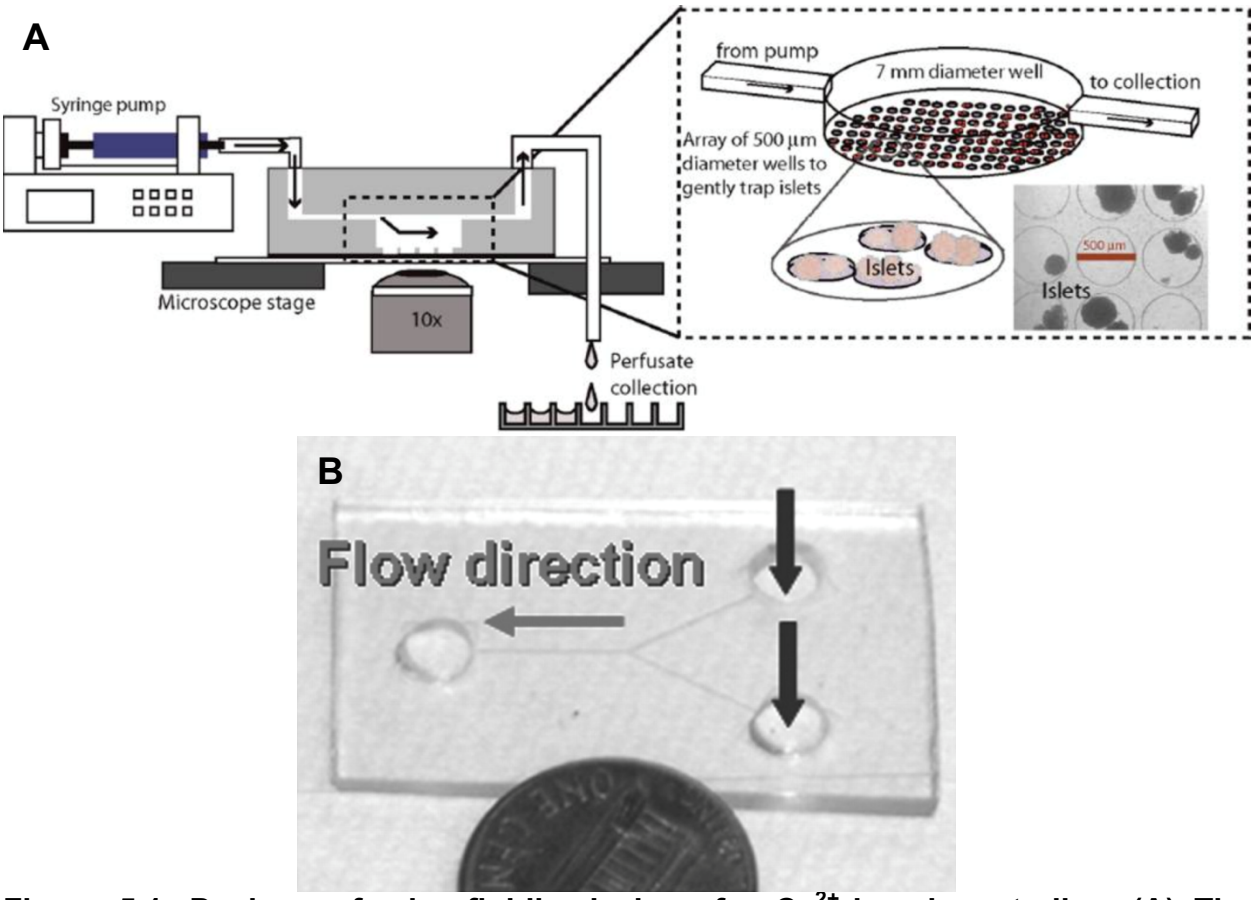

Figure 5.1. Designs of microfluidic devices for Ca^{2+} imaging studies. (A) The schematic on the left depicts the cross-section view and experiment setup and the isometric view of the PDMS device is shown in the inserted image. The chip contains three layers: The bottom layer consists of an array of small circular wells (500 μm diameter) to immobilize the islets; a middle layer consists of the 7 mm diameter circular well; and the top layer of the microfluidic channels. (B) A PDMS microfluidic device reversibly sealed by positioning onto a glass coverslip. Cells were loaded into the Y-microfluidic channel and allowed 45 min to adhere before [Ca^{2+}] monitoring. Arrows indicate perfusion direction. Reproduced from reference 13 and 15.

Here we demonstrate a polydimethylsiloxane (PDMS)/glass hybrid microfluidic chip for Ca^{2+} imaging applications. This device can accommodate a 5 × 5 mm square coverslip loaded with cells, and allows continuous perfusion over them during measurement. Excess buffer is removed from the top of the cell chamber and the temperature is well controlled. The reusable device is easy to fabricate and maintain, and allows easy cell loading and removing.

Experimental Section

Chemical and Reagents

Cell culture reagents were purchased from Life Technologies (Carlsbad, CA). Human insulin, dimethyl sulfoxide (DMSO), and hexamethyldisilazane (HMDS) were obtained from Sigma (St. Louis, MO). All other chemicals were from Fisher (Pittsburgh, PA). Krebs Ringer buffer (KRB) contained (in mM): 118 NaCl, 5.4 KCl, 2.4 $CaCl_2$, 1.2 $MgSO_4$, 1.2 KH_2PO_4, 20 HEPES and 0.5/25 glucose.

Microfluidic Chip Fabrication

The double layer PDMS portion of the device was fabricated with soft lithography techniques as previously described.[17–19] All the PDMS used in the chip fabrication was RTV-615 (Curbell Plastics, Livonia, MI) and had a base to curing agent ratio of 10:1. To fabricate the PDMS layer with microfluidic channels, HMDS was spun on a 3-in. silicon wafer (University Wafer, Boston, MA) to facilitate photoresist adhesion. SU-8 2075 photoresist (MicroChem, Newton, MA) was spun onto the wafer to create a 60 μm layer and was patterned using a dark-field photomask with the design shown as the black lines in **Figure 5.2**. A thick layer (~5 mm) of PDMS was poured over the mold and heated to 80 °C for at least 30 min. A ~0.5-mm-thick layer was created by pouring PDMS over a blank silicon wafer. It was allowed to settle for 10 min before heated to 80 °C for at least 30 min. Both layers were peeled away from the mold and bonded together using corona discharge and heated to 80 °C for 15 min. The bulk PDMS piece was cut to small pieces according to predefined rectangle shapes on the mold. The ends of the channels on each piece were exposed. A 7 mm diameter hole was punched at the center of each PDMS part as a cell chamber. Each piece was bonded to a glass

coverslip (Corning Cover glass, 50 x 24mm, Fisher) using corona discharge and heated again to 80 °C for 15 min.

Microfluidic Chip Operation

Fluidic connections were made by inserting 150 µm ID/ 360 µm OD fused silica capillaries (PolyMicro Technologies, Phoenix, AZ) to the beginning of the flow splitter from the open ends of the channels, as illustrated in **Figure 5.2**. The other ends of the capillaries were connected to perfusion buffer, pressurized with 30 psi of helium. Flow rate was adjusted to 40 µL min^{-1} on both sides to achieve a total flow rate of 80 µL min^{-1}. Two high pressure chambers were connected to a 4-port valve (VICI Valco Instruments, Houston, TX) allowing switching buffer during experiments without stop of perfusion during experiments.

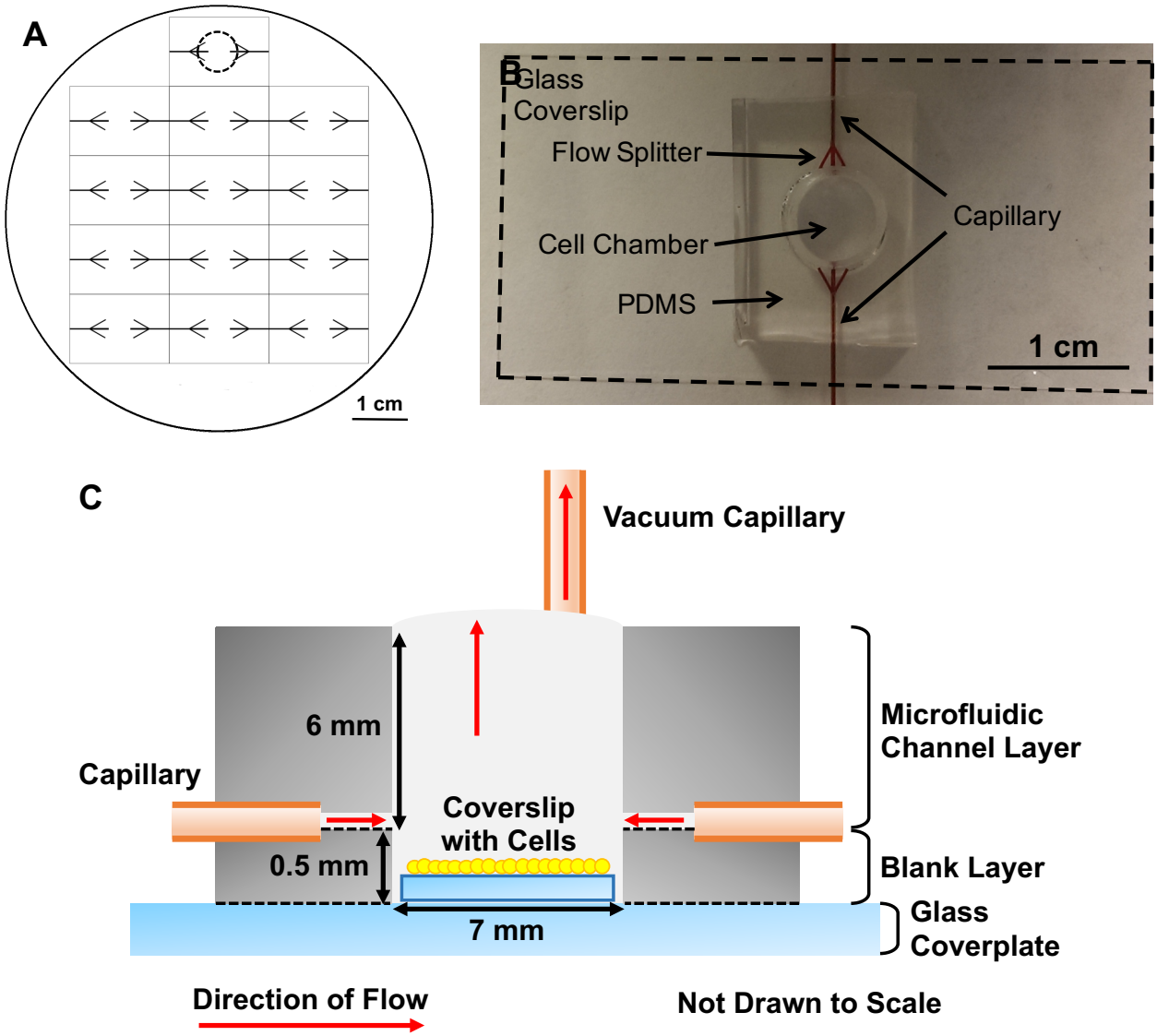

Figure 5.2. Open-top PDMS/glass microfluidic chip for Ca^{2+} imaging. (A) Design of the mold pattern for microfluidic channels. Solid lines indicate mold on a 3-in. silicon wafer (200 μm wide and 60 μm high). PDMS was poured on the mold and peeled away after dry, and cut to small rectangle pieces guided by the solid lines on mold. A dashed circle on the top-mid piece illustrates the location to punch the cell chamber. (B) Top view of a microfluidic chip. Dashed rectangle shape indicates the glass coverplate, where the PDMS piece is glued onto. Capillaries were inserted from the open end of the microfluidic channels on the side for fluidic access. The flow splitters are filled with red color food dye. (C) Side view of the microfluidic chip. The dashed lines represent the interfaces between layers bonded by corona discharge. Capillaries introduce buffer to the inlet of the flow splitters to allow uniform fluid profile in the cell chamber. Excess buffer is constantly removed on top of the cell chamber by a capillary connected to vacuum.

Cell Culture

Glucagon-secreting αTC6 cells were obtained from our collaborator and cultured as reported previously.[20] They were normally maintained in Corning 75 cm^2 cell culture flasks (Fisher). For Ca^{2+} imaging experiments, glass coverslips were cut to 5 × 5 mm squares. The coverslips were sterilized in 70% ethanol for at least 1 h and then dried in a sterile culture hood. Three to four coverslips were placed in each 35-mm petri dishes using sterile tweezers prior to seeding the cells. Cells were detached from the culture flasks with trypsin (0.25%, Life Technologies) and seeded to the petri dishes. Experiments were performed using 80-90% confluent cells. Cells were cultured in Dulbecco's modified Eagle's media containing 25mM glucose (DMEM, Life Technologies) supplemented with 10% fetal bovine serum (Life Technologies) and 100 unites mL^{-1} Penicillin/Streptomycin (Life Technologies) and stored in an incubator with 5 % CO_2.

Computational Modeling

Perfusion of the cell chambers was modeled using COMSOL Muitiphysics (COMSOL, Inc., Burlington, MA). The "laminar flow" and transport of diluted species models were used to monitor the flow split and theoretical temporal resolution. All simulations assumed water perfusion through the chip, with a density of 998 kg m^{-3} and a viscosity of 1.002×10^{-3} Pa·s' (20 °C). The cell chamber had dimensions of 7 mm diameter × 5 mm. The inlet channels for the cell chamber were modeled in 2D with the shallow channel set to 60 μm tall. The cell chamber inlet flow rate was set at 20 μL min^{-1} on both sides.

Cell Preparation and Loading

Cell permeable Fura-2-acetoxymethyl ester (Fura-2 AM, Life Technologies) was dissolved in DMSO to create a stock concentration of 1 mM. Prior to loading on the chip, the coverslip with cells to be measured was transferred to DMEM culture media with 0.5 mM glucose and 2 μM Fura-2 for 45 min at 37 °C to load with dye. The microfluidic chip was rinsed with 70% ethanol, water and 0.5 mM glucose KRB sequentially, with 80 μL KRB added to the cell chamber and filled in the perfusion channels. The cells were gently rinsed with 0.5 mM glucose KRB in another petri dish and loaded on the chip. After connected to perfusion, the cells were perfused with 0.5 mM glucose KRB for 10 min in dark (without measuring), before being treated with different conditions to measure [Ca^{2+}]. KRB containing 30 mM KCl was applied at the end of each experiments as positive control. A temperature probe was inserted to the bottom of the chamber to keep tracking it. The temperature was maintained at 37 °C with heating strip adhering at the bottom of the chip.

[Ca^{2+}] Measurements

The chip was placed atop the stage of a Nikon Diaphot 300 microscope. Fura-2 was alternately excited using a filter wheel with 340 and 380 nm light from a Xenon-arc lamp. The fluorescence emission from both excitation wavelengths was collected through a 510 ± 10 nm bandpass filter. Fluorescent images were collected at 1 Hz. Metamorph software was used to select single cells and integrate the intensity. [Ca^{2+}] was determined by calculating the calculating the ratio of the emission at 340 and 380 nm excitation following calibration. The calibration procedures can be found in previous works.[21]

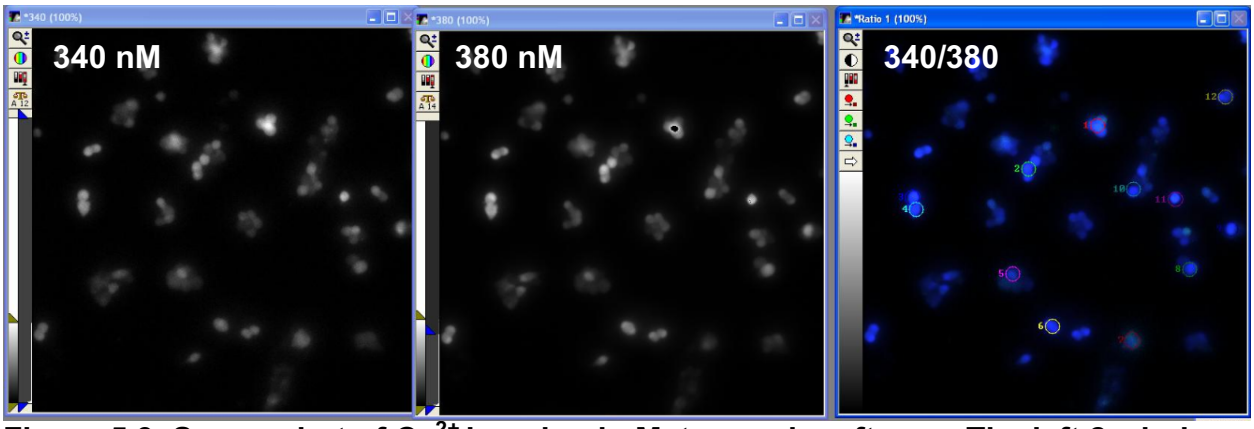

Figure 5.3. Screenshot of Ca^{2+} imaging in Metamorph software. The left 2 windows illustrate cells' fluorescent images when excited by 340 and 380 nM light. The ratio of 340/380 is demonstrated in the 3rd window. Several cells were selected as the colorful circles illustrated in the 3rd window and the average ratios of the emission were tracked to calculate [Ca^{2+}].

Statistical analysis

All data are expressed as mean ±SE and were analyzed with an unpaired two-tailed Student t test or ANOVA as appropriate. Differences were considered significant at $p < 0.05$.

Results and discussion

Overview of microfluidic chip design

A reversibly sealed chip was applied for Ca^{2+} imaging previously in our group.[22] Cells were also loaded on the chip with a coverslip and sealed in the middle of 2 pieces of glass or PDMS for measurements. Although useful, that design was relatively hard to operate and prone to leakage. Moreover, the reversible design allows further use of perfusate at downstream for measurements or other application (e.g. co-culture as illustrated in chapter 3), while such applications are not needed in Ca^{2+} measurement.

The open-top PDMS/glass microfluidic chip (**Figure 5.2**) we designed in this work allowed easier cell loading and removal and chip operation than the reversibly sealed chip. It also avoids leakage. In this application, temperature of the media at the bottom

of the cell chamber can be easily measured by inserting the temperature probe into the chamber. Other applications like electrochemistry measurements near cell can also be achieved if necessary.

In designing the microfluidic chip, the side-view illustrated in **Figure 5.2** demonstrated the 3-layer design: a thick layer with microfluidic channels, a blank thin layer and a glass coverslip supporting layer. The thin PDMS layer lifts the perfusion channels to allow fluid perfusing through the upper surface of the cells, preventing shear stress on the cells. The thin glass coverslip was applied as the supporting layer to fit the short working distance of the objective on the microscope. 13 microfluidic chips can be prepared once with one mold.

The 5 × 5 mm square coverslip helped better stabilize its position in the cell chamber. It matches the size of the 7 mm diameter cell chamber with 4 corners reaching the edge of the cell chamber. This snug fit prevented coverslip shifts during experiments.

Chip characterization

To assist in determining the flow conditions, a COMSOL model was developed to simulate the cell chamber as illustrated in **Figure 5.4**. Two rectangular shapes were labeled near the bottom of the cell chamber to mimic different areas of the coverslip and the mean concentration of each are probed.

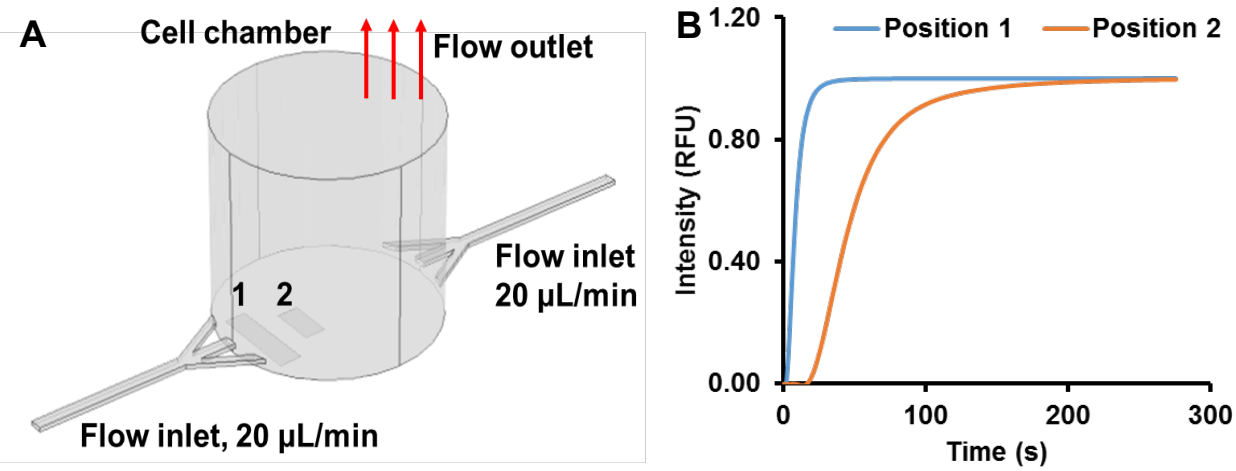

Figure 5.4. The cell chamber model built with COMSOL software and the mean concentration of different areas labeled near the bottom of the cell chamber. Flow rate from both ends were set at 20 µL min^{-1}. Top of the cell chamber was set as the flow outlet. Time resolved intensity change is illustrated while position 1 and 2 (B) are associated with the 1 and 2 labeled in the model (A).

Setting flow rate at 40 µL min^{-1}, the model suggested that the parts closest to the perfusion channel had almost instant response and rise time, while closer to the center, the delay time was 26 s and rise time from 10% to 90% was 64 s. Food dye was applied to measure the delay time in the capillary when switching buffer, which was found to be 8.7 ± 0.4 s. Food dye diffusion in the cell chamber is difficult to quantify, but the color was observed in the center of the chamber within 1 min.

In real cell culture experiments, only a small area of cells was aligned with the microscope objective for imaging (< 2 mm diameter circle). This characterization suggested using cells closer to the perfusion channel for faster response. Another way to evaluate rise and delay time was to 30 mM KCl to cells at the end of the experiment. High concentration KCl causes closure of K_{ATP} channel on the cell membrane to induce almost instant Ca^{2+} influx. The time from switching to 30 mM KCl to observance of K^+ induced Ca^{2+} influx, including delay and rise time in both the perfusion capillary and the cell chamber, was used as dead time and corrected for each measurement.

[Ca^{2+}] measurements

To access the mechanism of dysregulation of glucagon secretion in αTC6 cells, XBP1 knockdown cells (αXBPKD), control cells for KD, XBP1 overexpressing cells (αXBPOE) and control for OE were perfused with glucose concentrations of 0.5 mM, 25 mM and 25 mM + 100 nM insulin sequentially. Representative [Ca^{2+}] profiles of each cell type are illustrated in **Figure 5.5**. Our results show that these cells displayed bursts or spikes of Ca^{2+} that were modulated by different conditions. The data were analyzed by counting the [Ca^{2+}] spike per unit time as illustrated in previous reports.[4]

Consistent with previous reports[4,23], [Ca^{2+}] spikes in control cells were dampened by application of high glucose and insulin. A similar trend was evident in αXBPKD cells, but the response to high glucose and insulin was blunted compared with control cells. Meanwhile, the average [Ca^{2+}] level in αXBPKD cells was not significantly different from control cells in all different glucose conditions and with 100 nM insulin. The basal [Ca^{2+}] was significantly higher in αXBPOE cells compared with controls, although the [Ca^{2+}] spikes were similar between them. Although increased glucagon secretion was found in αXBPKD cells in the collaborative work,[24] the Ca^{2+} data suggest that [Ca^{2+}] alterations are not likely to underlie the dysregulation of glucagon secretion in XBP1 deficient α-cells. The lack of [Ca^{2+}] alteration in αXBPKD cells helped to draw the conclusion that cAMP[25] is a dominant second messenger in the regulation of glucagon secretion in α-cells with other experiments performed. This conclusion is consistent with a previous report that glucagon secretion at high glucose concentration does not require elevation of [Ca^{2+}].[22]

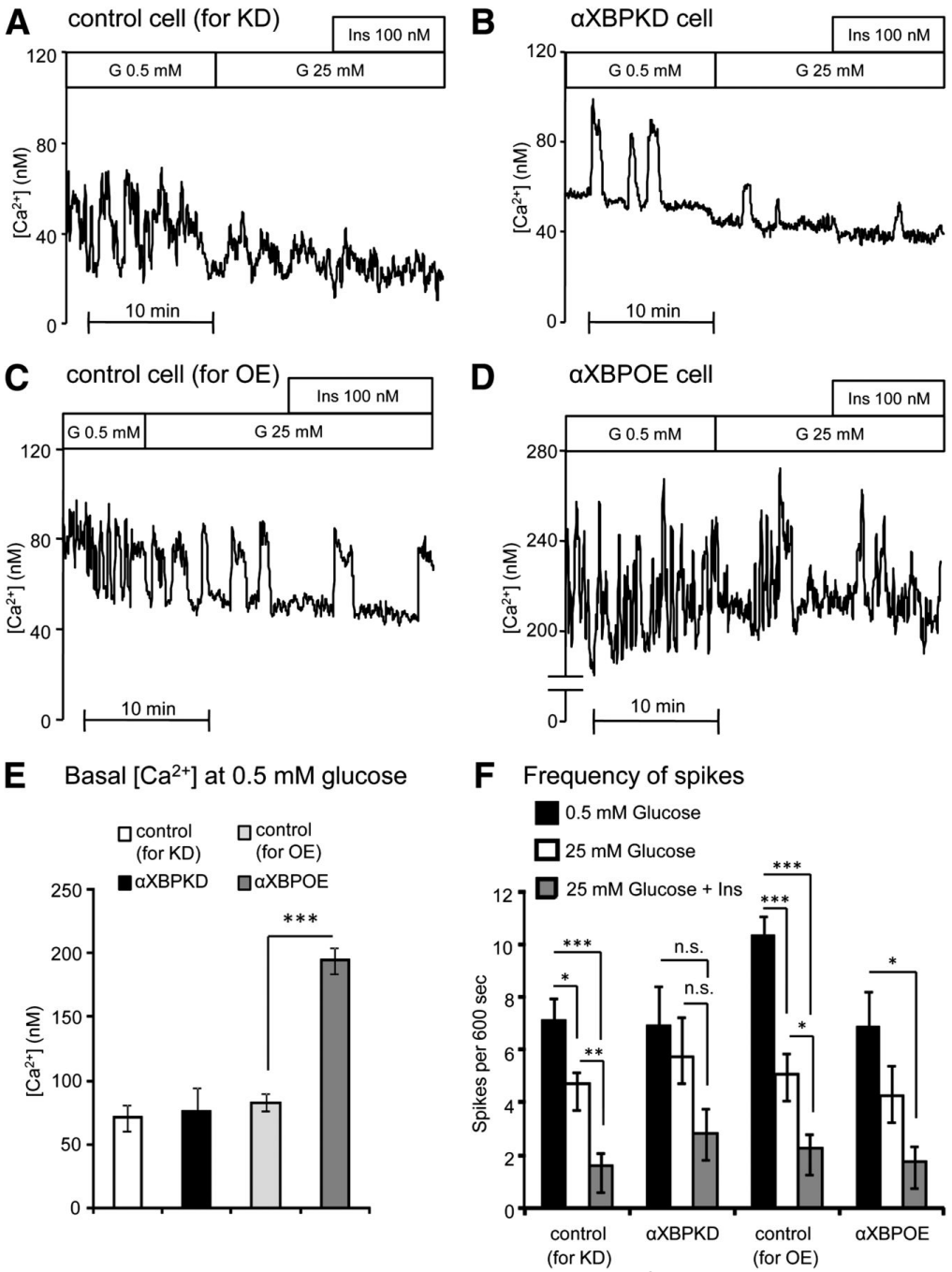

Figure 5.5. Effects of altered XBP1 expression on [Ca^{2+}] in aTC6 cells. The glucose (G) concentration was increased from 0.5 to 25 mM, and 100 nM human insulin was present as indicated. Representative traces are shown of single cells from control for KD (A), aXBPKD cell (B), control for OE (C), and aXBPOE cells (D). E: Basal [Ca^{2+}] is shown for each group (n = 9-15 in each group). Data are expressed as means ± SEM. ***P < 0.0001. F: Quantification of frequency of spikes from each group (n = 8-16). Data are expressed as means ± SEM. *P < 0.05, **P < 0.01, ***P < 0.001; n.s., not significant.

Conclusion

We have demonstrated a PDMS/glass hybrid microchip for Ca^{2+} imaging studies. The device is convenient to fabricate, and the open-top design allows easy cell manipulation and chip operation. Compared to previous developments, it has small chamber volume allowing fast buffer changing. The recessed well also prevent shear stress applied on cells. It has been applied in a biological study to compare [Ca^{2+}] among different cell types.

References

(1) Unger, R. H.; Aguilar-Parada, E.; Müller, W. A.; Eisentraut, A. M. *J. Clin. Invest.* **1970**, *49*, 837–848.

(2) Reaven, G. M.; Chen, Y. D. I.; Golay, A.; Swislocki, A. L. M.; Jaspan, J. B. *J. Clin. Endocrinol. Metab.* **1987**, *64*, 106–110.

(3) Baron, A. D.; Schaeffer, L.; Shragg, P.; Kolterman, O. G. *Diabetes* **1987**, *36*, 274–283.

(4) Ravier, M. A.; Rutter, G. A. *Diabetes* **2005**, *54*, 1789–1797.

(5) Moses, A. C.; Cohen, K. L.; Johnsonbaugh, R.; Peter Nissley, S. *J. Clin. Endocrinol. Metab.* **1978**, *46*, 937–946.

(6) Kawamori, D.; Kurpad, A. J.; Hu, J.; Liew, C. W.; Shih, J. L.; Ford, E. L.; Herrera, P. L.; Polonsky, K. S.; McGuinness, O. P.; Kulkarni, R. N. *Cell Metab.* **2009**, *9*, 350–361.

(7) Gerich, J. E.; Tsalikian, E.; Lorenzi, M.; Schneider, V.; Bohannon, N. V; Gustafson, G.; Karam, J. H. *J Clin Endocrinol Metab* **1975**, *41*, 1178–1180.

(8) Yoon, K. H.; Ko, S. H.; Cho, J. H.; Lee, J. M.; Ahn, Y. B.; Song, K. H.; Yoo, S. J.; Kang, M. Il; Cha, B. Y.; Lee, K. W.; Son, H. Y.; Kang, S. K.; Kim, H. S.; Lee, I. K.; Bonner-Weir, S. *J. Clin. Endocrinol. Metab.* **2003**, *88*, 2300–2308.

(9) Marchetti, P.; Bugliani, M.; Lupi, R.; Marselli, L.; Masini, M.; Boggi, U.; Filipponi, F.; Weir, G. C.; Eizirik, D. L.; Cnop, M. *Diabetologia* **2007**, *50*, 2486–2494.

(10) Eizirik, D. L.; Cardozo, A. K.; Cnop, M. *Endocr. Rev.* **2008**, *29*, 42–61.

(11) Lee, A.-H.; Heidtman, K.; Hotamisligil, G. S.; Glimcher, L. H. *Proc. Natl. Acad. Sci. U. S. A.* **2011**, *108*, 8885–8890.

(12) Tsien, R. Y.; Rink, T. J.; Poenie, M. *Cell Calcium* **1985**, *6*, 145–157.

(13) Mohammed, J. S.; Wang, Y.; Harvat, T. A.; Oberholzer, J.; Eddington, D. T. *Lab Chip* **2009**, *9*, 97–106.

(14) Tran, L.; Farinas, J.; Ruslim-Litrus, L.; Conley, P. B.; Muir, C.; Munnelly, K.; Sedlock, D. M.; Cherbavaz, D. B. *Anal. Biochem.* **2005**, *341*, 361–368.

(15) Chao, P.-H. G.; West, A. C.; Hung, C. T. *Am. J. Physiol. Cell Physiol.* **2006**, *291*, C718–C725.

(16) Morioka, T.; Dishinger, J. F.; Reid, K. R.; Liew, C. W.; Zhang, T.; Inaba, M.; Kennedy, R. T.; Kulkarni, R. N. *Mol. Endocrinol.* **2012**, *26*, 967–976.

(17) Unger, M. A.; Chou, H. P.; Thorsen, T.; Scherer, A.; Quake, S. R. *Science* **2000**, *288*, 113–116.

(18) Ng, J. M. K.; Gitlin, I.; Stroock, A. D.; Whitesides, G. M. *Electrophoresis* **2002**, *23*, 3461–3473.

(19) McDonald, J. C.; Duffy, D. C.; Anderson, J. R.; Chiu, D. T.; Wu, H.; Schueller, O. J.; Whitesides, G. M. *Electrophoresis* **2000**, *21*, 27–40.

(20) Philippe, J. *J. Clin. Invest.* **1989**, *84*, 672–677.

(21) Reid, K. R. PhD. Dissertation, University of Michigan, 2009.

(22) Clark, A. M.; Sousa, K. M.; Chisolm, C. N.; MacDougald, O. A.; Kennedy, R. T. *Anal. Bioanal. Chem.* **2010**, *397*, 2939–2947.

(23) Salehi, A.; Vieira, E.; Gylfe, E. *Diabetes* **2006**, *55*, 2318–2323.

(24) Akiyama, M.; Liew, C. W.; Lu, S.; Hu, J.; Martinez, R.; Hambro, B.; Kennedy, R. T.; Kulkarni, R. N. *Diabetes* **2013**, *62*, 2439–2449.

(25) Tian, G.; Sandler, S.; Gylfe, E.; Tengholm, A. *Diabetes* **2011**, *60*, 1535–1543.

CHAPTER 6

Summary and Future Directions

Summary

The overall goal of this work was to develop, refine, and apply new analytical instrumentation to study islets of Langerhans functions. Generally, we developed novel analytical tools and techniques to study insulin secretion, C-peptide secretion, and Ca^{2+} influx. The novel microfluidic device also allowed cell-cell interaction studies. Although islets, pancreatic α-cells and adipocytes are the model systems applied in this study, the developed analytical technology can be used to study other biological cells or systems.

Microchip Electrophoresis for Chemical Gradient Generation and Long-term Operation

The first tool was a microchip electrophoresis device for long-term cell culture and chemical monitoring, incorporating a method to automatically generate arbitrary glucose profiles and a method for automated calibration at defined times.

Insulin secreted from the islets was measured at 5-10 s intervals by an electrophoretic competitive immunoassay. Every few hours, a single pole double throw (SPDT) relay controlled electrical connection moved from the islet reservoir to the parallel insulin standard reservoir, allowing the electrophoretic sampling of insulin standards while maintaining the islet under perfusion.

Single islets were perfused with different concentration of glucose. Processes of sampling of insulin secreted by the islet, insulin and FITC-insulin mixing and their competitively reacting with insulin antibody were achieved by electroosmotic flow (EOF). A high-voltage relay will control continuous injection of sample plug to the separation channel, where free FITC-insulin and FITC-insulin bound to antibody were separated. The integrated system can perform 14,000 electrophoresis assays in 24 h and automatically control culture condition, thus allowing continuous monitoring of insulin under well-controlled conditions.

To control glucose, the system incorporates two independent syringe pumps loaded with low and high concentration glucose. Flow rates of both were controlled by a home-made LabView program. By mixing 2 syringe pumps' contents at different flow rates through a tee fabricated on the electrophoresis chip, arbitrary glucose gradients can be generated. The glucose gradient was applied to measure glucose sensitivity of islets exposed to various glucose concentrations overnight *in vitro*. The concentrations of glucose that able to trigger measureable insulin secretion were progressively reduced by 3 mM, 11 mM or 11 mM + Diazoxide (an insulin secretion inhibition drug) overnight treatment, suggesting an increase in glucose sensitivity.

A Microchip Electrophoresis System to Study Cell-cell Interactions

A microchip electrophoresis device was developed to study the impact of adipocytes on islet insulin secretion by co-culture both cells. During co-culture, buffer was pumped onto the chip through adipocytes and islets. Palmitic acid with concentration similar to the NEFAs secreted by adipocytes were used to treat islets as positive controls. During chemical monitoring, perfusion through adipocytes was

stopped and buffer was perfused directly to islets through a side channel. Insulin concentration was measured with the same manner as illustrated with the long-term chip.

Our work demonstrated that 3 h pretreatment with 80 μM palmitic acid enhances insulin secretion, suggesting short-term FFA treatment is a positive regulator of insulin secretion. The 2-fold augmentation compared with equivalent fatty acid (80 μM) stimulated by adipocytes may be due to either the mix of NEFAs that are released or to other secretory products such as adipokines. Although further validation may be required, the results here demonstrates the first positive regulation of short-term adipocytes pretreatment on insulin secretion, with potential amplified effects results from adipokines interplay.

Microchip for monitoring C-peptide-bearing Superfolder Green Fluorescent Protein (CpepSfGFP) Secretion from Living Islets

A microfluidic chip was developed to measure low concentration fluorescent labeled peptides. Modifications were made on the previously developed immunoassay chip by removing immunoassay channels to prevent dilution. The chip was applied to measure islet C-peptide-bearing Superfolder Green Fluorescent Protein (CpepSfGFP) secretion. To avoid the fluorescent label affecting metabolism, only ~0.04 % of total C-peptide were labeled, resulting in a very low signal intensity of C-peptide. With the modification applied, signal of CpepSfGFP was detected. Its intensity also increased when the islets were stimulated with high glucose. By comparing this results with insulin secretion, it was concluded that CpepSfGFP has identical *in vitro* kinetics with insulin secretion.

Investigation of the Role of X-Box Binding Protein 1 in Insulin Regulated Pancreatic α-cell Function with Ca^{2+} influx measurements

A polydimethylsiloxane (PDMS)/glass hybrid microfluidic chip for Ca^{2+} imaging applications was developed. This device can accommodate a 5 × 5 mm square coverslip loaded with cells, and allows continuous perfusion over them during measurement. Excess buffer is removed from the top of the cell chamber and the temperature is well controlled. The reusable device is easy to fabricate and maintain, and allows easy cell loading and removing.

The chip was applied to measure Ca^{2+} influx to study the role of XBP1 in pancreatic α-cell. XBP1 is a transcription factor that plays a critical role in mediating the Unfolded protein response (UPR). XBP1 deficiency in pancreatic β-cell has been reported causing β-cell dysfunction. Stable XBP1 knockdown and overexpression α-cell lines' [Ca^{2+}] were measured *in vitro*. Significant [Ca^{2+}] level alterations were observed, suggesting that [Ca^{2+}] alterations are not likely to underlie the dysregulation of glucagon secretion in XBP1 deficient α-cells.

Future Directions

Several advancements can be made to the devices studied and developed in this dissertation. For the long-term microchip, our goal is to develop a system combining automatic control of culture condition and long-term stability. The system can be improved in 2 aspects. To keep the cells healthy on chip for longer time, the perfusion media can be optimized to supply more nutrients. Improvements can also be applied to increase the stability of long-term electrophoresis operation.

For the cell-cell interaction studies, based on existing results, several directions can be further investigated including comparing short-term and long-term treatments, and applying inflamed adipocytes for co-culture, which are likely to impair islets' insulin function. The microchip can also be further developed to monitor multiple islets in parallel to improve throughput.

Improvement of Perfusion of Islets on Long-term Electrophoresis Chip

Although the islets studied in Chapter 2 of this paper exhibited intact shape and normal insulin secretion dynamics for more than 24 h, the islets were perfused with BSS buffer, which only contains necessary salts and glucose. It is more appropriate and desired to supply more nutrients allowing more optimized *in vitro* environment for the islets and potentially longer-term culture. Commercial cell culture medias such as RPMI 1640 or DMEM are not applicable for the reason as discussed previously[1], primarily due to the incompatibility between phosphate buffer system and relatively high concentration Ca^{2+} demand for insulin secretion. Compensating Ca^{2+} to a final 2.4 mM concentration in RPMI 1640 was attempted, but caused sedimentation in the media. Adding BSA or fetal bovine serum (FBS) to phosphate-free buffer (like Balanced salt solution) was another approach attempted to provide nutrients, however, protein can be attracted to the wall of the capillary. Existence of too much protein prevents EOF, making it incompatible with electrophoresis. Investigation done in this work showed 2% BSA already affected the EOF and caused broadened electropherograms. Although such buffer may not be appropriate for electrophoresis, they are still good candidates for on-chip cell culture. A potential practice is to apply protein rich buffer during cell culture (pretreatment), rinse and perform electrophoresis measurements with buffers containing

less protein. Besides proteins, to provide multi-vitamin and amino acid for the cells by adding them to the BSS buffer can also be an important portion to supply more nutrients. These methods require further investigation and optimization to achieve better performance.

Improvement of Long-term Stability of Electrophoresis

To better mimic *in vivo* glucose profile is our goal with the microchip electrophoresis. As illustrated in **Figure 1.7**, blood glucose profiles in animals usually fluctuate. Such profiles can be mimicked by the programmable gradient generator, and it has been applied to study glucose sensitivity of islets. However, to investigate long-term insulin studies with more physiologically relevant glucose patterns, the more challenging portion is to maintain the electrophoresis stable for more than 24 h. Although such time span has been achieved in this dissertation, the success rate was not sufficient to consistently replicate the experiments allowing biological conclusions being drawn. The main challenge to overcome, at least as perceived in my work, is clogs in the microfluidic channels.

The two main sources of clogs are broken tissue parts leaking into channels and buffer salts sedimentation. They were alleviated by improving cell culture and preventing salts sedimentation, as discussed in chapter 2. However, although clogs were well contained for short-term experiments (3-5 h), they still frequently happened after 12 h electrophoresis operating.

As discussed in chapter 2, all electrophoresis buffers were continuously perfused to keep fresh, when buffer vials were stored in room temperature for 24 h. Assuming such condition may lead to buffer degradation, measures were taken by storing

perfusion buffer in ice bath or changing fresh buffer preserved in fridge every few hours. However, these steps did not show significant improvement on electrophoresis stability. Another hypothesis is gradual sedimentation still builds up in channel due to electrolysis, despite the buffers are continuously refreshed. Mixing buffers with different recipe in such small channel can make the situation more severe. One way to alleviate effects of electrolysis is to apply high voltage with less amount of time. As illustrated in **Figure 6.1**, the constant high voltage at waste reservoir can be replaced by a relay, switching between high voltage and ground. During a long-term monitoring, by programming the position of the added relay, electrophoresis can be turned on and off performed intermittently (e.g. every 30 min). Although some secretion information is not recorded, it may worth the trade off if monitoring time can be extended.

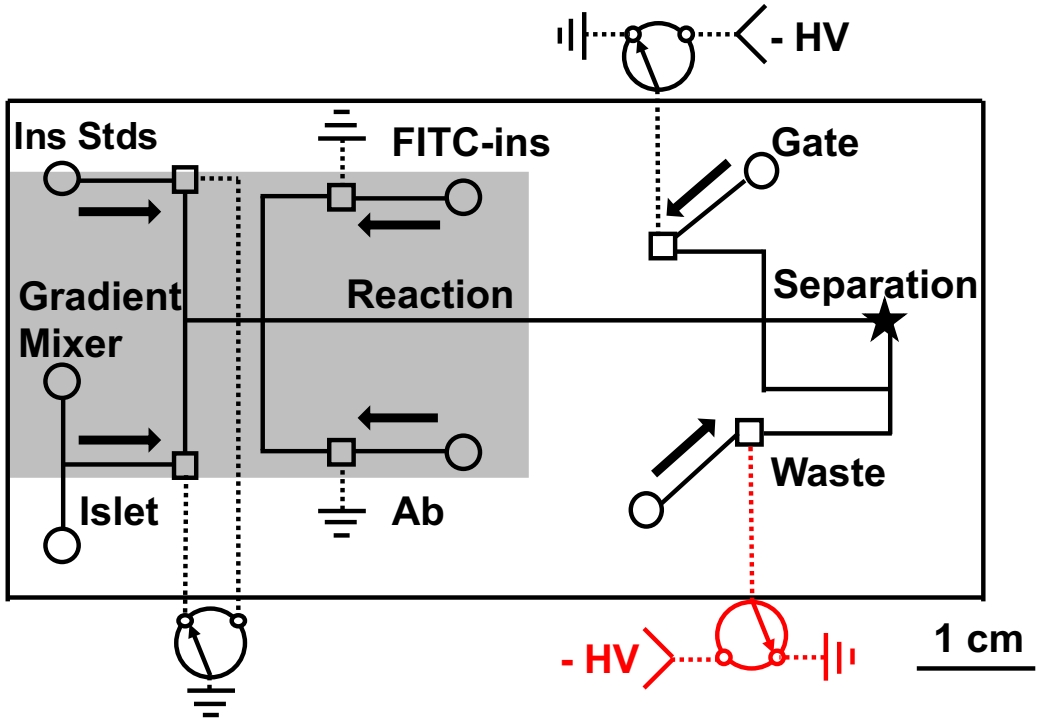

Figure 6.1. Diagram of the microchip electrophoresis. Modified application on waste channel is marked in red. Switching waste reservoir to ground stops the electrophoresis. Doing so in a long-term monitoring may protect the channels from clog.

Compare Short-term and Long-term Fatty Acid Pretreatment and Co-culture On-chip

Although it has been known that short-term NEFA treatment is a positive regulator of insulin secretion, most short-term studies were performed by administrating NEFAs during glucose treatment and measure insulin secretion immediately.[2–4] One study[5] pretreated islets with 0.5 mM palmitic acid at 4 mM glucose for ~30 min, and then stimulated them with 8 mM glucose. Palmitic acid showed a clear 2 fold potentiation of GSIS in that study. Another study[6] pretreated islets with 0.5 mM palmitic acid for 1 h but did not observe significant GSIS augmentation. The results in this dissertation demonstrated that short-term pretreatment of fatty acid enhances insulin secretion even with relatively low fatty acid concentration, suggesting short-term fatty acid pretreatment is a positive regulator of insulin secretion.

NEFA modulation of GSIS in islets, also termed as “lipid signaling”, can signal directly via a free fatty acid receptor, GPR40.[7–10] It is also known that intracellular metabolism of NEFAs resulting in the synthesis of lipid signaling molecules such as long-chain acyl-CoA (LC-CoA) and diacylglycerol (DAG), which are very important in NEFA’s role in modulating GSIS (see reference 11 for a review). In this dissertation work, 1 h and 2 h pretreatments with palmitic acid were also attempted, but produced inconsistent results, while 3 h pretreatment consistently enhanced GSIS. It is likely an indication that NEFA’s effect on insulin secretion is time dependent.[12,13] For a future direction, experiments can be applied to expose islets to different length of time, and compare the effects on insulin secretion. More than that, since metabolism is a factor of NEFA modulation in β-cells, it is also interesting to measure islet metabolomics. Our group previously have developed method using LC-MS for such applications with β-cell

lines.[14,15] Modifications on the method were also made to apply to islets, which can be used in applications of this work in the future.

Meanwhile, previous evidence suggested that chronic (~48 h) exposure of fatty acid resulted in impaired insulin secretion.[16] Such effects are illustrated in **Figure 6.2**. Saturated NEFAs have been known to reduce insulin biosynthesis and secretion and induce β-cell apoptosis.[11] Monitoring GSIS and metabolomics of islets pretreated with NEFAs for long-term (more than 48 h) may provide us better understanding of how this process happens. The results can also be compared with short-term treatments (less than 6 h).

Similar experiments can also be performed with adipocytes co-culture. Co-culture of adipocytes and islets cannot reproduce a completed *in vivo* environment without interacting with other tissue cells, however, it may potentially reveal the direct effects of adipocytes on islets. The receptors of several adipokines have been found on β-cells (see reference 17 and 18 for a review). Also, a lot of type 2 diabetes patients have been obese for a long time before hyperglycemia and dyslipidemia[19]. It is possible that adipose tissue already leads to β-cell dysfunction, even ahead of high level of blood glucose and NEFAs. In this dissertation, we demonstrated short-term adipocytes co-culture augments GSIS. It would be interesting in the future to investigate long-term adipocyte-islet co-culture. It is possible that the short-term enhancement may cause β-cell compensation, which ultimately lead to β-cell failure and defected insulin secretion.

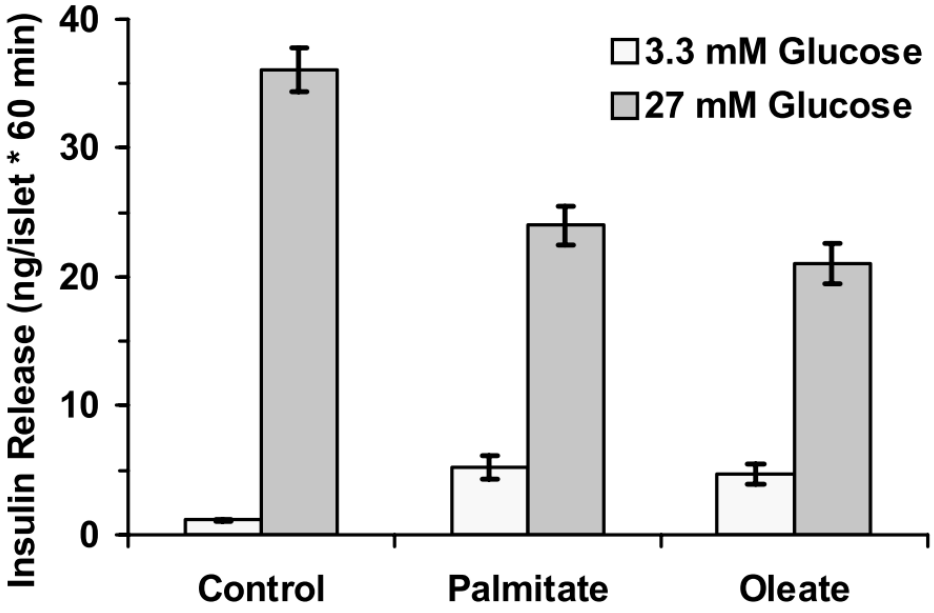

Figure 6.2. GSIS from islets chronically exposed to fatty acids. Islets were cultured for 48 h with 0.125 mM indicated fatty acid. Chronic exposure to palmitate and oleate increased basal insulin release and impaired GSIS (with 27 mM glucose). Chart recreated with data from reference 16.

Compare Inflamed and Normal Adipocytes' Effects on Insulin Functions

Secretion of NEFAs and several adipokines levels were found abnormal during obesity. TNF-α-an inflammatory cytokine and the first molecular link between inflammation and obesity-was found overexpressed in the adipose tissue of rodent obesity models[20,21] and obese humans[22–24]. With more inflammatory mediators being found exhibit patterns similar to TNF-α during obesity, transcriptional profiling studies verified that inflammatory and stress-response genes are the most regulated in adipose tissue of obese animals[25–27] (A list of alterations of many of these genes and other adipokines secretion can be found in reference 28). Disregulation of the inflammatory cytokines and adipokines may cause insulin resistance and β-cell compensation and ultimately lead to β-cell failure[18,28,29], but their roles in directly regulating insulin secretion were less studied and discussed. As a future direction, it would be interesting

to apply inflamed adipocytes directly on islets and study their effects on insulin secretion.

Inflammation in 3T3-L1 adipocytes can be induced with treatment of TNF-α as described previously.[30] Non-TNF-α treated adipocytes can be used as a negative control. Another approach is to directly use inflamed adipocytes from obese individuals. Although primary adipocytes are challenging to be cultured for more than 24 h, the experiments can be designed to use the adipocytes immediately after isolation. A microfluidic device was reported using primary adipocytes immediately after isolation and has been applied to measure adiponectin secretion.[31] Using the media cultured with adipocytes to treat islets is another approach. These studies can be used for further investigation of potential pathophysiological link between obesity and type 2 diabetes.

Qualification and quantification of NEFAs and adipokines secretion from adipocytes

Palmitic acid was applied as positive control of adipocytes in this dissertation. Although it is one of the major fatty acids secreted by adipocytes, a mixture of major NEFAs secreted by adipocytes can be used as a more representative positive control.[32,33] Characterizations of NEFAs and adipokines are also important directions, particularly to measure their alteration in inflamed adipocytes secretions. The Kennedy group recently developed methods coupling chips to mass spectrometry, providing a powerful way to identify and quantify multiple secretions from adipocytes.[34] **Figure 6.3** illustrated full scan analysis of mass spectrum of on-line elution profile from 3T3-L1 adipocytes. This experiment can be applied to characterize fatty acid secretion. The perfusate during co-culture can be collected and introduced to the on-line solid-phase extraction and mass spectrometry system for NEFAs identification and quantification.

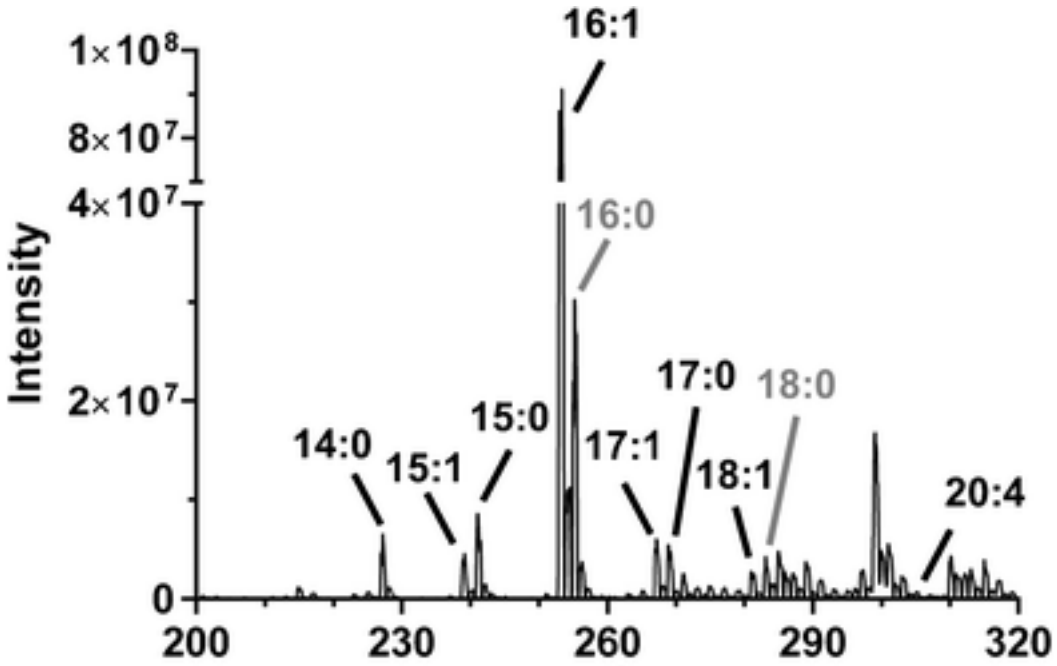

Figure 6.3. On-line elution profile from 3T3-L1 adipocytes. Full scan analysis of m/z ranging from 200 to 320 performed on a QQQ-MS. Adipocytes loaded in the cell chamber were stimulated with isoproterenol/forskolin. An on-line solid phase extraction bed was applied to load fatty acid samples and subsequently washed. Sample was eluted to the MS. Peaks are labeled with the NEFAs that associate with the appropriate m/z. Reproduced from Reference 34.

Adipokines were not identified or quantified in this dissertation work, although such measurements have been proceeded with 3T3-L1 adipocytes in previous studies.[35] **Figure 6.4** demonstrated protein expression of a few major adipokines. In the future, techniques like SDS-PAGE/LC-tandem MS[36,37] and gene expression analysis[30] can be applied to better assess adipokines secretion.

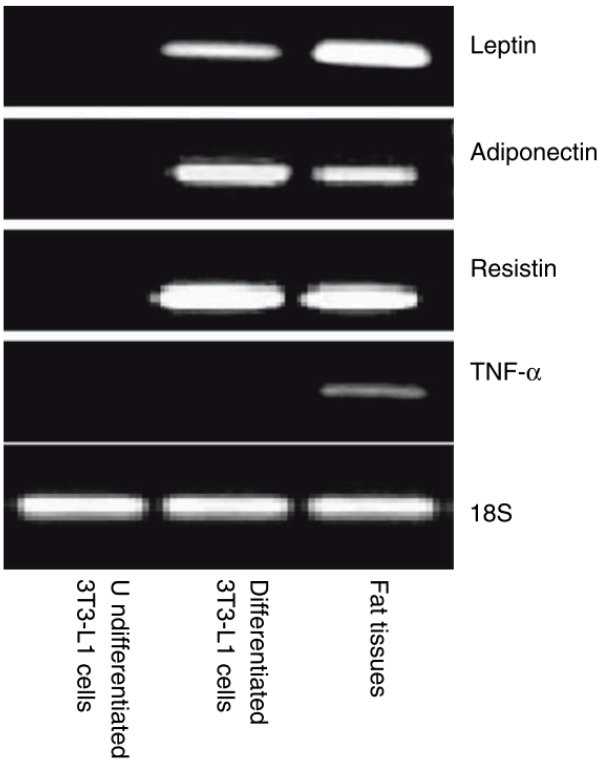

Figure 6.4. The expression of adipocyte-secreted factors in 3T3-L1 cells. Leptin, adiponectin and resistin are expressed in differentiated 3T3-L1 adipocytes and in fat tissues from mouse epididymis fat pad, but not in undifferentiated 3T3-L1 preadipocytes. TNF-α was only weakly detected in fat tissues. Reproduced from Reference 35.

Microfludic Device for Co-culture Studies in Parallel

The Kennedy group previously developed a microfluidic electrophoresis device for high-throughput, automated, online monitoring of insulin secretion from as many as 15 single islets in parallel[38], which has been described in chapter 1. Higher throughput analysis by parallel measurements results in reduced time and cost. Furthermore, for the co-culture studies, parallel measurements allow better control of islets culture conditions. To be more specific, islets with the same time after isolation can be placed on nearby locations on chip, while co-cultured with adipocytes, fatty acid standards or blank coverslip. **Figure 6.5** illustrated a microchip designed for 2 co-culture groups on the same chip. This chip was attempted for a few times but several challenges were not

well resolved yet. The adipocytes chambers portion was designed to be sealed with 2 sheets of acrylic plastic. Because this chip is wide, applying screws only on both ends easily bended the plastic sheets, leading to leakage in the adipocyte chambers in the middle. A better design is needed to seal the adipocyte chambers. The experimental protocol to maintain 2 islets is also tedious and prone to error, which may need further simplifying. The Pretreatment step takes 3 h and measurements of insulin secretion takes 1 h. To keep both islets pretreated for the same length of time, after the adipocytes are loaded and primed on chip for 30-40 min, one islet is loaded first for 1 h before the other. They will be sequentially measured for insulin secretion afterwards. It would be desired to realize simultaneous measurement of multiple islets. A method to simultaneously measure multiple channels signal was previously developed by our group.[39] It may also be useful to use a fluorescent camera for multichannel detection. These improvements can allow multiple islets pretreatment and insulin monitoring in parallel, thus increase throughput.

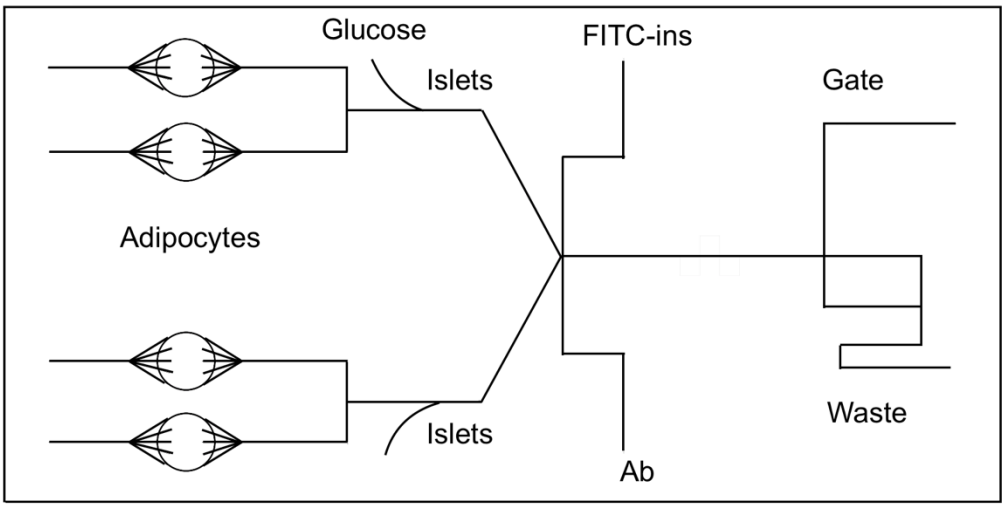

Figure 6.5. A microchip design culturing 2 islets. 2 co-culture groups are designed on the same chip while sharing the same insulin measurement part. During experiment, one islet is loaded first while the other is loaded in 1 h. Afterwards, insulin secretion are monitored in sequence.

Conclusion

To summarize, several microfluidic devices have been designed and developed in this dissertation for different applications, including unattended insulin secretion monitoring combining gradient generation, cell-cell interaction studies on chip, direct monitoring of fluorescent peptides, and $[Ca^{2+}]_i$ measurements. The future directions include several aspects, focused on improvement of the stability of the long-term MCE system, more complex biological applications with the co-culture chip to better understand the effects of NEFAs and adipocytes on islets' insulin function, and enhanced analytical methods to improve experimental throughput.

References

(1) Shackman, J. G.; Dahlgren, G. M.; Peters, J. L.; Kennedy, R. T. *Lab Chip* **2005**, *5*, 56–63.

(2) Alstrup, K. K.; Gregersen, S.; Jensen, H. M.; Thomsen, J. L.; Hermansen, K. *Metabolism* **1999**, *48*, 22–29.

(3) Thams, P.; Capito, K. *Diabetologia* **2001**, *44*, 738–746.

(4) Warnotte, C.; Gilon, P.; Nenquin, M.; Henquin, J. C. *Diabetes* **1994**, *43*, 703–711.

(5) Doliba, N. M.; Qin, W.; Vinogradov, S. A.; Wilson, D. F.; Matschinsky, F. M. *Am. J. Physiol. Metab.* **2010**, *299*, E475–E485.

(6) Tian, G.; Maria Sol, E. R.; Xu, Y.; Shuai, H.; Tengholm, A.; Sol, E. M.; Xu, Y.; Shuai, H.; Tengholm, A. *Diabetes* **2015**, *64*, 904–915.

(7) Itoh Y, Kawamata Y, Harada M, Kobayashi M, Fujii R, Fukusumi S, Ogi K, Hosoya M, Tanaka Y, Uejima H, Tanaka H, Maruyama M, Satoh R, Okubo S, Kizawa H, Komatsu H, Matsumura F, Noguchi Y, Shinohara T, Hinuma S, Fujisawa Y, F. M. *Nature* **2003**, *422*, 173–176.

(8) Latour, M. G.; Alquier, T.; Oseid, E.; Tremblay, C.; Jetton, T. L.; Luo, J.; Lin, D. C. H.; Poitout, V. *Diabetes* **2007**, *56*, 1087–1094.

(9) Kristinsson, H.; Smith, D. M.; Bergsten, P.; Sargsyan, E. *Endocrinology* **2013**, *154*, 4078–4088.

(10) Komatsu, M.; Takei, M.; Ishii, H.; Sato, Y. *J. Diabetes Investig.* **2013**, *4*, 511–516.

(11) Nolan, C. J.; Madiraju, M. S. R.; Delghingaro-Augusto, V.; Peyot, M.-L.; Prentki, M. *Diabetes* **2006**, *55*, S16–S23.

(12) Komatsu, M.; Sharp, G. W. G. *Diabetes* **1998**, *47*, 352–357.

(13) Komatsu, M.; Yajima, H.; Yamada, S.; Kaneko, T.; Sato, Y.; Hashizume, K.; Aizawa, T. *Diabetes* **1999**, *48*, 1543–1549.

(14) Lorenz, M. A.; Burant, C. F.; Kennedy, R. T. *Anal. Chem.* **2011**, *83*, 3406–3414.

(15) El-Azzouny, M.; Evans, C. R.; Treutelaar, M. K.; Kennedy, R. T.; Burant, C. F. *J. Biol. Chem.* **2014**, *289*, 13575–13588.

(16) Zhou, Y. P.; Grill, V. E. *J. Clin. Invest.* **1994**, *93*, 870–876.

(17) Eldor, R.; Raz, I. *Diabetes Res. Clin. Pract.* **2006**, *74*, S3–S8.

(18) Dunmore, S. J.; Brown, J. E. P. *J. Endocrinol.* **2013**, *216*, T37–T45.

(19) Scheen, A. J. *Acta Clin Belg* **2000**, *55*, 9–15.

(20) Hotamisligil, G. S.; Shargill, N. S.; Spiegelman, B. M. *Science* **1993**, *259*, 87–91.

(21) Sethi, J. K.; Hotamisligil, G. S. *Semin. Cell Dev. Biol.* **1999**, *10*, 19–29.

(22) Kern, P. A.; Saghizadeh, M.; Ong, J. M.; Bosch, R. J.; Deem, R.; Simsolo, R. B. *J. Clin. Invest.* **1995**, *95*, 2111–2119.

(23) Hotamisligil, G. S.; Arner, P.; Caro, J. F.; Atkinson, R. L.; Spiegelman, B. M. *J. Clin. Invest.* **1995**, *95*, 2409–2415.

(24) Saghizadeh, M.; Ong, J. M.; Garvey, W. T.; Henry, R. R.; Kern, P. A. *J. Clin. Invest.* **1996**, *97*, 1111–1116.

(25) Soukas, A.; Cohen, P.; Socci, N. D.; Friedman, J. M. *Genes Dev.* **2000**, *14*, 963–980.

(26) Weisberg, S. P.; McCann, D.; Desai, M.; Rosenbaum, M.; Leibel, R. L.; Ferrante Jr., A. W. *J. Clin. Invest.* **2003**, *112*, 1796–1808.

(27) Xu, H.; Barnes, G. T.; Yang, Q.; Tan, G.; Yang, D.; Chou, C. J.; Sole, J.; Nichols, A.; Ross, J. S.; Tartaglia, L. A.; Chen, H. *J. Clin. Invest.* **2003**, *112*, 1821–1830.

(28) Wellen, K. E.; Hotamisligil, G. S. *J. Clin. Invest.* **2005**, *115*, 1111–1119.

(29) Stein, D. T.; Stevenson, B. E.; Chester, M. W.; Basit, M.; Daniels, M. B.; Turley, S. D.; McGarry, J. D. *J. Clin. Invest.* **1997**, *100*, 398–403.

(30) Pinent, M.; Espinel, A. E.; Delgado, M. A.; Baiges, I.; Bladé, C.; Arola, L. *Food Chem.* **2011**, *125*, 513–520.

(31) Godwin, L. a.; Brooks, J. C.; Hoepfner, L. D.; Wanders, D.; Judd, R. L.; Easley, C. J. *Analyst* **2015**, *140*, 1019–1025.

(32) Abdelmagid, S. A.; Clarke, S. E.; Nielsen, D. E.; Badawi, A.; El-Sohemy, A.; Mutch, D. M.; Ma, D. W. L. *PLoS One* **2015**, *10*, e0116195.

(33) Sera, R. K.; Mcbride, J. M.; Higgins, S. A.; Rodgerson, D. *J. Clin. Lab. Anal.* **1994**, *8*, 81–85.

(34) Dugan, C. E.; Grinias, J. P.; Parlee, S. D.; El-Azzouny, M.; Evans, C. R.; Kennedy, R. T. *Anal. Bioanal. Chem.* **2017**, *409*, 169–178.

(35) Zhao, Y. F.; Feng, D. D.; Hernandez, M.; Chen, C. *Endocrine* **2007**, *31*, 52–60.

(36) Brockman, D.; Chen, X. *Adipocyte* **2012**, *1*, 25–37.

(37) Lehr, S.; Hartwig, S.; Lamers, D.; Famulla, S.; Müller, S.; Hanisch, F.-G.; Cuvelier, C.; Ruige, J.; Eckardt, K.; Ouwens, D. M.; Sell, H.; Eckel, J. *Mol. Cell. Proteomics* **2012**, *11*, M111.010504.

(38) Dishinger, J. F.; Reid, K. R.; Kennedy, R. T. *Anal. Chem.* **2009**, *81*, 3119–3127.

(39) Dishinger, J. F.; Kennedy, R. T. *Anal. Chem* **2007**, *79*, 947–954.